UNIVERSITY OF BELGRADE
FACULTY OF PHYSICS

Danica Stojiljković

KINETICS AND MORPHOLOGY OF PARTICLE DEPOSITION AT HETEROGENEOUS SURFACES

Doctoral Dissertation

Belgrade, 2022

УНИВЕРЗИТЕТ У БЕОГРАДУ
ФИЗИЧКИ ФАКУЛТЕТ

Даница Стојиљковић

КИНЕТИКА И МОРФОЛОГИЈА ДЕПОЗИЦИЈЕ ЧЕСТИЦА НА ХЕТЕРОГЕНИМ ПОВРШИНАМА

докторска дисертација

Београд, 2022. година

Thesis Defense Committee

Thesis advisor:

Dr. Slobodan Vrhovac
Research Professor
Institute of Physics Belgrade
University of Belgrade

Committee member:

Dr. Julija Šćepanović
Assistant Research Professor
Institute of Physics Belgrade
University of Belgrade

Committee member:

Prof. Dr. Sunčica Elezović-Hadžić
Professor
Faculty of Physics
University of Belgrade

Committee member:

Prof. Dr. Đorđe Spasojević
Professor
Faculty of Physics
University of Belgrade

Acknowledgements

First, I would like to thank Dr. Slobodan Vrhovac for allowing me to be a part of his team and for guiding me through the complexity of seemingly simple models. I am grateful for the shown trust, generous help, and tremendous patience and understanding. I am thankful to our associates, Dr. Nenad Švrakić for introducing us to the subject and for fruitful discussions, and to Dr. Julija Šćepanović for many constructive conversations and immense support.

I wish to express my eternal gratitude to Dr. Antun Balaž for his continuous support over the years, for being available even when he's busy, for his professional and personal guidance, and for pushing me to do better, work harder and be wiser. He is the most remarkable boss, colleague, and friend, who has introduced me to the world of theoretical physics and (numerical) research.

Many thanks to Dr. Aleksandar Bogojević and Dr. Aleksandar Belić for accepting me to be a member of the first generation of the SCL family, giving me the chance to work at CERN, the most exciting place in the world for any physicist, and for broadening my professional interests beyond the frame of science. Many thanks to all of my colleagues at IPB, former and current, especially to numerous office-mates, for creating an enjoyable working atmosphere and for interesting everyday chats on a wide range of subjects, from daily weather to the meaning of it all.

And finally, and most importantly, my most sincere gratefulness goes out to my family for all of their love and support. To my mother who always encouraged me to be persistent and to fulfil my potential. To my father who taught me how to always look on the bright side and enjoy small moments. To my brother for never-ending discussions on every subject one could think of. To my husband for standing by my side. To my two lovely sons, who motivated me to re-learn how to play and investigate. And to many others...

Abstract

Monolayer and multilayer thin film formation on solid or liquid surfaces is a growing multidisciplinary area of research of great interest for new and emerging technologies in photonics, microelectronics, nanotechnology, plasmonics, biosensors, bio-medical devices, etc. Adsorption and deposition (irreversible adsorption) of colloids, proteins, and other bio-materials on solid/liquid interfaces are of large significance for many practical and natural processes such as filtration, paper-making, chromatography, separation of proteins, viruses, bacteria, pathological cells, immunological assays, thrombosis, biofouling, biomineralization, etc. Controlled adsorption of colloid particles on sites of nanometric scale can also be exploited for direct visualization of surface features.

The Random Sequential Adsorption (RSA) model is one of the basic models used to describe the irreversible formation of monolayer deposits of microscopic and mesoscopic particles. Inter-particle interactions are approximated classically with the hard-core exclusion model, which means that overlaps between the particles are not allowed. Particles can only adsorb if they are in direct contact with the substrate. This feature ensures a monolayer deposition. Irreversible adsorption means that the adsorbed particle stays permanently fixed to the substrate and diffusion or desorption processes are not allowed. Previously adsorbed particles block a certain area of the substrate for new adsorptions and consequently, the system becomes jammed. Heterogeneities of a substrate impose further limitations on the positions of adsorbed particles. Our aim is to quantify structural changes in the jammed state that are introduced by different patterns of substrate heterogeneities. We use the RSA approach to analyze the deposition of identical spherical particles of a fixed radius on non-uniform flat surfaces covered by rectangular cells. Two different types of patterns are of interest: randomly positioned cells and square lattice centred cells.

In the first part of the dissertation, the configuration of the cells (heterogeneities) was produced by performing RSA simulations to a prescribed coverage fraction $\theta_0^{(\text{cell})}$. Adsorption was assumed to occur if the particle (projected) centre lies within a rectangular cell area, i.e., if the sphere touches one of the cells. The jammed-state properties of the model were studied for different values of the cell size α (comparable with the adsorbing particle size) and density $\theta_0^{(\text{cell})}$. Numerical simulations were carried out to investigate adsorption kinetics, jamming coverage, and structure of coverings. Structural properties of the jammed-state coverings were analyzed in terms of the radial distribution function $g(r)$ and distribution of the Delaunay 'free' volumes $P(v)$. It was demonstrated that adsorption kinetics and the jamming coverage decreased significantly, at a fixed density $\theta_0^{(\text{cell})}$, when the cell size α increased. The predictions following our calculation suggest that the porosity (pore volumes) of the deposited monolayer can be controlled by the size and shape of landing cells, and by the anisotropy of the cell deposition procedure.

The second direction of research in this thesis analyses the adsorption of spherical particles of a fixed diameter on nonuniform surfaces covered by square cells arranged in a square lattice pattern. To characterize such a pattern two dimensionless parameters are used: the cell size α and the cell-cell separation β, measured in terms of the particle diameter d_0. We focus on the kinetics of the deposition process in the case when no more than a single disk can be placed onto any square cell ($\alpha < 1/\sqrt{2} \approx 0.707$). We find that the asymptotic approach of the coverage fraction $\theta(t)$ to the jamming limit θ_J is algebraic if the parameters α and β satisfy the simple condition, $\beta + \alpha/2 < 1$. If this condition is not satisfied, the late time kinetics of the deposition process is not consistent with the power-law behaviour. However, if the geometry of the pattern approaches "noninteracting conditions" ($\beta > 1$), when adsorption on each cell can be decoupled, the approach of the coverage fraction $\theta(t)$ to θ_J becomes closer to the exponential law. Consequently, changing the pattern parameters in the present model allows for interpolating the deposition kinetics between the continuum limit and the lattice-like behaviour. Structural properties of the jammed-state coverings are studied in terms of the radial distribution function $g(r)$ and the spatial distribution of particles inside the cell. Various, non-trivial spatial distributions are observed depending on the geometry parameters of the pattern.

Сажетак

Формирање једнослојних и вишеслојних танких филмова на чврстим и течним површинама је растућа мултидисциплинарна област истраживања од великог интереста у фотоници, микроелектроници, нанотехнологијама, плазмоници, за биосензоре, биомедицинске уређаје, итд. Адсорпција и депозиција (иреверзибилна адсорпција) колоида, протеина и других биоматеријала на чврстим/течним површинама су од велике важности за многе практичне и природне процесе као што су филтрација, производња папира, хроматографија, сепарација протеина, вируса, бактерија и патолошких ћелија, имунолошки тестови, тромбоза, биоминерализација, итд. Контролисана адсорпција колоидних честица на структурама на нанометарској скали се такође могу искористит за директну визуализацију структурних карактеристика.

Модел случајне секвенцијалне адсорпције (RSA модел) је један од основних модела за описивање формирања једнослојних депозита мезоскопских честица. Међучестична интеракција је апроксимирана класичним моделом крутих тела, што значи да је забрањено међусобно преклапање честица. Честице се могу адсорбовати једино ако су у директном контакту са супстратом. Ова особина доводи до формирања једнослојних депозита. Појам иреверзибилна адсорпција поразумева да су адсорбоване честице трајно причвршћене за подлогу, а процеси дифузије или десорпције су забрањени. Претходно адсорбоване честице блокирају одређени део подлоге за адсорпцију нових честица што доводи до загушења система. Нехомогеност супстрата намеће додатна ограничења на позиције адсорбованих честица. Наш циљ је да квантификујемо структурне промене загушеног стања настале услед разлличитих хетерогених образаца на адсорбујоћој подлози. Користимо RSA приступ за анализу депозиције идентичних сферних честица на нехомогене равне површине покривене правоугаоним ћелијама. Од интереса су два различита типа распореда: случајно распоређене ћелије и ћелије распоређене у чворовима квадратне решетке.

У првом делу истраживања у оквиру ове тезе, конфигурација ћелија се формира помоћу RSA симулације док се не постигне жељена покривеност супстрата $\theta_0^{(cell)}$. До адсорпције долази ако (пројектовани) центар честице лежи унутар правоугаоне ћелије, тј. ако сферна честица додирује неку од ћелија. Особине загушеног стања су изучаване за различите вредности величине ћелија α (упоредивих са величином честице) и различите густине ћелија $\theta_0^{(cell)}$. Извршене су нумеричке симулације како би истражили кинетику адсорпције, покривеност у загушењу и структуру депозита. Структурне особине загушеног стања анализиране су помоћу парне корелационе функције $g(r)$ и дистрибуције Делонејевих слободних површина. Резултати наших симулација сугеришу да се контрола порозности једнослојног депозита може постићи подешавањем величине, облика и оријентације прихватних ћелија.

Други правац истраживања у тези је анализа адсорпције сферних честица фиксног пречника на хетерогеним површинама прекривеним квадратним ћелијама распоређеним у чворове квадратне решетке. За карактеризцију овог шаблона користимо два бездимензиона параметра: величину квадратне ћелије α и размак између две суседне ћелије β. За јединицу мере користимо пречник адсорбујућих ћелија d_0. У фокусу истраживања је кинетика процеса депозиције у случају када било која прихватна ћелија може да адсорбује највише једну честицу ($\alpha < \sqrt{2}/2$). Покривеност $\theta(t)$ асимптотски тежи граничној вредности θ_J по алгебарском закону ако параметри α и β задовољавају услов $\beta + \alpha/2 < 1$. Ако овај услов није испуњен, кинетика касне фазе процеса депозиције није конзистента са степеном законитошћу. Ипак, како се геометрија подлоге приближава неинтерагујућем режиму ($\beta > 1$), асимптотски прилаз покривености се приближава експоненцијалној закоости. Сходно томе, промена параметара патерна субстрата у овом моделу омогућује интерполацију између два гранична случаја адсорпције на континууму и на квадратној решетки. За изучавање структурних особина загушеног стања користимо парну корелациону функцију $g(r)$ и просторну дистрибуцију честица унутар ћелија. Примећене су разноврсне нетривијалне просторне дистрибуције у зависности од геометрије патерна подлоге.

Contents

List of figures

Chapter 1

Introduction

Adsorption is a general term for the processes responsible for the formation of deposits (a.k.a adsorbates). It represents the adhesion of foreign particles to the solid or liquid surfaces commonly termed as adsorbants or substrates. It is a common phenomenon that has great scientific and industrial importance as it has been linked to a wide range of applications in biology [3–6], nanotechnology [7, 8], device physics [9–11], physical chemistry [12, 13], and materials science [14]. Depending on the application in question, the depositing objects could be colloidal particles, polymer chains, globular proteins, nanotubes, DNA segments, or general geometrical shapes, such as disks, polygons, etc. Due to its wide range of applications, there has been a continuous effort to enrich our understanding of deposition processes and experimentally observed structural properties of the adsorbed phase [7, 15, 16].

One of the basic models for studying a thin film formation is known as Random Sequential Adsorption (RSA). It models the process of adsorption of objects in a sequential manner (one by one). The new object is randomly positioned on the substrate, and adsorption is successful if it doesn't overlap any of the previously adsorbed objects. If overlap occurs, the object is rejected and a new adsorption attempt is made. All accepted objects stay permanently fixed on the substrate, thus forming a monolayer deposit. They block certain areas of the substrate for the adsorption of new objects. The blocked area of the substrate expands as the number of adsorbed objects grows, and the adsorption rate slows down. A finite substrate eventually reaches a jammed state where the complete substrate is blocked for the adsorption of new objects. When a substrate is infinitely large, the jammed state is reached in the limit as time goes to infinity.

This is the most general description of the RSA process. The two general terms, 'substrate' and 'object', represent suitable entities in any adsorption process we aim to describe. We can choose whether the substrate is discrete, continuous, pre-patterned, regular, lattice-based, 1D, 2D, 3D, or (in theory) anything we can think of. In practice, our model will seek to describe a physical system within a wide range of applications in biology, nanotechnology, device physics, physical chemistry, and materials science. Most systems of interest would have flat 2D substrates, but other shapes such as spheres, cylinders and rings can also be of interest. The term 'object' can stand for line segments, circles, squares, ellipses, polygons, or any other shape representing real objects such as colloidal particles, polymer chains, globular proteins, nanotubes, DNA segments, etc. New and emerging technologies enable us to precisely tailor the shape and size of the deposition objects on micro and

even nanoscale. All this makes RSA the tool for various interdisciplinary studies.

A desorption is a process in which adsorbed particles detach from a surface. It competes with the adsorption and slows down or even prevents a deposit growth. Other processes that play their roles in kinetics and dynamics of adsorbate formation are diffusion, surface relaxation, hoping of particles, inter-particle interactions, etc. In this work, we will focus on processes in which the time needed to reach the jammed state is much smaller than the relaxation time. Relaxation processes can be neglected and we can assume that after each particle is adsorbed, it stays rigidly and irreversibly fixed to the substrate.

New technologies enable the production of particles with precise shapes on micro and even nanoscale, and the effects of particle properties on deposits and the adsorption process have been thoroughly investigated. Besides adsorbate particles, it is evident that adsorbant surface structure is just as important. Many surfaces of adsorbants are inherently heterogeneous, or they can be modified by the use of coupling agents bound to interfaces, e.g., polyelectrolytes, ligands, surfactants, polyvalent ions, or chemical coupling agents. In each stated case, adsorption occurs at heterogeneous surfaces bearing isolated adsorption sites. This enables us to create deposits with precisely tailored properties, such as coverage and morphology. A deeper theoretical understanding of these systems enhances the effectiveness of the process, rather than using the trial-error method.

We are interested in the kinetics of an adsorption process, as well as in the adsorbate structure in terms of coverage evolution, maximum (jamming) coverage, density/pair correlation function, porosity, etc. Due to the problem complexity, very few simple models can be solved analytically and those are mostly models of one-dimensional substrate. Pioneer work in this field was done by Paul Flory who studied the attachment of pendant groups in a polymer chain [17]. This problem translates to the adsorption of dimers on a one-dimensional regular lattice (see figure 1.1(a)). Flory found that if unreacted groups of a polymer chain randomly pair with its unreacted neighbour, 13.53% of them are prevented from reacting due to isolation between reacted pairs. In terms of the adsorption of dimers on and infinite 1D lattice, the exact jamming coverage is $1 - 1/e^2 \approx 08647$. In 1958, a Hungarian mathematician Alfred Rényi solved the following problem: given a street of given length and cars
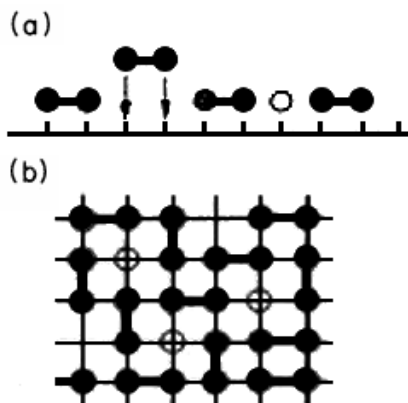
Figure 1.1: (a) Dimer filling on a 1D lattice; (b) Dimer filling on a square lattice. Isolated empty sites, which can never fill, are shown as "o" [15].
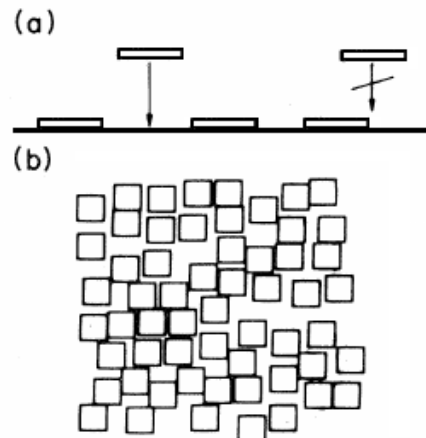
Figure 1.2: (a) Continuum "car parking" of unit length intervals on the line; (b) jammed state for RSA of aligned squares in the plane [15] .

of constant length that park on a random free position on the street, what is the density of cars when there are no more free positions [18]? This translates to the adsorption of line segments of fixed length onto a one-dimensional continuous substrate (figure 1.2(a)). An exact jamming density on an infinite parking line is known as the Rényi's parking constant (≈ 0.7475979203).

Typical configurations of hard sphere deposits created in an RSA process radically differ from configurations of a gas in thermodynamic equilibrium, as shown by Widom [19]. The RSA process favors configurations in which pairs of spheres are distant. Radial distribution function of deposit configurations created in an RSA process that is stopped when the deposit coverage reaches a predetermined value θ below the jamming coverage θ_J, differs from the one of the equilibrium hard-sphere gas of the same density θ. Also, the system in equilibrium may be in a state with density θ that is higher than jamming density θ_J, which an RSA system can never surpass. Widom [19] also showed that if we want to use RSA to approximate equilibrium systems, this will only be correct up to the second and third virial coefficients, or cluster integrals, but incorrect fourth and higher-order ones.

Many variants of RSA systems have been studied in order to investigate the influence of shape, size, orientation and dispersion of adsorbing particles, finite-size effects, defects and impurities of a substrate [20–40]. Main focus of these studies was on systems with homogeneous substrates, but in many adsorption processes the substrate is manifestly heterogeneous. Motivated by affinity chromatography, in which solute particles bind only to ligands that are immobilized on the substrate surface, Jin et al. [41] investigated the so-called random-site surface model (RSS). They considered cases of randomly distributed ligands that are much smaller than solute particles and can be modeled as points. They found an exact mapping between the kinetics of this process and of the adsorption on a smooth continuous surface. The mapping is given by relation $\tau = \alpha(1 - e^{-t/\alpha})$, where t and τ are measuring the elapsed time in RSS and continuous surface RSA, respectively, and α is a dimensionless parameter related to the site density.

Based on a substrate type, research studies of RSA processes could be roughly divided into two groups: adsorption on a continuum substrate and adsorption on discrete sites, usually lattices. The crossover between two substrate types is usually treated in a way that the continuous substrate is considered as the limit case of a lattice substrate where distances between neighbouring sites are infinitely small. Another line of research tackles this crossover differently: particles can be adsorbed only within non-overlapping finite-size areas or objects, called cells, that are distributed over a flat substrate and form a desired pattern. This model can also be interpreted as adsorption on a discrete set of point-like adsorption sites that allow for error in particle positioning of the order of the size of the cell, thus treating adsorbing sites as cells of finite size.

The first generalization of the RSA model where lattice sites were treated as objects of finite size was the adsorption of dimers to equidistant adsorbing segments on a line, analyzed analytically and numerically by Bonnier et al. [42]. In the same fashion, Adamczyk et al. [43, 44] generalized the Random Site Surface model and considered surface heterogeneities as finite-size hard disks (or spheres) of fixed radius, positioned randomly in the preceding RSA process. The RSS model can also be generalized by using randomly placed adsorption cells of different shapes. A research direction exploited in this dissertation uses adsorbing cells shaped as squares or rectangles of different elongation.

Araújo et al. [45] and Marques et al. [13] numerically investigated the adsorption of disk-shaped particles on a two-dimensional pre-patterned substrate that consists of equal square cells centered at

(a)   (b)
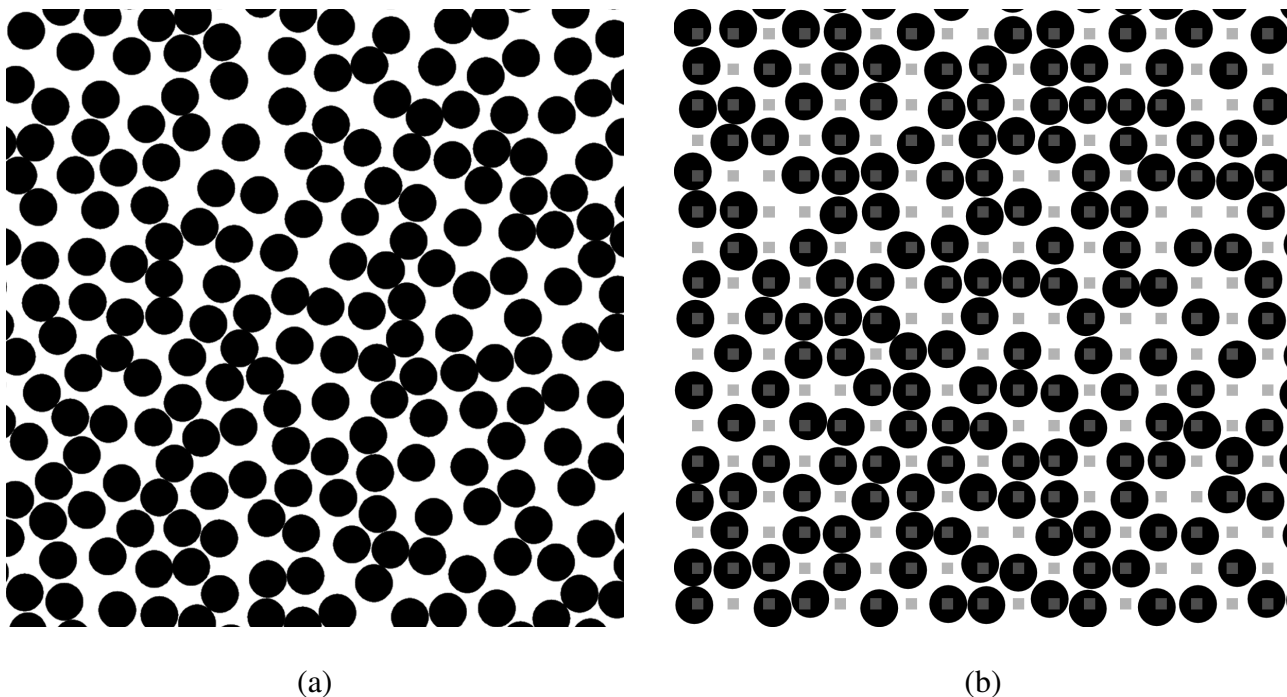
Figure 1.3: Typical configuration of jammed state yielded with random sequential adsorption (RSA) of disks on a flat continuous surface (a) and on a regular pre-patterned surface (b).

the vertices of a square lattice (Fig. 1.3(b)). They studied effects of a regular substrate pattern and particle polydispersity on the deposit density morphology, as well as on the in-cell particle population. They focused on the morphology of the final state. In this dissertation we analyze the kinetics of this model and investigate features of the deposition structure in more depth.

Privman and Yan [1] and Verma and Privman [2] analyzed the extended model of deposition of segments of length a in one-dimension, on a lattice of spacing l between its sites. Unlike sites of the precise lattice that have no size, sites of imprecise lattice are symmetrically broadened into segments of width w in which the centers of the depositing objects can land. They reported that even an arbitrarily small imprecision in the lattice-site localization ($w \gtrsim 0$) changes the convergence to jamming from fast, exponential, to slow, power-law. Our study in a similar spirit investigates the rapidity of the approach to the jamming state in the case of a two-dimensional (2D) pre-patterned substrate, elucidating the crossover between discrete and continuous substrate in a different light.

This dissertation

This thesis is organized as follows. In chapter 2, following this introduction, we overview the properties of the system necessary to analyze and understand the growth of a monolayer deposit and its structure. A historical overview of related research of the Random Sequential Adsorption model on various substrate types is given in chapter 3. Chapter 4 gives the details of the numerical simulation that we have developed and used to obtain the results presented in this thesis. The classical RSA model was modified to take into account the substrate inhomogeneities and adsorption was assumed to occur only if the (projected) particle center lies within a rectangular cell area, i.e., if a sphere touches one of the cells. In chapter 5, we investigated the RSA of spherical particles on a randomly patterned substrate, in which the configuration of the cells was produced by performing RSA simulations to a prescribed coverage fraction. Chapter 6 analyses the adsorption of spherical particles on surfaces covered by square cells arranged in a square lattice pattern. In the final chapter 7 we summarize the presented work and give some concluding remarks.

Chapter 2

Monolayer growth kinetics and structure

In this chapter, we describe the parameters and distributions used for the monolayer deposit characterization. The kinetic properties of a deposition process are described by the temporal evolution of the substrate coverage $\theta(t)$. To gain basic insight into the "microstructure" of the jammed state, we use the radial correlation function and size distribution of pores (patches of unoccupied spaces between particles).

2.1 Adsorption kinetics, jamming coverage and asymptotic behaviour

The most common parameter used to characterize the kinetic properties of a deposition process is coverage $\theta(t)$, defined as a fraction of the substrate area covered by adsorbed particles at moment t. It is calculated by dividing the size of the occupied substrate space by the total size of the substrate. In the case of adsorption of mono-dispersed particles, the coverage at a time t is calculated with the formula

$$\theta(t) = N_p(t)\frac{S_p}{S_s}, \tag{2.1}$$

where $N_p(t)$ is the number of adsorbed particles at a time t, S_p is the size of the substrate that a single particle occupies and S_s is the total size of the substrate. In the case of adsorption on a lattice substrate, S_p is the number of the lattice nodes that are occupied by adsorbed particles and S_s is the total number of nodes in the substrate sample. In the case of a one-dimensional continuous substrate, size refers to a length, while in the two-dimensional case it is a surface area. In experiments, the most relevant case is the adsorption of three-dimensional particles on two-dimensional surfaces, in which case the particle size S_p is calculated as the area of a particle projection onto the substrate. For example, adsorption of N_p non-overlapping identical spherical particles of radius r_0 to a square flat surface with a side of length L will give the coverage as

$$\theta(t) = N_p(t)\frac{r_0^2\pi}{L^2}. \tag{2.2}$$

The adsorption rate $u \equiv \mathrm{d}\theta(t)/\mathrm{d}t$ is proportional to the number of particles striking the unit surface area per second (flux j) and to the so-called sticking coefficient $S(\theta)$, which is the probability that an impinging particle actually sticks to the substrate: $u = jS(\theta)$. The sticking coefficient is equal to the fraction of the substrate surface that is available for new adsorptions $B(\theta)$, known as the available space function or the blocking function, multiplied by the probability P that a particle sticks to the substrate on contact: $S(\theta) = PB(\theta)$. RSA model assumes that adsorption is inevitable whenever a particle strikes the substrate at a location that satisfies the non-overlapping condition. In other words, the interaction energy between the substrate area and a particle is infinite at contact and equals zero otherwise and the probability P equals 1. Hence, the sticking coefficient equals the available space function $S(\theta) = B(\theta)$.

In the RSA model, the flux of the impinging particles j is considered to be uniform and at a constant rate. Time scaling $t^* = jt$ enables us to take the flux to be unitary and yield the adsorption rate as

$$u(t^*) = \frac{\mathrm{d}\theta(t^*)}{\mathrm{d}t^*} = B(\theta(t^*)). \tag{2.3}$$

in the further text, for the sake of simplicity and without loss of generality, we will only use the scaled time and omit the asterisk in the scaled time symbol.
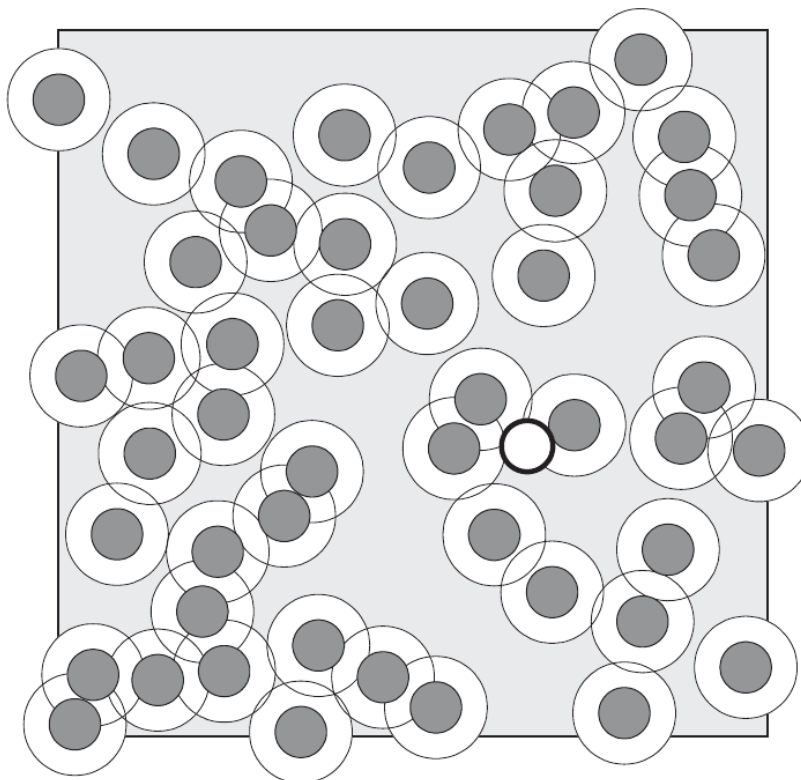
Figure 2.1: A typical configuration of particles adsorbed at an interface (dark disks); the white annuli show the exclusion areas, whereas the shadowed zones represent the areas (targets) available for the centre of the wandering particle depicted by the white disk. Figure from Adamczyk [46].

The typical RSA configuration of spherical (disk-like) particles adsorbed on a flat surface is illustrated in figure 2.1 [46]. Dark disks represent particle projections, while white annuli around them compose the space blocked for the centres of new particles. Gray surface is the "free" space available for the adsorption of new particle centres and its area represents the available space function. We get coverage versus time dependencies as shown in figure 2.2(a) by calculating the available space function and solving the equation 2.3. The available space function can be exactly calculated only in a few simple one-dimensional cases and we rely on numerical Monte Carlo simulations for its estimate. The sum of coverage θ and available space function $B(\theta)$ is less than 1 due to unfilled space around particles that are blocked for centres of new particles (white annuli in figure 2.1). These annuli overlap each other making the exact calculation of its area practically impossible.

Some features of the temporal evolution of the coverage are common for all RSA systems. At the start of the process, the entire surface of the substrate is available for adsorption of particles and all adsorption attempts are successful. Each adsorbed particle blocks the surrounding area for the adsorption of new particle centres and affects the geometry of all later placements. This is why $\theta(t)$ grows linearly at the start and slows down due to the interaction with previously adsorbed particles (the non-overlapping condition). Due to the blocking of the substrate area by already adsorbed particles, the available space function decreases as more particles are being adsorbed and coverage growth gets slower and slower.

At large times the coverage $\theta(t)$ asymptotically approaches the jammed-state value θ_J where only gaps too small to fit new particles are left in the monolayer. In the analysis of the asymptotic approach to jamming, a plot of $\theta_J - \theta(t)$ on a logarithmic scale strongly depends on the precise calculation of θ_J. Instead, we will examine the adsorption rate $u(t)$, i.e. the coverage growth of adsorbed particles per unit time and surface area. It is yielded by the differentiation of coverage $\theta(t)$ and the adsorption rate equals zero in the jammed state by definition ($u(t \to \infty) = 0$). A typical shape of the adsorption rate is shown in figure 2.2(b).
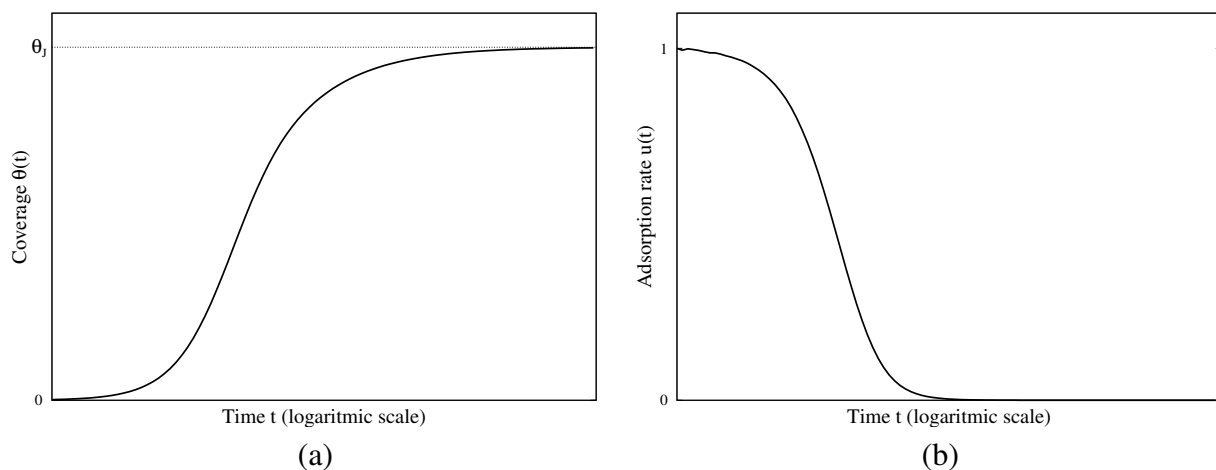
Figure 2.2: (a) Qualitative dependence of coverage θ on time and (b) corresponding dependence of the adsorption rate u on time (t).

2.2 Radial distribution function (pair correlation function)

Radial distribution function $g(r)$, also known as the pair-correlation function, provides a simple yet powerful encoding of the distribution of inter-particle gaps. It gives information about the long-range inter-particle correlations and their organization [47]. It is central in experimental applications of geometrical concepts to physical systems since it defines the scattering function measured in light, X-ray, and neutron diffraction experiments [48].

By definition, the pair correlation function measures the probability that a particle centre is found at a distance r from the referent particle, relative to the one of an ideal gas. In two-dimensional systems, it can be calculated from the expression

$$g(r) = \frac{S_s}{N_p} \frac{\Delta \overline{N}_a(r)}{2\pi r \Delta r},$$ (2.4)

where r is the radial coordinate, S_s is total surface area, N_p is total number of particles adsorbed over the surface, and $\Delta \overline{N}_a(r)$ is the average number of particles within the annulus of radius r and thickness Δr whose centre coincide with a particle centre (see figure 2.3). If $N_a(r; r^*)$ is the number of particles whose centre lies inside of a circle of radius r centred at a position r^*, then averaging this value over all circles whose centres coincide with particle centres will give us $\overline{N}_a(r)$. For a set of N_p particles
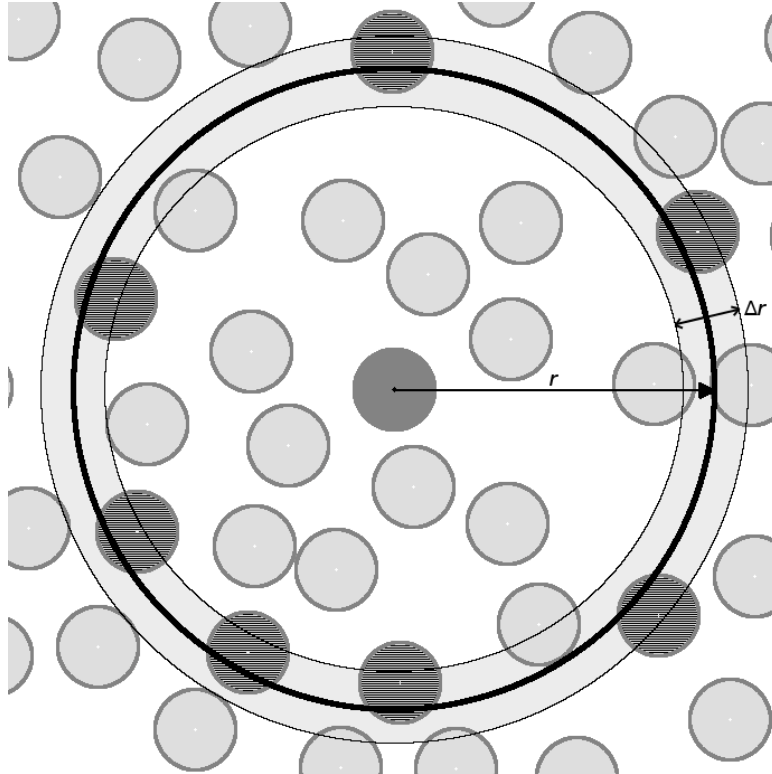
Figure 2.3: Radial distribution function: average density of particles at distance r from the centre of a reference particle.

positioned at $r_1, r_2, ..., r_{N_p}$ this is written as

$$\overline{N}_a(r) = \frac{1}{N_p} \sum_{j=1}^{N_p} N_a(r; r_j) = \frac{1}{N_p} \sum_j \sum_{i \neq j} \eta(r - |r_j - r_i|),$$ (2.5)

where $\eta(x)$ is the Heaviside step function. From equation (2.5), we obtain

$$\Delta \overline{N}_a(r) = \frac{1}{N_p} \sum_j \sum_{i \neq j} [\eta(r + \frac{\Delta r}{2} - |r_j - r_i|) - \eta(r - \frac{\Delta r}{2} - |r_j - r_i|)],$$ (2.6)

which then gives

$$g(r) = \frac{S_s}{2\pi r \Delta r N_p^2} \sum_j \sum_{i \neq j} [\eta(r + \frac{\Delta r}{2} - |r_j - r_i|) - \eta(r - \frac{\Delta r}{2} - |r_j - r_i|)].$$ (2.7)

Equation (2.7) is used in practice for calculating the pair correlation function of systems generated in Monte Carlo simulations. For each generated system, we find distances between particles in all pairs, bin them into a histogram, and normalize the histogram according to equation (2.7). The histogram is then further averaged over all generated systems.

Special caution should be taken in calculations of a finite system when the reference particle is closer to the edge of a surface and parts of the circle of radius r around it fall outside of the surface. Contributions of such points to the histogram should be appropriately corrected and this can be done in
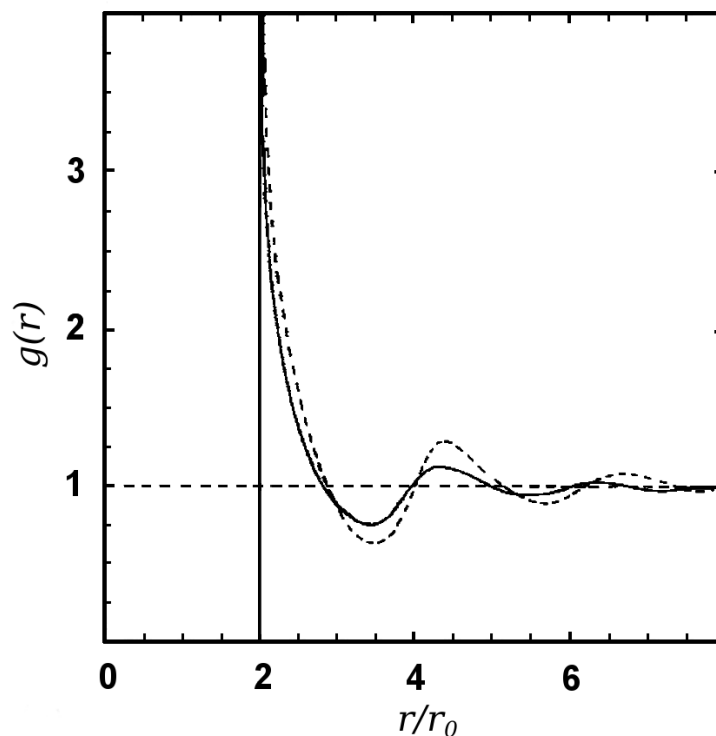
Figure 2.4: The pair correlation function for monolayers of density $\theta = 0.547$: the continuous line shows the smoothed numerical results for random monolayer and the dashed line shows the theoretical results for a 2D hard-sphere equilibrium. Figure from Adamczyk [46].

one of three ways: (i) completely disregarding those particles; (ii) calculating the part of the circle that falls into the surface, and replacing $2\pi r\Delta r$ with the surface of the truncated annulus; and (iii) using periodic boundary conditions to extend the surface area and fill in the missing part of the annulus. The latter can only be done if the periodic boundary condition has been used throughout the entire simulation and it applies to the generated configurations of a system.

In the case of a system of identical hard spheres, two particles can not be at a distance smaller than $2r_0$, hence $g(r < 2r_0) = 0$. Since there can not be correlation between two infinitely separated particles, $g(r)$ approaches 1 for $r \to \infty$. As an illustration, figure 2.4 shows the pair correlation function calculated for the RSA of identical disks on a flat continuous substrate derived from numerical simulations and theoretical results for the models of hard spheres in equilibrium [46]. Both systems are at the same density equal to the jamming coverage of the RSA system. For $r/r_0 > 5$, radial distribution function is strongly damped so that the RSA configuration looks uncorrelated (i.e., $g(r) = 1$), and it has a logarithmic divergence at contact $r = 2r_0$ [5, 48–50].

2.3 Pore distribution

Gap size distribution is widely used to characterize the structure of a straight line covered with rods [19, 51–54]. A pore is analogous to a gap in a two-dimensional system and systems of higher dimensions. Defining a pore is a challenging task in a more-than-one dimensional system where inter-particle space is connected. The Delaunay triangulation is commonly used as a geometrical tool to break apart an inter-particle space into separate pores. The size distribution of pores $P(v)$ is commonly used to characterize the structure of disordered granular packings and to quantify the structural changes during the compaction process [55–59].

Triangulation is a technique for creating a mesh of contiguous, non-overlapping triangles whose vertices belong to and exhaust a given set of points $\mathbf{P}$. By definition, a triangulation of a finite set of points on a plane $\mathbf{P} \subset \mathbf{R}^2$ is called a Delaunay triangulation if the circumcircle of every triangle is empty, that is, there are no points from $\mathbf{P}$ in its interior. A prominent characteristic of a Delaunay triangulation is that it maximizes the minimal angle of all possible triangulations, with a unique property of local equiangularity. It is also helpful in defining the nearest neighbours as two vertices of the same Delaunay triangle. An extensive review and comparison of 9 different Delaunay triangulation algorithms are given by Su and Scot Drysdale [60]. In this thesis, we used the Quickhull algorithm [61] in MATLAB® programming language to compute the Delaunay triangulation for a given set of disk centres on a plane.

By definition, the circumcircle of a Delaunay triangle is empty, i.e. it doesn't contain other points from the set. Let's view this in the context of a flat monolayer deposit of hard disks with a fixed radius r_0. The disk centres are the base set of points for a Delaunay triangulation. We single out any of the triangles and denote the radius of its circumcircle as R. Three particles of diameter r_0 lie centred on the triangle vertices, and an imaginary disk with radius $R - r_0$, concentric with the triangle circumcircle, touches all three particles (red disk in figure 2.5). These inscribed disks are the definition of inter-particle pores.

The maximum diameter of a circular pore is less than r_0 when a monolayer deposit adsorbed on

a continuous surface is in a jammed state. Otherwise, an additional particle could be adsorbed in the pore larger than r_0 which is contrary to the jammed state definition. This is not true if the substrate is patterned: even if there is enough space between adsorbed particles to fit a new particle, the second condition requires that the centre of the particle must fall within the predefined cells. This allows for bigger pores in the jammed state. On the other hand, a smart design of substrate pattern can impose a certain ordering of deposit that can lead to a denser packing of particles than the one in the case of a non-patterned substrate.

The above definition of pores has a few shortcomings. In the first place, circular pores can overlap each other. This problem can be solved by carefully excluding the smallest among overlapping pores, which is not a straightforward task in the case of overlaps of multiple pores. Another flaw of this definition is that a set of circular pores does not fill up the whole volume of the inter-particle space. To avoid these two problems, we use another definition of a pore as the part of a Delaunay triangle that is not covered by disk particles (illustrated by the striped area in figure 2.5). The advantage of these pores over the circular pores is that the former ones completely cover the inter-particle space without overlapping each other. On the other hand, a pore volume doesn't indicate if the pore is big enough to fit an additional particle and can not be used to check if the jammed state condition is satisfied even in the case of a continuous substrate.

Another analysis at the *microscopic* scale is based on the Voronoi tessellation [63]. It unambiguously decomposes any arbitrary region occupied by disks into space-filling, non-overlapping convex polygons. Formally, for any set of points **P** in a two-dimensional space, a polygonal shape surrounds each point p from the set **P** such that any point in the polygon is closer to p than to any other point
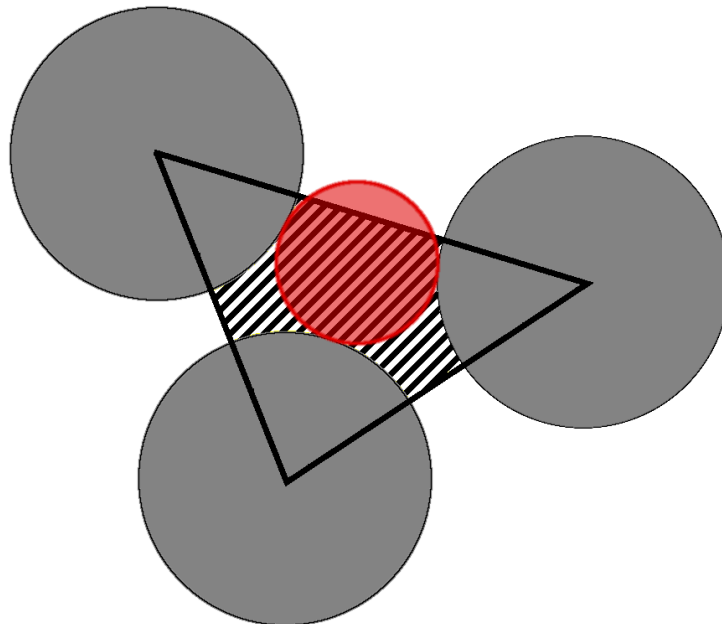
Figure 2.5: Inter-particle pore defined as (i) largest disk that is touching all three particles centred at the vertices of a Delaunay triangle (red disk); (ii) empty part of a Delaunay triangle (striped area).
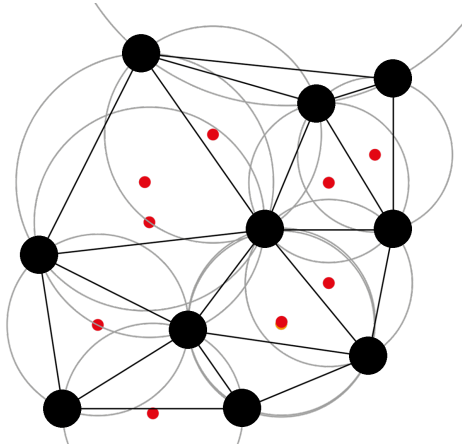
Figure 2.6: Delaunay triangulation of a set of points (black dots) with empty circumcircles and its centres marked with red dots. Figure copied from [62].
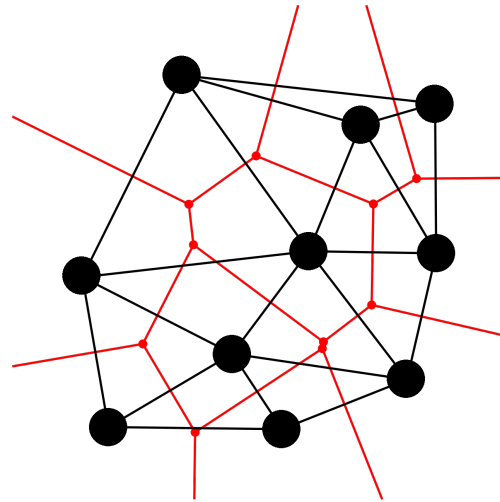
Figure 2.7: Relation between Delaunay triangulation (black lines) and Voronoi tessellation (red lines). Centres of empty circumcircles coincide with vertices of Voronoi polygons. Figure copied from [62].

from the set **P**. These polygons are known as Voronoi cells. They are convex and their edges join at trivalent vertices. Each vertex is equidistant to three neighbouring disks. Voronoi tessellation is dual to Delaunay triangulation: vertices of Voronoi polygons are centres of Delaunay empty circumcentres and edges of Voronoi polygons bisect the edges of Delaunay triangles. Two points are considered to be nearest neighbours if associated Voronoi cells are contiguous, which is equivalent to the definition of nearest neighbours given earlier in this section.

Figure 2.6 shows an example of a Delaunay triangulation for a set of 10 points, along with all empty circumcircles and their centres marked with red dots. Figure 2.7 shows a Voronoi diagram for the same set of points alongside the Delaunay triangulation. Each object (denoted by a black circle) is located in a separate polygon. Figure 2.7 also illustrates close relation between the Delaunay triangulation and Voronoi tessellation: centres of empty circumcircles coincide with the vertices of Voronoi polygons and each side of a polygon bisects one of the triangle sides.

Chapter 3

Random Sequential Adsorption model

The kinetics of an adsorption process has been mainly studied through the formulation of different models, aiming to capture the essential features of the process. Random Sequential Adsorption (RSA) is a simple model that can provide the generic features of the adsorption phenomenon in the case of a very strong interaction between particles and substrate. The adsorption process is treated as the sequential addition of particles on the substrate such that at each time step only one particle is added to the substrate at a randomly selected position. During the process of addition, newly added particles are forbidden from overlapping with the already adsorbed particles, and any attempt of adsorption that results in overlap is rejected. The adsorbed particles are permanently fixed at their spatial positions so that they affect the geometry of all later placements. Under these conditions, the system evolves rapidly toward non-equilibrium conditions, and the kinetics becomes essentially dominated by geometrical exclusion effects between particles. Evans [15] gives a thorough historical review of RSA models and their applications.

It must be stressed that the classical RSA approach can be used for modelling the kinetics of an idealized process only, consisting of the creation of particles at a given distance from the interface with a constant rate and in a consecutive manner. For particles of a sub-micrometre size range, in addition to hydrodynamic and electrostatic forces, Brownian motion significantly affects their trajectories and transport to boundary surfaces. It is not possible, within the framework of the RSA model, to find a unique relationship between the kinetics of this idealized process and the kinetics of the particle adsorption process governed by various transport mechanisms. One has, therefore, to rely on approximate models being useful for specific transport mechanisms of particles [46].

3.1 RSA on a discrete substrate

A discrete substrate represents a set of isolated adsorbing sites, restricting binding positions of particles only to those sites. A basic example of the RSA on a discrete substrate is the adsorption of monomers on a lattice when one particle binds to a single site without blocking any other sites. Eventually, all sites will be occupied, regardless of the dimensionality and lattice configuration, making the jamming density equal to 1. With the assumption that the particle flux is unitary, from

$\mathrm{d}\theta(t)/\mathrm{d}t = 1 - \theta(t)$ it is easy to calculate the time evolution of the coverage and yield that

$$\theta(t) = 1 - e^{-t}. \tag{3.1}$$

The adsorption of dimers on a lattice turns out to be a non-trivial case. A dimer is adsorbed at a random position and occupies two neighbouring sites. Two adjacent dimers can have a single isolated site between them that can never be occupied. Consequently, the jamming coverage is smaller than 1. Jamming coverage of a one-dimensional case was first calculated by Flory [17]. He studied the condensation of pairs of consecutive substituents X of a polymer composed of -CH$_2$-CHX-, and found that fraction of unreacted groups equals e^{-2} and the jamming coverage equals $1 - e^{-2} \approx 0.8647$. The asymptotic approach to jamming limit retains the exponential form in the case of the infinitely long lattice.

Adsorption of dimers on a 2D square lattice was the subject of several studies [64–66]. Although it can't be solved analytically, numerous approximations and numerical calculations showed that $\theta_J = 0.9068$ [65]. Vette et al. [66] studied dimers filling on triangular, square and hexagonal lattices. Further studies of adsorption of k-mers on 2D lattices concluded that in lattice RSA models [27, 67–69], the approach of the coverage fraction $\theta(t)$ to its jamming limit θ_J is given by the time dependence:

$$\theta_J - \theta(t) \sim \exp(-t/\sigma), \tag{3.2}$$

where parameter σ depends on the orientational freedom of depositing objects, and on the dimensionality of the substrate [68, 69].

3.2 RSA on a continuous substrate

When the adsorbing particles, such as proteins or colloids, are much larger than the structural details of the substrate surface, the surface can be considered continuous on a mesoscopic scale and the adsorption of particles is an off-lattice process. The one-dimensional case of the RSA of equal rods on a continuous line is known as Renyi's car parking problem after the Hungarian mathematician. He was the first to propose and solve this model [18]. The calculated jamming coverage ($\theta_J = 0.7476...$) is significantly lower than the close packing coverage which equals 1. Late time approach to the jamming limit displays power-law behavior $\theta_J - \theta(t) \sim t^{-1}$. The pair correlation function at long distances behaves super-exponentially, unlike equilibrium systems with characteristic exponential decay [70].

Feder [5] calculated the jamming coverage of disks on a flat plane to be approximately equal to 0.547. He used numerical simulations to show that the asymptotic approach of coverage to its jamming limit obeys the power-law t^{-p} with exponent $p \approx -1/2$. Pomeau [50] proposed that the exponent p equals $1/D$ where D is the dimensionality of a system. Swendsen [49] pointed to a geometrical argument which predicts that a late-stage asymptotic approach of coverage for spheroids obeys the power-law

$$\theta_J - \theta(t) \sim t^{-1/D}, \tag{3.3}$$

where D is the dimensionality of the system. For aligned squares, the power-law relation is modified by a logarithmic factor. The same arguments were used to show that the pair correlation function in the jammed state diverges logarithmically at contact.

Relation 3.3 was numerically and analytically confirmed by many investigators [5, 36, 49, 50, 71]. Swendsen's arguments initially appeared to be valid for any particle shape, but soon it was proven by numerical calculations that even though the power-law is universal for various shapes (spherocylinders, ellipses, rectangles, and needles) and elongations, the value of the exponent varies depending not only on the dimensionality but on the number of degrees of freedom [20–22, 25, 26, 29, 48]. Viot et al. [29] showed that two critical regimes exist in the late stage of the process in the limit of very small elongations of various objects. In the first regime, the asymptotic approach obeys Feder's law, $t^{-1/2}$, and it is directly followed by a regime in which $t^{-1/3}$ law is obeyed. They found that the time when the crossover occurs is directly linked to the parameter that measures the anisotropy of adsorbing particles.

3.3 RSA on a patterned substrate

Although the basic RSA model may accurately reproduce many experimental situations, its extension to more complex surfaces having an intrinsic structure is by no means trivial. For example, the supporting surface may be pre-patterned with preferential sites for specific particle attachments, which alters the kinetics of the process and the structure of the adsorbed layer. With the use of photo-lithographic techniques, high-power lasers, chemical treatments, etc., such surface modifications are routinely realized on the micro-scale, or even on the nano-scale [72–75].

There is well-developed literature on irreversible adsorption of various types of two-dimensional (2D) patterned surfaces [13, 41, 43, 45, 76–80]. Historically, Jin et al. [41] were the first to study pre-patterned substrates in a model of irreversible deposition on a random site surface (RSS) where the sites are represented by randomly distributed points. Their work was motivated by affinity chromatography in which ligands are fixed on the adsorbent surface and the desired solute (or a class of solutes) can attach only to those ligands. They found a remarkable, yet simple mapping between elapsed time of the adsorption on a continuous surface τ and on a random site surface t, given through relation

$$\tau = \alpha(1 - e^{-t/\alpha}),\qquad(3.4)$$

where α is an average number of adsorbing sites per surface unit. This mapping is valid in any dimension, but it is applicable only if adsorbing sites are randomly distributed.

The random-site model is only suitable if the size of ligands is much smaller than the size of adsorbing particles. The finite size of ligands will result in arrangements that are not strictly random, and the mapping given by the equation (3.4) is inapplicable. Adamczyk *et al.* [43, 44] have extended the RSS model to the situation where the size of the landing sites is finite and comparable with the size of adsorbing spheres. They explored two cases of the ligand shape: circular disks and spherically shaped sites (see figure 3.1). They concluded that in the case of circular disks, Jin's mapping holds if the disk radius is at least ten times smaller than the particle radius, but when its radius exceeds 20% of the particle radius, the behaviour radically differs from the RSS model. Their results prove that the spherically shaped sites are much more effective in binding particles than the disk-shaped sites.

Araújo et al. [45] have investigated the adsorption of disk-shaped particles on a patterned substrate that consists of equal square cells centred at the vertices of a square lattice. They investigated the
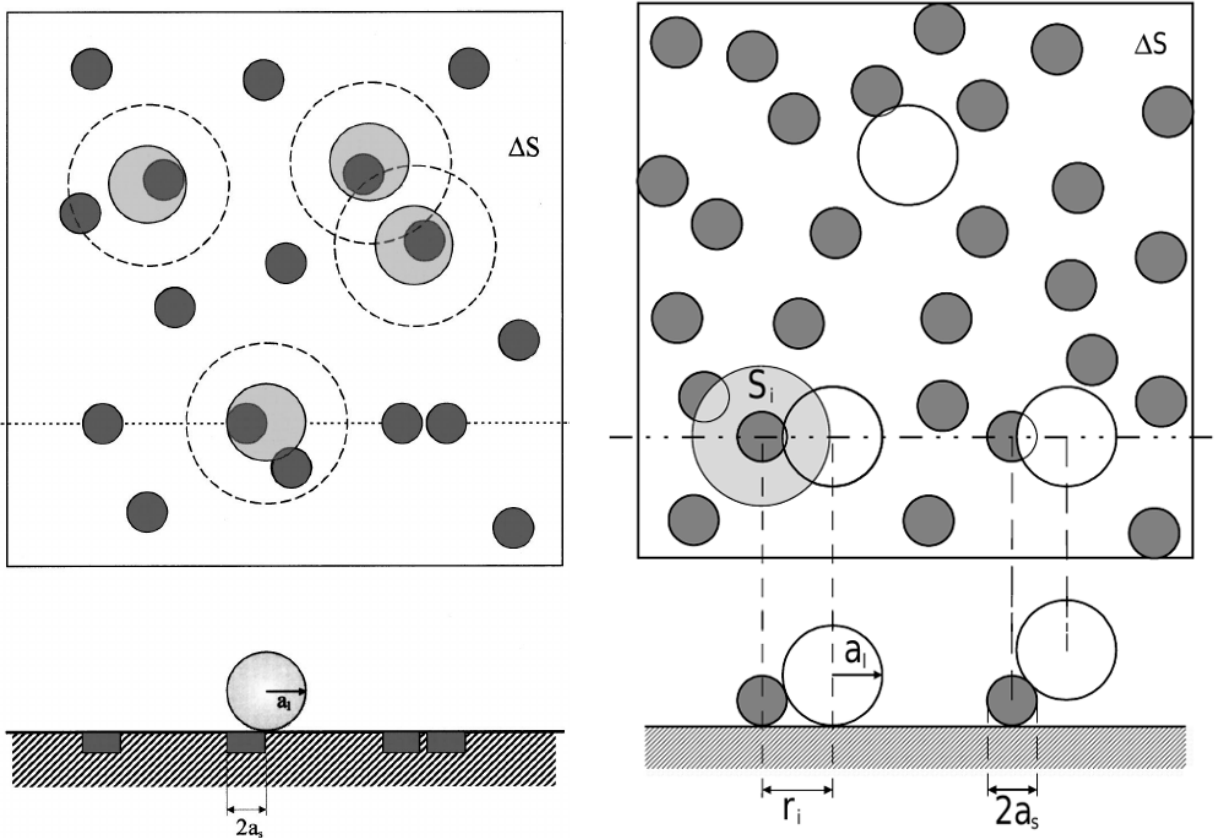
Figure 3.1: A schematic representation of particle adsorption over heterogeneous surfaces bearing disk-shaped (left) and spherically shaped (right) adsorption sites [43, 44]

phase space of parameters α and β which stand for the size of the square cell side and the cell-cell separation, respectively, measured in units of adsorbing particle diameter (see figure 3.2). Based on the size of the square cell α, one can discriminate between a *single-particle per cell* (SPPC) and a *multiple particles per cell* (MPPC) regime. SPPC regime is in force for $\alpha < \sqrt{2}/2$ when at most single particle can be adsorbed on any cell. Another division is based on the measure of the cell-cell separation β. If β is greater than 1, the blocked area of a particle attached to a cell can't reach any other cells and this mode is named *non-interacting cell-cell adsorption*. The *interacting cell-cell adsorption* regime requires that β is less than 1. The phase diagram is illustrated in figure 3.3. The main focus of the work of Araújo et al. [45] was on the morphology of the jammed state. The ordering effect of the substrate competes with the randomness in particle positions and excluded volumes, yielding a variety of deposit morphologies: lattice-like, locally homogeneous or locally ordered.

In addition, Araújo [81] has discussed the influence of the pattern on the adsorption kinetics. He has pointed out that time evolution towards the jammed state can be consistent with exponential or power-law behaviour, depending on the geometry of the pattern. Marques et al. [13] studied the effect of the presence of a regular substrate pattern and particle polydispersity on the deposit morphology and density, as well as on the in-cell particle population.
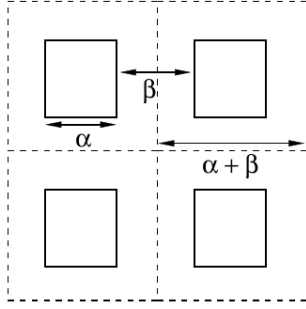
Figure 3.2: Landing sites are squares of size αr_0, with centres positioned at square lattice with lattice constant $(\alpha + \beta)r_0$ [45].
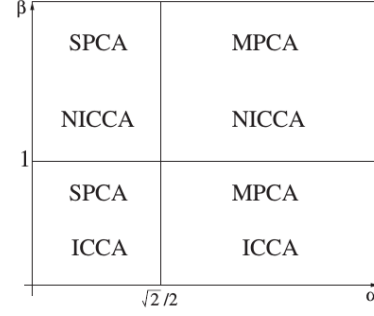
Figure 3.3: Phase diagram in (α, β) space, separating interacting from non-interacting cell-cell adsorption, and single particle per cell from multiple particle per cell mode [45].

3.4 RSA on a patterned straight line

Understanding the kinetics of a model of RSA on a patterned substrate relies heavily on numerical simulations. However, analytical tools can be used to study cases of one-dimensional substrates. In [1] and [2] authors studied the adsorption on an imprecise lattice and identified regions of different types of convergence to jamming that form a repeating pattern in the phase space of model parameters. Bonnier et al. [42] studied the adsorption of dimers on a dashed line, a model that is equivalent to a special case of the adsorption on an imprecise lattice, studied in [2]. Both papers report that there are four types of an asymptotic approach to the jamming limit: continuous-like algebraic, anomalous algebraic, lattice-like exponential and modified exponential. In this subsection, we outline their main arguments and results.

The late-stage asymptotic behaviour of the RSA on a continuous surface is explained using the assumption that there exists a moment t_a after which predominant adsorptions of new particles happen at holes small enough to fit only one particle [49, 50]. The presence of larger holes is negligible and the probability that a new hole is created after the moment t_a equals zero. The probability $n(h; t > t_a)$ that a small hole gets filled is proportional to its size $a \sim h^d$, where h is the characteristic linear dimension of a hole and d is the system dimensionality. Therefore, the hole size distribution declines exponentially with time:

$$n(h; t > t_a) = n(h; t_a)e^{-Rh^d t}. \tag{3.5}$$

Difference between the jamming coverage and the coverage at any instant t after the moment t_a is given by:

$$\begin{aligned}
\Delta\theta(t) = \theta_J - \theta(t) &= A \int_0^{h_{max}} n(h; t)\, \mathrm{d}h \\
&= A \int_0^{h_{max}} n(h; t_a)e^{-Rh^d t}\, \mathrm{d}h,
\end{aligned} \tag{3.6}$$

where A is the area of a single particle projection onto the substrate.
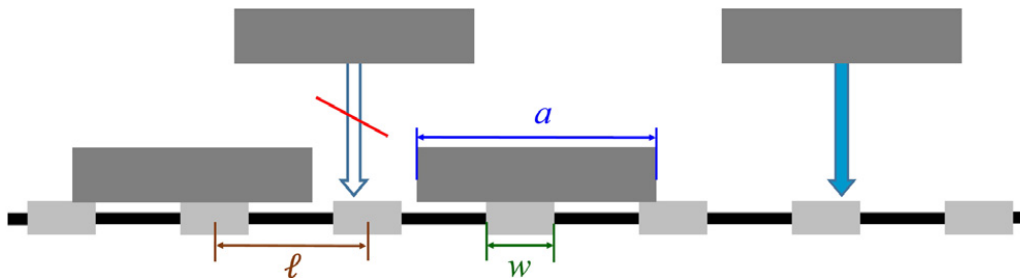
Figure 3.4: Random sequential adsorption of segments on imprecise lattice [1, 2].

The form of the hole size distribution in the small hole limit at moment t_a is crucial for determining the type of asymptotic approach. Pomeau [50] and Swendsen [49] assumed that $n(h \to 0, t_a)$ is finite and that it can be approximated by a constant in the range of interest $h \in [0, h_{max}]$. As a result of this assumption, the asymptotic approach to the jamming coverage is algebraic $\Delta\theta(t) \sim t^{-1/d}$ for spheroid particles in d-dimensional space and it has the form of $\Delta\theta(t) \sim t^{-1}(\ln t)^{d-1}$ for aligned hyper-cubes [49]. Other forms of hole size distribution $n(h \to 0, t_a)$ appear in models of RSA on patterned substrates, leading to different asymptotic approaches [2]. This includes cases where it is impossible to have holes smaller than a threshold h_{min}, i.e. $n(h < h_{min}, t_a) \equiv 0$. Accordingly, the small hole size distribution of interest is in the limit of h slightly larger than the threshold h_{min}, i.e. $n(h \to h_{min}^+, t_a)$.

Privman and Yan [1] and Verma and Privman [2] numerically explored the model of adsorption on a one-dimensional imprecise lattice. Particles of size a can attach to the substrate if their centres fall on a lattice site that is symmetrically broadened around the lattice site position without overlapping previously adsorbed particles (see figure 3.4). The size of a broadened site is w, while the lattice constant is l. The authors identified regions of different convergence types in the phase space of scaled parameters of the model, $(w/l, a/l)$, based on the numerical analysis of the hole size distribution in a late stage of the process. Rectangular blocks of phase space that lie between $w/l \in [0, 1]$ and $a/l \in (k-1, k)$, where $k = 1, 2, 3...$, are identical in terms of the late-stage asymptotic behavior. A representative block of the phase diagram for $k = 2$ is presented in figure 3.5. The authors identified the following regions with different forms of small hole size distribution, yielding different types of convergence to jamming:
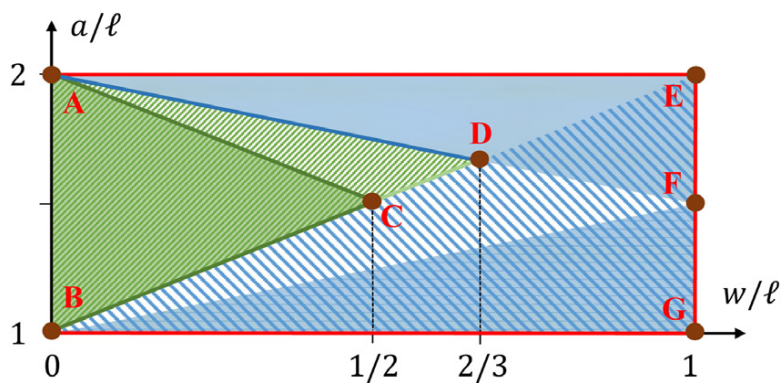
Figure 3.5: Different regions of convergence to jamming as described in the text [2].

(i) Triangle **ABC**, including edges, excluding point **B**: exponential convergence, exact (k)-mer on a lattice adsorption dynamics
$$n(h, t_a) \sim \delta(h - w) \implies \Delta\theta(t) \sim e^{-Rt}$$

(ii) Pentagon **ADBGE**, excluding edges: algebraic convergence
$$n(h \to 0, t_a) \sim const. \implies \Delta\theta(t) \sim 1/t$$

(iii) Lines **(AE)**, **[EG]** and **[GB]**: exact car parking solution
$$n(h \to 0, t_a) \sim const. \implies \Delta\theta(t) \sim 1/t$$

(iv) Triangle **ACD**, including edge **(CD)** and excluding edges **[AC]** and **[AD]**: modified exponential convergence
$$n(h \to h_{min}^+, t_a) \sim const. \text{ and } n(h < h_{min}, t_a) = 0 \implies \Delta\theta(t) \sim e^{-\Phi h_{min} t}/t$$

(v) Line **(AD)**: anomalous algebraic convergence
$$n(h \to 0, t_a) \sim h \implies \Delta\theta(t) \sim 1/t^2$$

Bonnier et al. [42] studied the following model: point-like adsorbing sites lie on a straight line at a distance l apart from each other and rods of length r are sequentially adsorbed at a random position on a line if they cover exactly one adsorbing site without overlapping any of the previously adsorbed rods. They pointed out that this model is equivalent to the RSA of dimers of length $d + r$ on extended adsorption sites of size l, with distance d between every two adjacent sites. Adsorption occurs if both ends of a dimer fall on two adjacent sites without overlapping each other. Depending on the ratio r/l, asymptotic approach to the jamming coverage is similar to the normal continuous case $(\Delta\theta(t) = A/t)$ if $r/l \in (2/3, 3/2)$, to the monomer adsorption on a lattice if $r/l \in (0, 1/2]$ or to the dimer adsorption on a lattice if $r/l \in [3/2, 2)$ $(\Delta\theta(t) = \exp(-\sigma t))$. In addition to the two usual late-stage approaches to jamming (algebraic and exponential), authors identified and termed asymptotic behaviour for $r/l \in (1/2, 2/3)$ as non-trivial lattice dynamics given by

$$\Delta\theta(t) = \exp(-\sigma t)/t^2. \tag{3.7}$$

and for $r/l = 2/3$ they found anomalous continuous dynamics:

$$\Delta\theta(t) = A/t^2. \tag{3.8}$$

We recognized that Bonnier's model is equivalent to a special case of the RSA on an imprecise lattice, the model studied in [1, 2]. In the first model, a line segment of length r sticks to the surface if it falls over exactly one localized site. In the second model, a line segment of length a will stick to an empty surface if its centre projection falls within an extended site of width w. To find the mapping of parameters between the two models let's look at the possible positions of the segment centre relative to the corresponding adsorbing site (for illustration see figure 3.6). We distinguish between two different cases:

- $r < l$: when segment size r is smaller than the distance between two adjacent sites l, its centre can be as far as $r/2$ to the left or right from the adsorbing site. This means that the extended site width is $w = r$;

Figure 3.6: Illustration of equivalency of two models: (I) deposition of segments on localized adsorbing sites and (II) deposition of particles on extended lattice sites. On the left is a case of $r < l$ and on the right a case of $l < r < 2l$.

- $l < r < 2l$: when segment size r is larger than the distance between two adjacent sites l, its centre can be as far as $l - r/2$ to the left or right from the adsorbing site due to the limitation that it can cover only one site. This means that the extended site width is $w = 2l - r$.

Non-overlapping conditions in two models are mutually consistent only if the length of the segment in the first model is equal to the length of the segment in the second model, i.e. $r = a$. Therefore, the first part of the phase space that Bonnier studied, having $0 < r < l$, corresponds exactly to a line $a = w$ in the first quadrant of Verma's phase diagram (matching the line **B**-**C**-**D**-**E** in figure 3.5). The second part, where $l < r < 2l$, corresponds exactly to the line $a = 2l - w$ in the second quadrant (line **G**-**C**-**A**).

There is a discrepancy between the results of the two studies [2] and [42] regarding the convergence to the jamming in the range of $r \in (1/2, 2/3)$ which corresponds to a copy of the line **(CD)** in the first quadrant of the phase diagram (figure 3.5). Analytical study presented in [42] claims that asymptotic approach in this region has the form $\Delta\theta(t) = \exp(-\sigma t)/t^2$. Numerical analysis in [2] suggests the form $\Delta\theta(t) = \exp(-\sigma t)/t$. The authors presented only results for the second quadrant, but they claim that the results they obtained for the first quadrant are qualitatively the same. The quadratic correction to the exponential approach that Bonnier et al. [42] predict would result from a small hole size distribution that linearly vanishes at a non-zero threshold h_{min}. This type of distribution was not found by Verma and Privman [2]. The conclusions regarding the convergence to jamming in other segments are in complete agreement, with emphasis on point **D** ($w = r = 2l/3$) where the anomalous algebraic approach is found: $\Delta\theta(t) \sim 1/t^2$. We will come back to this in section 6.2 where we find similar anomalous convergence for RSA on a two-dimensional imprecise lattice.

Chapter 4

Numerical simulation

Manipulation of the substrate pattern can yield monolayer deposits with desired properties. Our goal is to investigate the influence of substrate inhomogeneities on the coverage growth rate and the geometry of the final (jammed) state. In two-dimensional systems, it is possible to make some conjectures and reasonable ad hoc arguments to predict asymptotic behaviours, but for most practical purposes we turn to numerical simulations that are based on the Monte Carlo method. We developed a small C++ library to create and position landing cells and particles of various shapes and sizes and investigate relations between them. Using this library we easily created applications that simulated the process of random sequential adsorption of particles on a flat 2D pre-patterned substrate.

4.1 Monte Carlo method

The Monte Carlo method relies on random numbers, probability theory and statistics to estimate the probability of possible outcomes of an uncertain event. It is heavily exploited for numerical calculations of analytically unsolvable problems or problems with a large number of degrees of freedom in physics, mathematics, economy, finance, engineering, etc. It is used to estimate the solution of problems that are deterministic, as well as for predicting the outcomes of problems with inherently uncertain input variables. We used the Monte Carlo method in our simulation and estimated values of interest by averaging over a large number of generated RSA configurations.

Randomness is essential in our analysis, not just because we use the Monte Carlo method: the R in the RSA abbreviation stands for the word *random*. Adsorption of every particle is attempted at a randomly chosen position. This is why it was very important to use a good random number generator, capable of providing a large number of long, reproducible, unique, and independent streams of random numbers. It is time-consuming and expensive to obtain true random numbers in large quantities and numerical simulations often rely on a pseudo-random number generator. Our choice was the SPRNG library, available for FORTRAN and C/C++ programming languages. It provides high-quality pseudo-random numbers in a computationally inexpensive and scalable manner, reproducible streams of parallel pseudo-random numbers, independent of the number of processors used in the computation and of the loading produced by sharing of the parallel computer and allows for the cre-

ation of unique pseudo-random number streams on a parallel machine with minimal inter-processor communication [82]. Out of 6 available SPRNG generators, we opted for Combined Multiple Recursive Generator (CMRG) because of the good speed/quality ratio in regard to our use case. The period of this generator is around 2^{219}. The number of distinct streams available is over 10^8. It ensures that for a given fixed seed, each one of N total streams is independent of and uncorrelated to any other stream. To clarify, by stream we mean a unique sequence of random numbers generated by a given generator. We used the SPRNG library, version 4.4, in all of our simulations.

4.2 Simulation of Random Sequential Adsorption on patterned substrates

We study irreversible monolayer deposition of identical spherical particles with hard-core exclusion on a prepared flat nonuniform substrate. The substrate heterogeneities are represented by identical non-overlapping rectangular cells that are fixed on the substrate surface. The basic assumption of our model is that a particle can only be adsorbed if it is in contact with one of the cells, i.e. if the centre of its disk-shaped projection lies within one of the rectangles. The substrate can be prepared in many ways by arranging the rectangles to form different patterns. In this thesis, we are particularly interested in two types of patterns: (i) Random pattern, formed by RSA deposition of square or rectangular cells, arbitrary oriented or aligned, and (ii) square lattice pattern, formed by square cells with midpoints at the vertices of a square lattice and with sides parallel to the lattice main axes. The non-overlapping condition for cells is in force in both cases. Consequently, in the case of a square lattice pattern, the distance between cell centres (lattice constant) must be greater than the cell sides.

In our study, the radius of depositing particles is fixed and comparable with the typical geometrical cell length. Moreover, we assume that the size of the particles is much larger than the length scale between binding sites so that adsorption over the length scale of cell linear dimensions can be regarded as an off-lattice process.

Our model forbids the deposited particles to diffuse along or desorb from the substrate on the time scale of the dense coverage formation. This means that adsorbed particles are permanently fixed to their spatial positions. The deposit growth rate depends on a flux of incoming particles, and for all of our purposes, we considered that this flux is uniform and at a constant rate. To reduce the effects of a finite substrate, we use periodic boundary conditions in both directions. These assumptions are typical of the RSA model.

The entire simulation procedure consists of three main stages:

1. Initialization:

   Simulation parameters are set in accordance with provided input arguments.

2. Substrate preparation:

   Identical rectangle cells are positioned over the simulation area to form a selected type of pattern, with respect to the input parameters. Upon completion of this phase, the substrate is completely prepared and stays unchanged through the rest of the simulation.

3. Deposit formation:

    An attempt of single-particle deposition is repeated in a loop. The deposition attempt starts by generating a random position of a test particle within the simulation area. Next, we check if the disk's centre falls outside of all landing cells and if it overlaps any of the previously adsorbed disks. The disk deposition attempt fails if any of these two checks are true. If the deposition attempt is successful, the particle becomes a permanent part of the deposit at its fixed position.

Simulation input parameters are following: particle radius $r_0 = d_0/2$, cell sides α and $\kappa\alpha$, cell coverage $\theta_0^{(cell)}$ (for random pattern) or lattice constant $\gamma = \alpha + \beta$ (for regular substrate), substrate size L, maximum number of adsorption attempts N_{max}, maximum number of failed adsorption attempts N_{idle}, and random number generator initialization parameters (seed, stream ordinal number and total number of streams). Simulation outputs the particle position and the ordinal number of deposition attempts for every successful adsorption. The ordinal number is converted to time as explained later in section 4.3.

Formations of random and regular patterns in the simulation are governed by different rules and sets of parameters, and both of them are individually described in the sections that follow. While for a random pattern we have to prepare substrate differently for every run, a regular pattern is always the same for the same parameters.

4.2.1 Preparation of randomly patterned substrate

At the start, the simulation substrate surface is an empty flat square area of size $L \times L$. We used $L = 256d_0$, as this value gave us sufficient precision in the available amount of computer time. Substrate preparation starts by performing the basic RSA algorithm with rectangular cells: a cell is randomly positioned at the substrate, and it is permanently attached to the surface if it doesn't overlap any of the previously adsorbed cells. If an overlap occurs, the adsorption of the cell is rejected. New adsorption attempts are repeated in the same way, up to the point when we reach the desired coverage fraction. This coverage must be smaller than the jamming coverage for landing cells ($\theta_0^{(cell)} \leq \theta_J^{(cell)}$). In this way, we can prepare randomly patterned heterogeneous substrate with a statistically reproducible density $\theta_0^{(cell)}$.

In the random pattern model, each landing cell is a rectangle with sides a and κa ($\kappa \leq 1$) whose midpoint is located on a continuous substrate. The cells can take arbitrary orientations, but in some numerical simulations, we introduced alignment in the deposition procedure for landing cells. This simple modification introduces a preferential direction in the deposition process and, depending on the aspect ratio of deposited rectangles, imposes specific "patterning" on the deposited layer. We re-scale the lengths relative to the diameter of the disks d_0, and define three dimensionless parameters:

$$\alpha = \frac{a}{2r_0}, \quad \lambda = \frac{a}{\kappa a} \tag{4.1}$$

$$\gamma = \frac{\alpha}{\sqrt{\theta_0^{(cell)}}} \tag{4.2}$$

The parameter γ (an average distance between cell centres) is a meaningful measure only if the landing cells are squares ($\lambda = 1$).

25

For a few fixed pairs of values of parameters α and λ, simulations were carried out for various values of $\theta_0^{(\text{cell})}$, ranging from 0.10 to 0.50. For each case, the simulations are carried out up to 10^{10} deposition attempts, or up until $L^2 \times 10^4$ consecutive deposition attempts are rejected. The results are obtained by averaging over 100 simulation runs.

4.2.2 Preparation of regularly patterned substrate

We investigated a regular pattern that consists of square cells whose midpoints are positioned in the nodes of a regular square lattice. Cell sides are parallel to the main axes of the lattice. The geometry of the regular pattern is controlled by the two dimensionless parameters, α and β, measured in terms of the particle diameter $d_0 = 2r_0$. Parameter α is the cell side size, and parameter β is the shortest distance between the parallel sides of the nearest neighbouring cells. The distance between neighbouring cell midpoints is $\gamma = \alpha + \beta$. We considered only configurations in which cells do not overlap each other ($\beta > 0$). The case of $\beta = 0$ is equivalent to a homogeneous substrate for all values of α. Cases where cells can accommodate one particle at most ($\alpha < \sqrt{2}/2$) and cell-cell separation is larger than the particle diameter ($\beta > 1$) are equivalent to the lattice site adsorption in regard to kinetics.

One or more disks can attach to each cell depending on the cell size α. For $\alpha < 1/\sqrt{2} \approx 0.707$, at most a single disk can be adsorbed at any given square cell. We denote this case as single-particle per-cell adsorption (SPCA). For squares with $\alpha \geq 1/\sqrt{2}$, more than a single disk can be placed in the square cell, and we denote this as multi-particle per-cell adsorption (MPCA). If distances between neighbouring cells are smaller than particle diameter ($\beta < 1$), a disk attempting adsorption on a given cell can overlap with a previously adsorbed one belonging to a neighbouring cell, resulting in a failed adsorption attempt. This excluded volume "interaction" between particles during adsorption at *different* cells affects the overall structure of the adsorbed layer and causes a slower asymptotic approach of the coverage fraction $\theta(t)$ to its jamming limit [45, 83]. Such regime is denoted *interacting cell-cell adsorption* (ICCA). For $\beta \geq 1$, disks attempting adsorption cannot overlap other disks in neighbouring cells, yielding the *non-interacting cell-cell adsorption* regime (NICCA). Deposition kinetics in the regime of NICCA is completely determined by the kinetics of adsorption of particles on a finite-size substrate (a single cell) with appropriate boundary conditions [45, 83].

We performed the Monte Carlo simulations on a planar substrate with typically 256×256 landing cells. Some cases of landing-cell configurations required more precise measurements and we had to increase the size of the substrate to 1024×1024. We also needed to increase the number of average adsorption attempts per cell, which resulted in a longer simulation execution time.

4.2.3 Particle deposition

After the substrate is prepared, we start the RSA process for identical spherical particles of diameter d_0. Since the adsorption was only possible within the landing cells, we optimized the simulation accordingly. Adsorption attempts were only made within the randomly selected cell. We omit out-of-cell adsorption attempts and therefore testing whether particle fell on the cell becomes redundant. To make up for this omission we have to scale the time step between consecutive attempts by the factor

(total area)/(total cell area). We generate and position particles, one by one, within a randomly chosen landing cell, and then test if they do not overlap previously adsorbed particles. If the condition is met, the test particle becomes a permanent part of the deposit.

The adsorption attempts are repeated until we reach the jammed state, where only gaps too small to accommodate new particles are left on the cells. In some cases, it can take a very long time to fill in every single gap. For practical reasons, we modified the simulation termination condition. The simulation ends when a given total number of attempts is reached or when a number of consecutive failed attempts exceeds the given maximum idle time. These two numbers are given as input parameters to the simulation at run-time, and they differ depending on the system size and parameters. In the case of single-particle per cell, an additional condition is given: simulation can end when every cell in the substrate adsorbs a particle. Note that this condition can never be met for some pattern configurations.

4.3   Time scaling and optimizations

The dimensionless adsorption time t is set to zero at the beginning of the second stage. It is then gradually increased by an increment Δt, given by $\Delta t = \pi r_0^2 / L^2$, each time an attempt is made to deposit a disk of radius $r_0 = d_0/2$ on a square surface (collector) of area L^2. Consequently, we define dimensionless adsorption time $t = N_{att} \pi r_0^2 / L^2$, where N_{att} is the overall number of attempts to place disk particles. By plotting coverage $\theta(t)$ versus the adsorption time t, defined above, one can simulate the kinetics of particle adsorption.

To optimize the computing time in the case of a regular pattern, deposition is attempted only inside the cells. We chose a random cell and attempt to deposit a particle at a random position within that cell. This optimization affects time scaling, so that the time increment can be calculated as $\Delta t = \frac{\pi r_0^2}{L^2} \frac{(\alpha + \beta)^2}{\alpha^2}$. In some cases, we wanted to reach very large times which required further optimizations of our calculations. When cells are small enough and can be occupied by one particle at most, we try to achieve the deposition events only in free cells. Then, the time t is increased after every deposition attempt by an increment $\Delta t = \frac{\pi r_0^2}{N_{free}} \frac{(\alpha + \beta)^2}{\alpha^2}$, where N_{free} is the number of free cells. These optimizations do not affect typical jammed state configurations nor the statistically averaged value of $\theta(t)$. However, the standard deviation of $\theta(t)$ is significantly reduced.

Chapter 5

Randomly patterned substrates

This chapter explores the effect of the presence of randomly patterned substrate on the structural properties of the jammed state of the monolayer deposit. Heterogeneities of a substrate impose further limitations on the positions of adsorbed particles. We consider the irreversible deposition of disks of a fixed diameter d_0 whose centres must fall inside one of the cells arranged at the surface. For simplicity, we will use the length scale in which $d_0 = 1$ throughout the whole chapter. The cells are positioned in a prior, independent RSA process, conducted until the desired cell density $\theta_0^{(cell)}$ is reached. Following the rules of RSA, cells do not overlap each other and they are permanently fixed to their spatial positions. A prepared substrate surface stays unaltered throughout the disk deposition process.

In the first part of this chapter, we present and discuss the results of numerical simulation for random deposition of identical disks on pre-patterned substrates covered by randomly positioned squares of arbitrary orientation. We characterize the jammed state in terms of the radial distribution function of the particle centres and the distribution of the Delaunay "free" volumes. In addition, we compare the impact of a regular vs. random pattern on the deposit structure. The second part of this chapter is devoted to the analysis of the adsorption of disks on randomly positioned rectangular cells deposited with arbitrary and fixed orientations.

5.1   Square cells

We are interested in the adsorption of disks on substrates prepared by random sequential adsorption of identical square cells of arbitrary orientation. The cell size α determines how many particles can attach to a cell, provided that the attachment condition is that a particle centre lies inside of the cell. We investigate the cells whose size is comparable with the size of adsorbing particles, and the number of disks adsorbed per cell is a small number (less than five). With α_k we denote the largest size of a square that can fit at most k disks. For $\alpha < \alpha_1 = 1/\sqrt{2}$, at most one disk can be adsorbed at any given square cell. We denote this case as single-particle per-cell adsorption (SPCA). More than one disk can be placed in the square cell if $\alpha \geq 1/\sqrt{2}$, and we denote this as multi-particle per-cell adsorption (MPCA). The cases of up-to-two, -three and -four disks per square cell are obtained, respectively, for
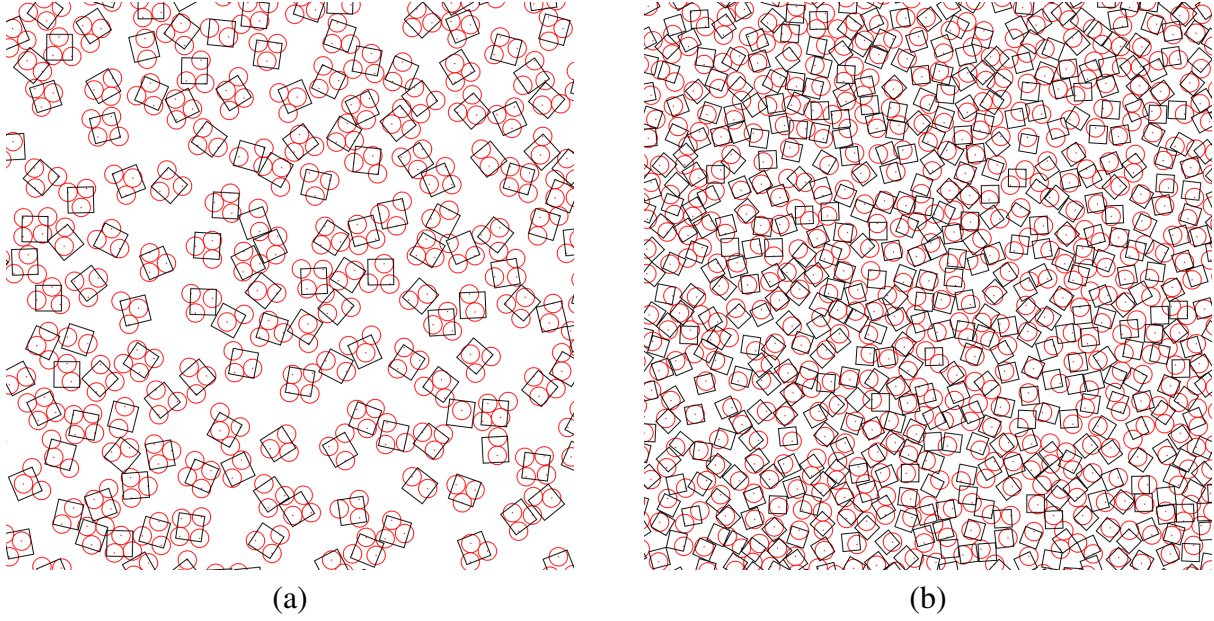
Figure 5.1: Typical jammed-state configuration of a region of size 30×30 in units of the disk diameter d_0, for (a) $\theta_0^{(\text{cell})} = 0.3$, $\alpha_4 = \sqrt{2} \approx 1.41$, and (b) $\theta_0^{(\text{cell})} = 0.5$, $\alpha_2 = (1 + \sqrt{3})/(2\sqrt{2}) \approx 0.966$.

α smaller than $\alpha_2 = (1 + \sqrt{3})/(2\sqrt{2}) \approx 0.966$, $\alpha_3 = 1$ and $\alpha_4 = \sqrt{2}$.

The effect of density of landing cells $\theta_0^{(\text{cell})}$ on the adsorption process is illustrated in figure 5.1 by snapshots of the jammed-state coverings for (a) $\theta_0^{(\text{cell})} = 0.3$ and (b) $\theta_0^{(\text{cell})} = 0.5$, for two values of the cell size α, namely, $\alpha_4 = \sqrt{2} \approx 1.41$ [figure 5.1(a)] and $\alpha_2 = (1 + \sqrt{3})/(2\sqrt{2}) \approx 0.966$ [figure 5.1(b)]. For low values of $\theta_0^{(\text{cell})}$, adsorption on a given cell is weakly affected by disks previously adsorbed on neighboring cells. Therefore, most of the cells shown in figure 5.1(a) contain at least three discs. However, in the case shown in figure 5.1(b) one can see a significant impact of the cell-cell excluded volume interaction on the cell population. Although each cell has enough area to accommodate up to two disks, only one disk is attached to the majority of the cells.

5.1.1   Adsorption on low cell density substrate

In the low limit of cell density $\theta_0^{(cell)} \to 0$, the average distance between two cells is much larger than the diameter of a disk. It is very rare that a particle from one cell can block the available space in another cell. This limit is called the non-interacting mode in which the cell-cell interactions are negligible. The adsorption kinetics is then equivalent to the adsorption kinetics on a single cell if time is appropriately scaled to account for the low cell density. The jamming limit is also dictated by the RSA on a single cell:

$$\theta_J = \frac{\langle n(\alpha) \rangle \pi \theta_0^{(cell)}}{4\alpha^2}, \tag{5.1}$$

where $\langle n(\alpha) \rangle$ is the average number of disks on a single jammed cell, attached in a RSA process. Equation (5.1) estimates the jamming density well for sufficiently low cell densities $\theta_0^{(\text{cell})} \lesssim 0.2$.
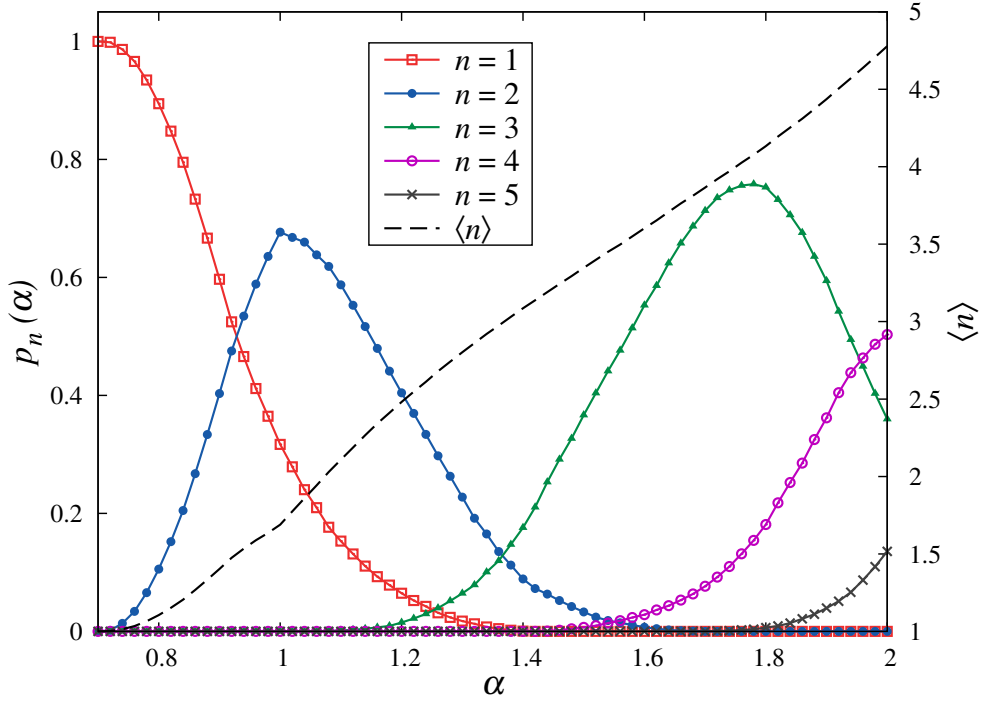
Figure 5.2: Simulation results for the probability that the configurations with $n = 1, 2, \ldots, 5$ disks occur on square cell of size α in the non-interacting cell-cell adsorption regime (left-hand axis). The dashed line is plotted against the right-hand axis and gives the simulation results for the average number of particles per cell $\langle n \rangle$ as a function of the cell size α in the non-interacting cell-cell adsorption regime.

The dashed (black) line in figure 5.2 shows the simulation results for the mean number of particles per cell $\langle n(\alpha) \rangle$ as a function of cell size α in the non-interacting cell-cell adsorption regime (i.e., in the case of single-cell on a substrate). In addition, in figure 5.2 we show the probabilities that the jammed square cell of size α captures $n = 1, \ldots, 5$ disks in the non-interacting cell-cell adsorption regime. If $\alpha = \alpha_1 \approx 0.707$, each landing cell (square) can contain no more than one disk. If $\alpha = \alpha_2 \approx 0.966$, the number of cells with one and two disks is approximately equal and $\langle n(\alpha_2) \rangle \lesssim 1.6$. However, if density $\theta_0^{(cell)}$ is constant, then the increase of the cell size $\alpha_1 \to \alpha_2$ reduces the total number of landing cells on the substrate by a factor ≈ 2. A reduction in the number of adsorbed disks is a consequence of these two effects. In figure 5.2 we see that the growth of $\langle n(\alpha) \rangle$ only slightly deviates from linear in the shown range of $\alpha_1 < \alpha < 2$. Due to the quadratic dumpenning factor in equation (5.1), which indicates that the jamming density θ_J decreases with cell size α at fixed density $\theta_0^{(cell)}$, which is illustrated in figure 5.3. The solid line shows the relative jamming coverage $\theta_J / \theta_0^{(cell)}$ in the non-interacting mode, while the dashed line represents the case of maximum packing per cell. Although the maximal packing density function is quite jagged with discontinuous jumps at $\alpha = \alpha_k$, the randomness in the positioning of particles in an RSA process smooths out the jamming density function.
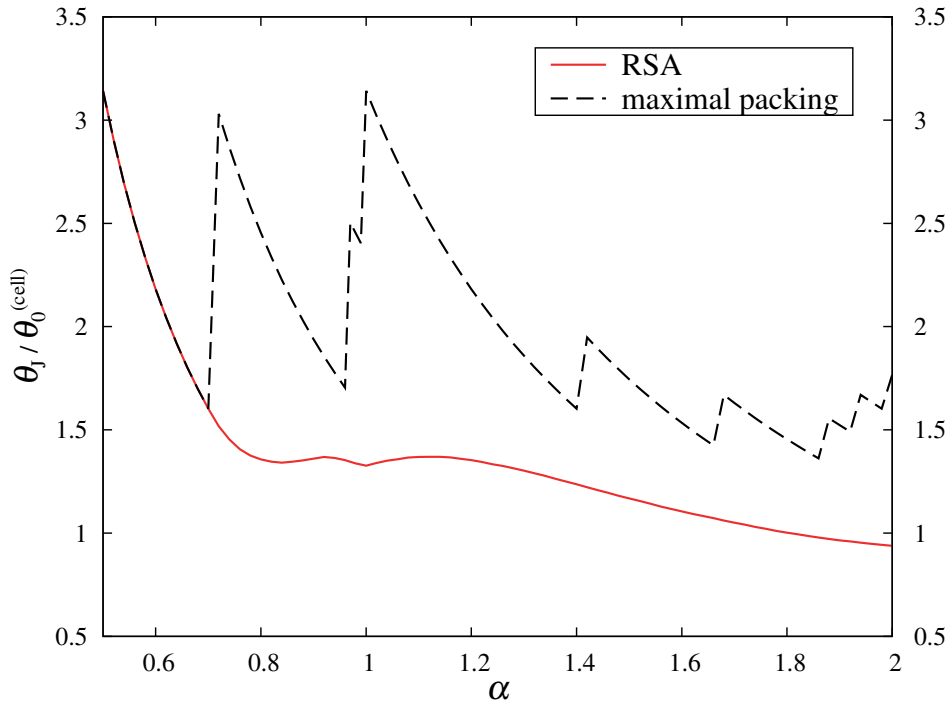
Figure 5.3: RSA jamming density (solid line) vs. maximal packing density (dashed line) relative to the cell density in the non-interacting mode.

5.1.2 Densification kinetics

Kinetics of the irreversible deposition of disks is illustrated in figures 5.4(a) – 5.4(e) where the plots of time coverage behavior $\theta(t)$ are given for the five values of coverage fraction of landing cells, $\theta_0^{(\text{cell})} = 0.1, 0.2, 0.3, 0.4, 0.5$. Here the plots of such time-dependence are shown for various values of the cell size, α_k ($k = 1, 2, 3, 4$). It can be seen that for a fixed density of landing cells $\theta_0^{(\text{cell})}$, jamming coverage $\theta_J = \lim_{t \to \infty} \theta(t)$ decreases with increasing the cell size α_k. This effect is clearly visible in the case of the lowest density of the landing cells $\theta_0^{(\text{cell})} = 0.1$ (figure 5.4(a)), when the average distance between the squares γ (equation (4.2)) is several times larger than the diameter of the disks, as discussed in previous section.

As can be seen from figure 5.4, the time coverage behaviour $\theta(t)$ is markedly slowed down with the increase of the cell size α for the fixed density of landing cells $\theta_0^{(\text{cell})}$. Indeed, in the MPCA case, large times are needed for filling small isolated vacant targets on landing cells, remaining in the late stages of deposition. Furthermore, in this regime, density curves $\theta(t)$ show a noticeable slowing down of the deposition process at coverages that are significantly smaller than jamming densities. Coverage growth starts to slow down at the moment when the number of adsorbed disks reaches the number of landing cells. After this initial filling of the landing cells, adsorption events take place on isolated islands of partially occupied cells. This extends the time interval between successful consecutive adsorption events and causes a slowing down of the densification.

The results for the time evolution of the coverage $\theta(t)$ in the case of up-to-two disks per square cell
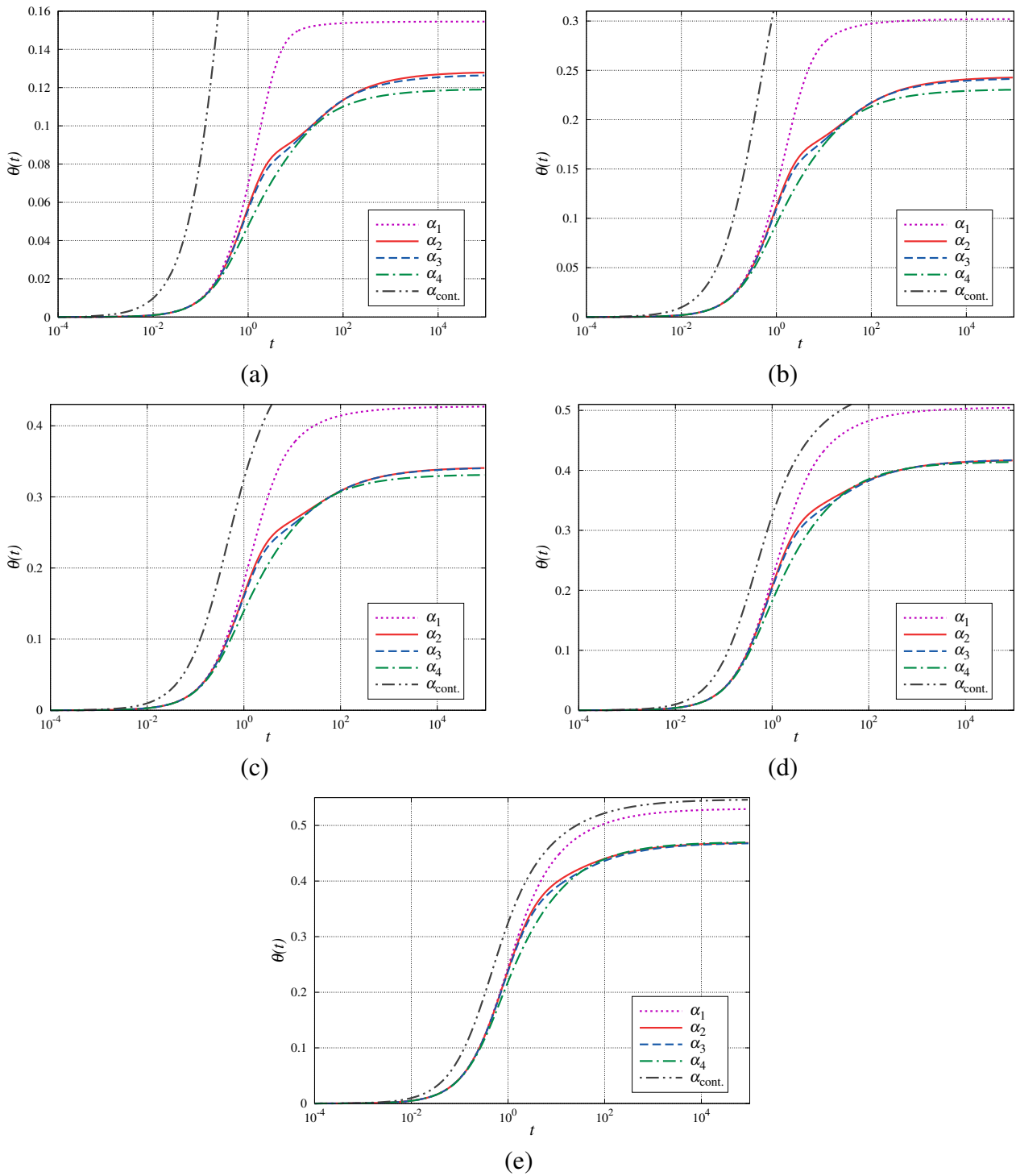
Figure 5.4: Shown here is the time evolution of the coverage fraction $\theta(t)$ for the five values of density of landing cells, $\theta_0^{(\text{cell})} = 0.1$ (a), 0.2 (b), 0.3 (c), 0.4 (d), 0.5 (e). The curves in each graph correspond to various values of the cell size, α_k ($k = 1, 2, 3, 4$), as indicated in the legend. The α_{cont} line shows the time dependence of the coverage $\theta(t)$ for RSA of disks on a continuous substrate. The entire α_{cont} curve can be seen in plot (e).
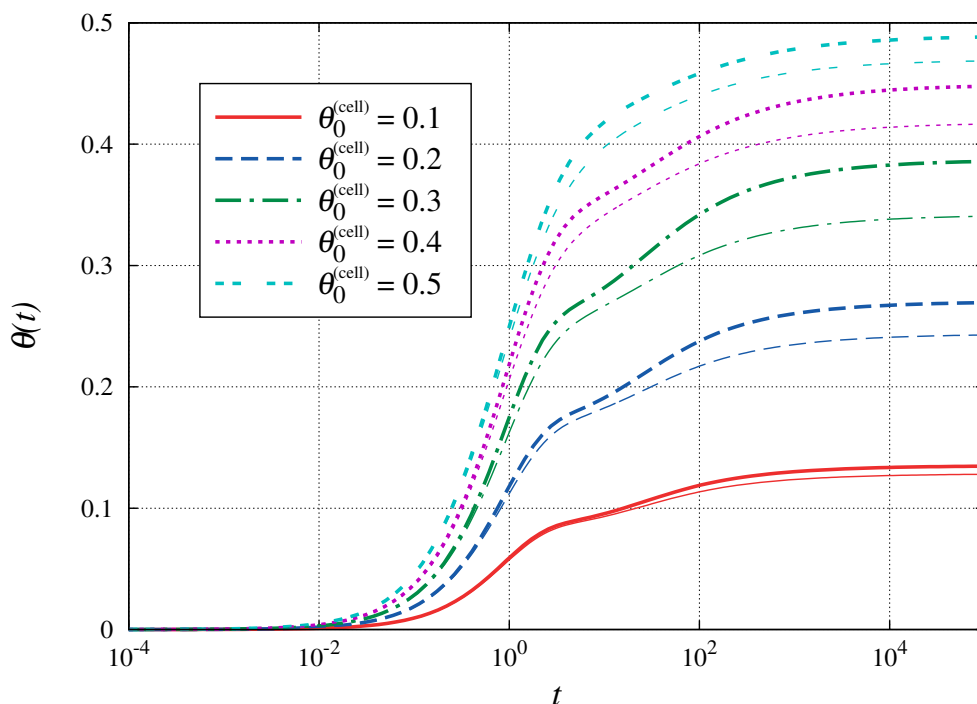
Figure 5.5: Temporal behavior of the coverage $\theta(t)$ for various values of $\theta_0^{(\text{cell})}$ in the case of up-to-two disks per square cell (cell size: $\alpha_2 = (1 + \sqrt{3})/(2\sqrt{2}) \approx 0.966$). The curves correspond to various values of density $\theta_0^{(\text{cell})} = 0.1 - 0.5$, as indicated in the legend. Thick lines represent results obtained for regular substrate pattern while thin lines are results for random pattern case.

($\alpha = \alpha_2$) are shown in figure 5.5 for various values of $\theta_0^{(\text{cell})}$. Qualitatively similar results are obtained with landing cells of other sizes α. As expected, the jamming density θ_J increases with higher coverage fraction of landing cells $\theta_0^{(\text{cell})}$. At high values of $\theta_0^{(\text{cell})} \lesssim 0.5$ when $\gamma \sim 1$, a disk attempting adsorption can overlap with a previously adsorbed one belonging to a different cell, resulting in a failed adsorption attempt. This excluded volume interaction between particles during adsorption at *different* cells causes an even slower asymptotic approach of the coverage fraction $\theta(t)$ to its jamming limit. In addition, the analysis of the time evolution of the coverage $\theta(t)$ was carried out for deposition on square cells centred at the vertices of a square lattice. Consequently, the temporal evolution of the coverage $\theta(t)$ obtained for regular substrate pattern is included in figure 5.5. Here, the size α and density $\theta_0^{(\text{cell})}$ of landing cells are the same as those used in our previous calculations for the random pattern cases. It can be seen that lower values of the jamming coverage fraction are reached by the deposition process involving randomness in the pattern compared to a deposition process in the presence of a regular substrate pattern, regardless of the value of the density $\theta_0^{(\text{cell})}$.

5.1.3 Asymptotic behaviour

Below we try to characterize quantitatively the time dependence of the approach to the jammed state at large times. Depending on the system of interest modelled by RSA, the substrate can be continuous (off-lattice) or discrete. The asymptotic approach of the coverage fraction $\theta(t)$ to its jamming limit,

$\theta_J = \theta(t \to \infty)$, is known to be given by an algebraic time dependence for continuous substrates [5, 36, 49, 50, 71]:

$$\theta(t) \sim \theta_J - At^{-1/d}, \qquad (5.2)$$

where A is a constant coefficient and d is interpreted as substrate dimension [49] in the case of spherical particles adsorption or, more generally, as a number of degrees of freedom [48]. For lattice RSA models, the approach to the jamming coverage is exponential [27, 67–69, 84, 85]:

$$\theta(t) \sim \theta_J - \Delta\theta \exp(-t/\sigma), \qquad (5.3)$$

where parameters θ_J, $\Delta\theta$, and σ depend on the shape and orientational freedom of depositing objects [68, 69].

Representative examples of the double logarithmic plots of the first derivative of coverage $\theta(t)$ with respect to time t are shown in figure 5.6(a), for various values of the cell size, α_k ($k = 1, 2, 3, 4$), and for high density of landing cells, $\theta_0^{(cell)} = 0.5$. The time derivatives of $\theta(t)$ are calculated numerically from the simulation data. In the case of the algebraic behavior of the coverage fraction $\theta(t)$ (equation (3.3)), a double logarithmic plot of the first time derivative $\frac{d\theta}{dt} \propto t^{-\frac{1+d}{d}}$ is a straight line. One can see that the curves shown in figure 5.6(a) are straight lines in the late stage of a deposition process. However, the same is not valid for all values of densities of landing cells $\theta_0^{(cell)}$. The double logarithmic plots of the numerically calculated derivatives of $\theta(t)$ for the data obtained in the case of a low density of landing cell $\theta_0^{(cell)} = 0.1$ are shown in figure 5.6(b). As it can be seen, at the very late times of the deposition process the plot of the first derivative of coverage fraction $\theta(t)$ with respect to time t is not linear on a double logarithmic scale, indicating that the approach to the jamming limit is not consistent with the power-law behaviour given by equation (3.3). The deviation from the power law is particularly pronounced in the case of single-particle per-cell adsorption (SPCA).

Kinetics of the irreversible deposition under SPCA conditions is illustrated in figure 5.7 where a

(a) (b)
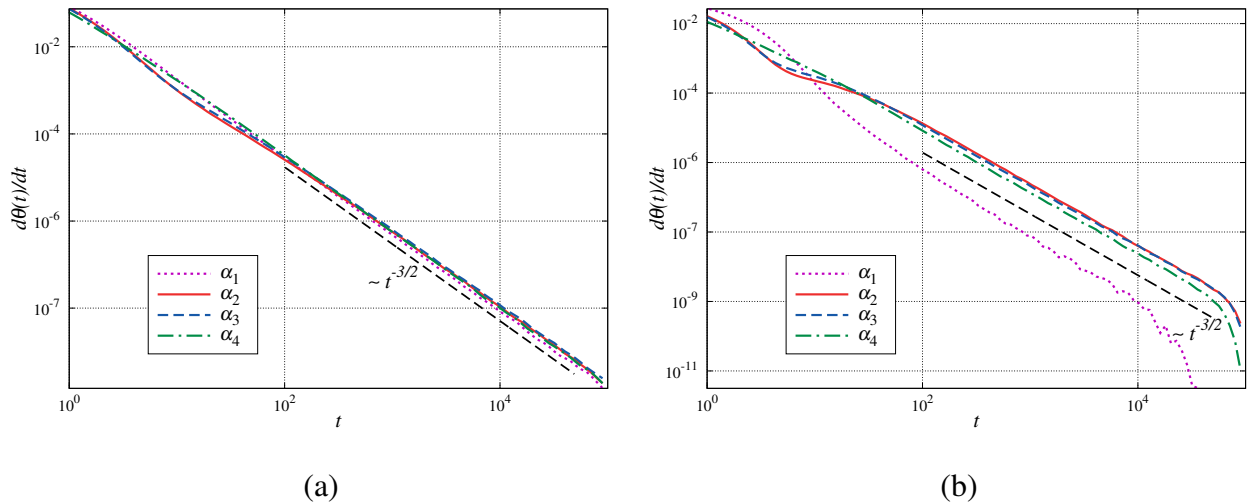
Figure 5.6: Test for the presence of the algebraic law (3.3) in the approach of the coverage $\theta(t)$ to the jamming limit for different densities of landing cells: (a) $\theta_0^{(cell)} = 0.5$, and (b) $\theta_0^{(cell)} = 0.1$. The curves in each graph correspond to various values of the cell size, α_k ($k = 1, 2, 3, 4$), as indicated in the legend. Straight-line sections of the curves show where the law holds. The dashed black line has the slope $-3/2$ and is a guide for the eye.
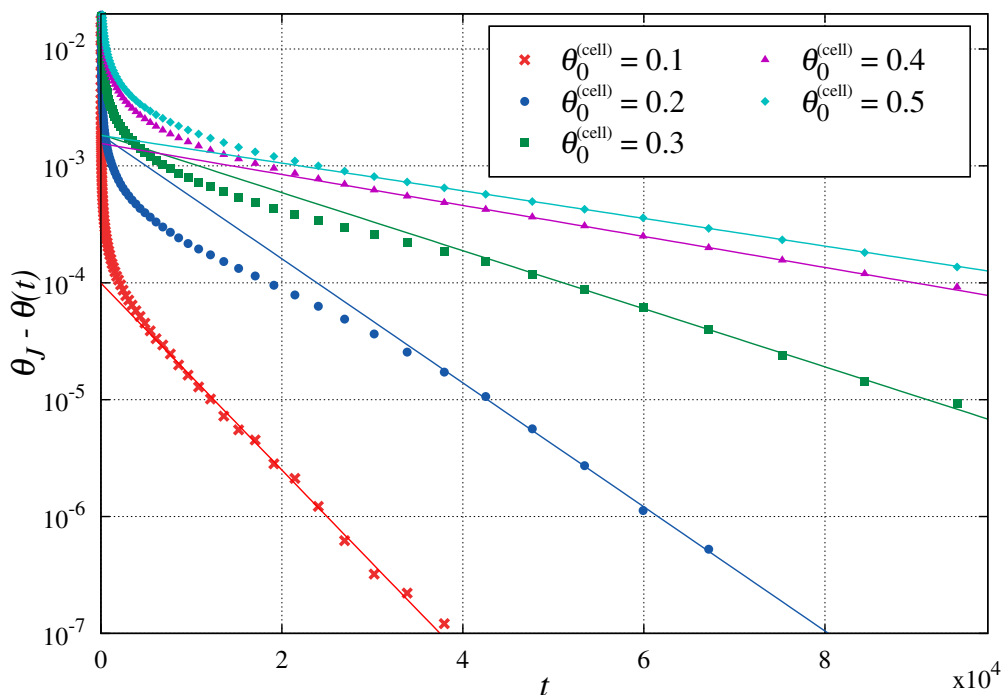
Figure 5.7: Plots of $\theta_J - \theta(t)$ versus t in the single particle per-cell adsorption case for various densities of landing cells $\theta_0^{(\text{cell})} = 0.1 - 0.5$. The solid lines are the exponential fit of equation (5.3).

logarithmic plots of $\theta_J - \theta(t)$ vs t are shown for various densities of landing cells $\theta_0^{(\text{cell})}$. These plots are straight lines for the late times of deposition, suggesting that in the case of SPCA the approach to the jamming limit is indeed exponential, as in lattice RSA models. Indeed, the kinetics of deposition in the SPCA case is determined by the kinetics of adsorption processes on finite-size landing cells. The difference relative to the lattice RSA is in the particle positions, which here are uncertain within the order of the size of the cell.

5.1.4 Radial distribution function

Here we compare quantitatively the structural characteristics of jamming coverings corresponding to different values of the cell size α for various densities $\theta_0^{(\text{cell})}$. In order to gain basic insight into the "microstructure" of the jammed state, we first consider the radial distribution function $g(r)$ (or pair-correlation function) which gives information about the long-range inter-particle correlations and their organization [47]. In absence of external forces, the pair correlation function can be calculated from the expression

$$g(r) = \frac{S}{N} \frac{\overline{N}_a(r)}{2\pi r \Delta r}, \tag{5.4}$$

where r is the radial coordinate, S is the surface area, N is the total number of particles adsorbed over this area, and $\overline{N}_a$ is the averaged number of particles within the annulus of the radius r and the thickness Δr. In figure 5.8(a) we compare the radial distribution function $g(r)$ at various densities $\theta_0^{(\text{cell})} = 0.1 - 0.5$ in the SPCA case. As expected, the random deposition process never leads to

correlation distances between the deposited particles exceeding two or three particle diameters. The position of the first peak measures typical distances between the closest disks. Decreasing the value of $\theta_0^{(cell)}$ in the SPCA case increases the uncertainty in the position of the particles which leads to peak broadening. The shape of radial distribution $g(r)$ is more structured at higher densities, showing higher first and second peaks, because, when the system gets denser, particles will be deposited closer to one another. As can be seen from figure 5.8(a), the minima of $g(r)$ curves shift to shorter distances ($\sim \sqrt{3}$) when the density $\theta_0^{(cell)}$ increases. At very low densities, the broad minima are located near the distance $\sim 2d_0$. Indeed, since the particles are added at random, the probability that disks are connected as a three-bead chain is negligible.

The results for $g(r)$ in the MPCA case are shown in figures 5.8(b) – 5.8(d). The shape of the radial distribution function $g(r)$ is significantly affected by the values of the cell size α. In the case of up-to-two disks per square cell (figure 5.8(b)) the peak which appears at a unit distance is the most pronounced for low densities of landing cells $\theta_0^{(cell)}$. For low values of $\theta_0^{(cell)}$, one expects a lower impact of the cell-cell excluded volume interaction on the cell population. However, as

(a)

(b)

(c)

(d)
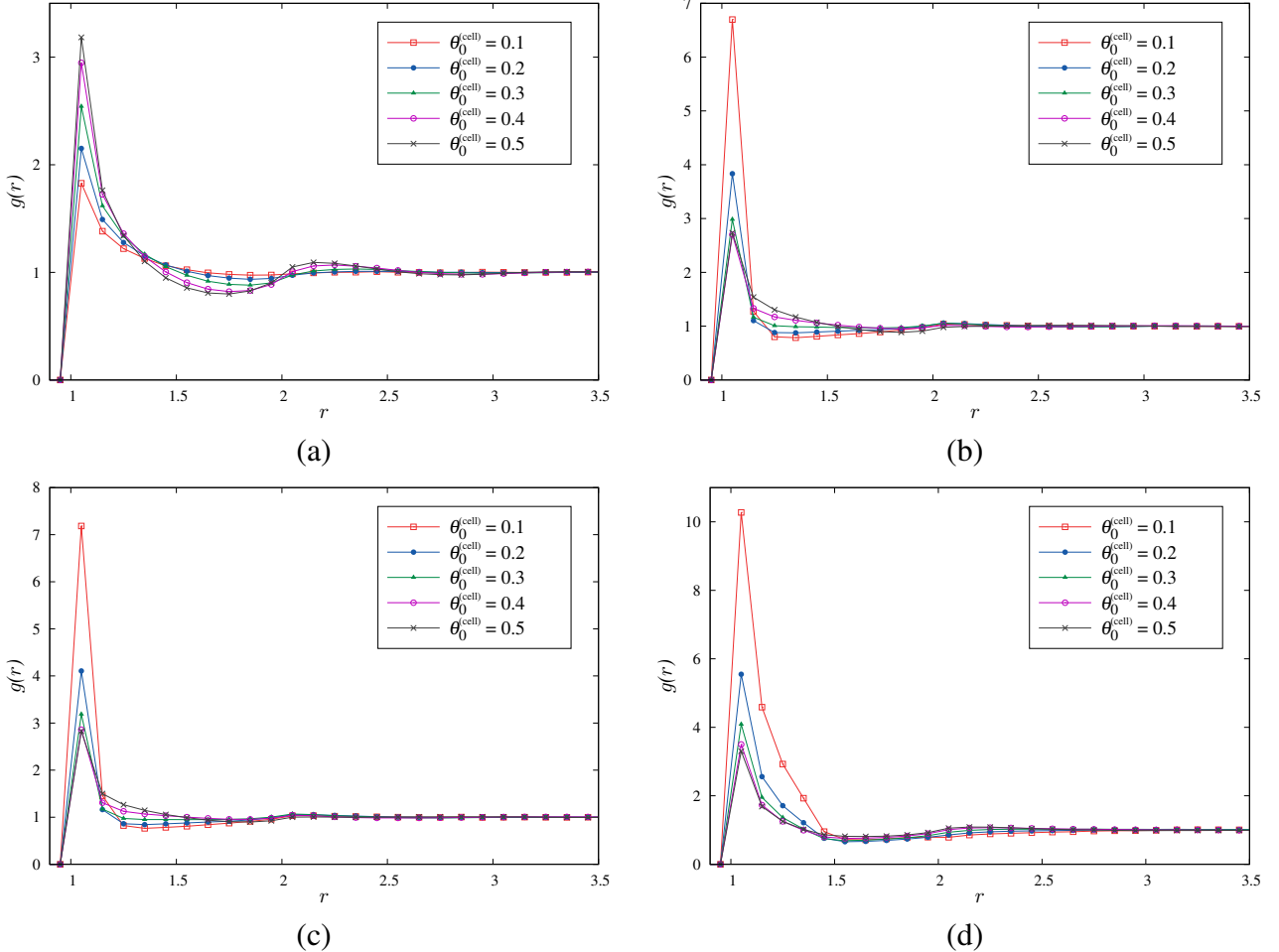
Figure 5.8: Radial distribution function $g(r)$ for jamming coverings as a function of separation r (in units of the disk diameter d_0) for various values of the cell size α: (a) $\alpha_1 = 1/\sqrt{2}$, (b) $\alpha_2 = (1+\sqrt{3})/(2\sqrt{2})$, (c) $\alpha_3 = 1$, (d) $\alpha_4 = \sqrt{2}$. The curves in each graph correspond to various values of density $\theta_0^{(cell)} = 0.1, 0.2, 0.3, 0.4, 0.5$, as indicated in the legend.

$\theta_0^{(cell)}$ increases, the first peak of $g(r)$ becomes broader because excluded volume interaction with disks belonging to neighbouring cells reduces the average number of adsorbed disks per cell. This is opposite to what is observed under SPCA conditions (figure 5.8(a)), where the distance to the closest disk, on average, is determined by the distance of the nearest-neighbour landing cells.

The comparison of figures 5.8(b) and 5.8(c) shows that the results for $g(r)$ in the case of up-to-two and up-to-three disks per square cell are very similar. This arises as a direct consequence of the fact that cells with sizes $\alpha_2 \approx 0.966$ and $\alpha_3 = 1$ have very similar population of particles (see figure (5.2)). Figure 5.8(d) shows the radial distribution function $g(r)$ of jamming coverings at several densities $\theta_0^{(cell)}$ obtained in simulations carried out with the cell size of $\alpha_4 = \sqrt{2}$. For this value of the parameter α, each cell is of sufficient size to accommodate up to four particles. As can be seen in figures 5.8(b) – 5.8(d), increasing the value of parameter α in the MPCA case increases the uncertainty in the position of the disk within the cell, i.e., it leads to peak broadening.

5.1.5 Volume distribution of pores

The jammed-state coverings are analyzed in terms of volume distributions of the pores. The convenient definition of a pore is based on the Delaunay triangulation (DT), which is a natural way to subdivide a 2D structure of disks into a system of triangles with vertices at the centres of neighbouring disks. Consequently, the circle circumscribing a Delaunay triangle has its centre at the vertex of a Voronoï polygon. In this work, we define the pore as a part of the Delaunay triangle not occupied by the disks (Delaunay "free" volume) [57, 58]. The pore volume v is normalized by the "volume" of the disks, $v_0 = d_0^2 \pi / 4$. In figure 5.9 we show Delaunay triangulation of typical jammed-state covering obtained for the same conditions as in figure 5.1(a) ($\theta_0^{(cell)} = 0.3$, $\alpha_4 = \sqrt{2} \approx 1.41$). Looking at the diagram of figure 5.9, one can observe variations in the area of Delaunay triangles, which indicates the presence of pores of various sizes in the deposit.

Here we consider the probability distribution $P(v)$ of the Delaunay "free" volume v. The distribution function $P(v)$ represents the probability of finding a pore with volume v. Fluctuations in the measurements of $P(v)$ are reduced by averaging over 100 different simulations, performed under the same conditions. We compare volume distribution of the pores $P(v)$ for jamming coverings corresponding to different values of the cell size α and various densities of landing cells $\theta_0^{(cell)}$, as illustrated in figures 5.10(a) – 5.10(e). Here, the pore distributions $P(v)$ obtained for densities $\theta_0^{(cell)} = 0.1, 0.2, 0.3, 0.4, 0.5$ have been plotted. At very low value of $\theta_0^{(cell)} = 0.1$ (figure 5.10(a)), the curves of volume distribution $P(v)$ are asymmetric with a quite long tail on the right-hand side, which progressively reduces while the cell size α increases at the fixed density. At the same time, the distribution $P(v)$ becomes narrower and more localized around the low values of the pore volume v. This behavior of the distribution $P(v)$ was not observed for all densities of landing cells $\theta_0^{(cell)} = 0.1 - 0.5$ (see figures 5.10(a) – 5.10(e)). For densities $\theta_0^{(cell)} \geqslant 0.2$, the pore distributions $P(v)$ obtained for deposition on square cells of size α_2 and α_3 are broader and shifted to higher values of volumes v compared to the pore distribution $P(v)$ corresponding to SPCA case (α_1). Qualitative interpretation of this result is given below.

In the case of up-to-four disks per square cell ($\alpha_4 = \sqrt{2}$), we observe the appearance of pronounced peak of $P(v)$ at low values of v, approximately at $v = 0.15 - 0.20$. It is easy to understand
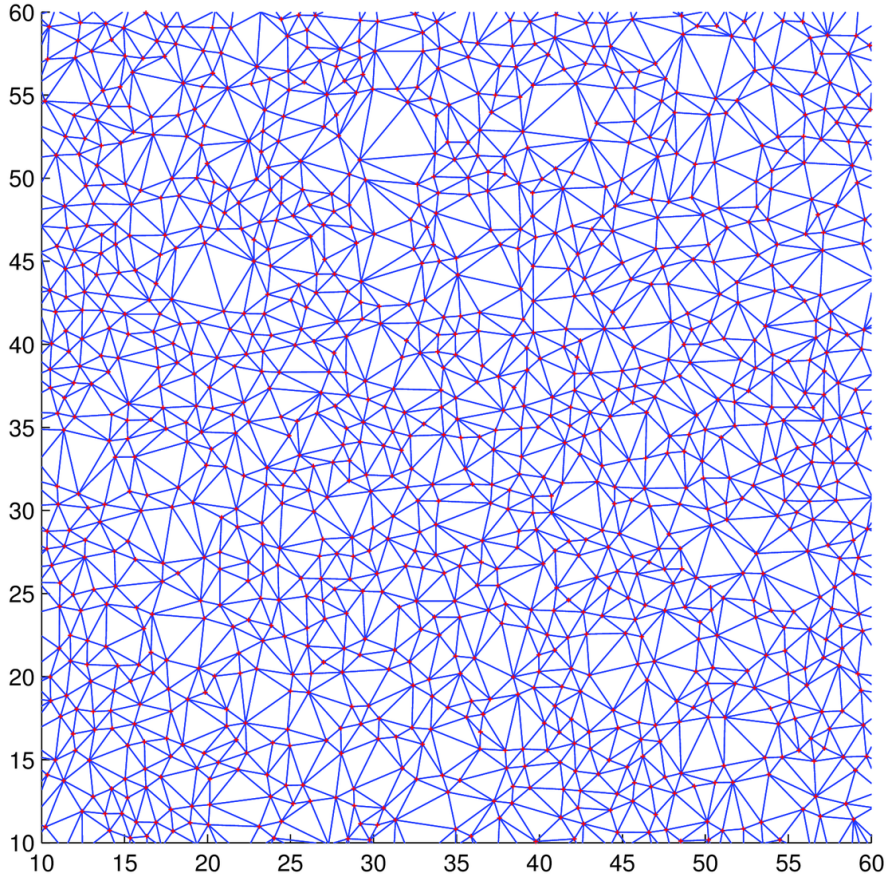
Figure 5.9: Delaunay triangulation of a set of points (centres of disks). Diagram corresponds to jammed-state covering obtained for density of landing cells $\theta_0^{(\text{cell})} = 0.3$ and cell size $\alpha_4 = \sqrt{2}$; see figure 5.1(a) for a typical configuration. The red dots are the centres of the adsorbed disks. Length is measured in units of the disk diameter d_0.

which kind of local configuration contributes mostly to this peak of the $P(v)$. The Delaunay cells with free dimensionless volume $v_{\text{hex}} = \sqrt{3}/\pi - 1/2 \approx 0.051$ correspond to the local arrangements of hexagonal symmetry when three disks are all in touch with each other with centres on the vertices of a unilateral triangle. The cells with free volume $v_{\text{quad}} = 2/\pi - 1/2 \approx 0.13$ correspond to the local configurations of quadratic symmetry when centres of four touching disks are positioned on the vertices of a square. These are minimal values of pore volumes that can be formed with three and four disks deposited on a single landing cell of size $\alpha_4 = \sqrt{2}$. However, the probability that the previously described structures of quadratic and hexagonal symmetry arise during the process of random deposition is negligibly small. Therefore, the "free" volumes formed with random deposition of disks into a single cell are larger than the minimal values $v_{\text{hex}} \approx 0.051$ and $v_{\text{quad}} \approx 0.13$, so that observed peak of $P(v)$ is around $v \lesssim 0.20$.

At high values of density of landing cells $\theta_0^{(\text{cell})} = 0.5$ (figure 5.10(e)), distribution $P(v)$ obtained under SPCA conditions becomes very similar to pore volume distribution for RSA of disks on a continuous substrate, as expected. The results for the volume distribution of the pores $P(v)$ obtained in the cases of up-to-two and up-to-three disks per square cell are almost identical at all densities $\theta_0^{(\text{cell})}$ (see figure 5.10). The similarity of these distributions at small values of pore volumes can be explained by the results shown in figure 5.2. Small pores appear due to the presence of configurations with three
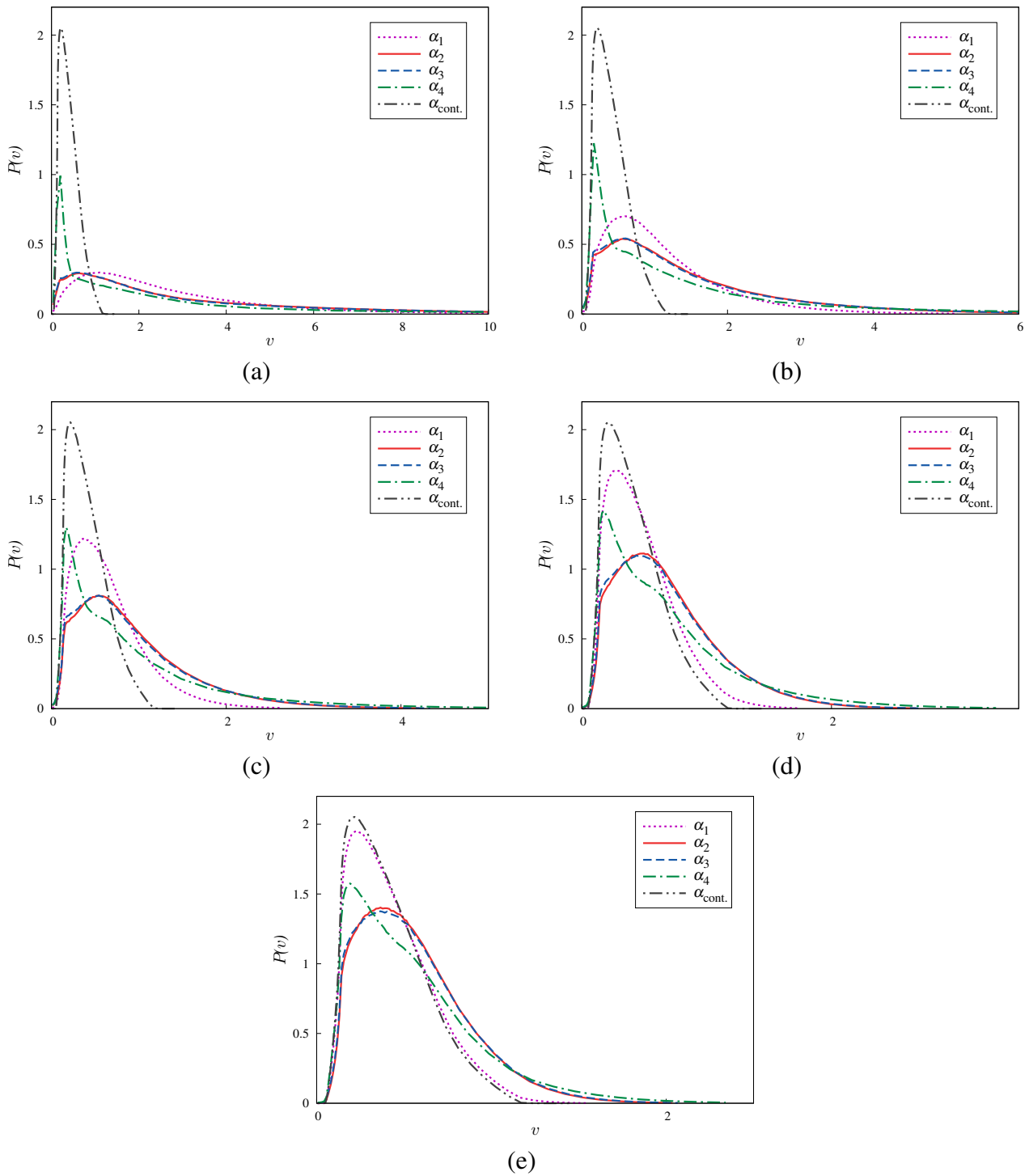
Figure 5.10: Volume distribution of the pores $P(v)$ in the case of random pattern are shown for jamming coverings at different values of density of the landing cells corresponding to $\theta_0^{(\text{cell})} = 0.1$ (a), 0.2 (b), 0.3 (c), 0.4 (d), 0.5 (e). The curves in each graph correspond to various values of the cell size, α_k ($k = 1, 2, 3, 4$), as indicated in the legend. The α_{cont} line shows distribution $P(v)$ for jamming covering in the case of the irreversible disks deposition on a continuous substrate.

or more disks on a single landing cell. But, in the case of up-to-three disks per square cell, the number of in-cell configurations with three disks is considerably smaller than the number of configurations with one or two disks. Consequently, the broad maximum in $P(v)$, centred at $v = 0.4 - 0.6$ is caused by the contribution of large pores formed mostly in the space between the landing cells.

5.1.6 Impact of pattern regularity

Further, we study the effect of the presence of a regular substrate pattern of squares on the volume distribution of the pores $P(v)$. Distributions $P(v)$ for jamming coverings corresponding to $\theta_0^{(cell)} = 0.1$ – 0.5 and different values of the cell size α_k ($k = 1, 2, 3, 4$) are shown in Figure 5.12. At low density of landing cells $\theta_0^{(cell)} = 0.1$ and for large cell size $\alpha \geqslant \alpha_4 = \sqrt{2}$ (see figure 5.12(a)) we observe the appearance of three peaks of $P(v)$. The first peak at $v \approx 0.2$ is due to Delaunay triangles with their vertices inside a single landing cell (see T1 triangle in figure 5.11). The third peak at $v \approx 8$ corresponds to Delaunay triangles with vertices located in different landing cells (see T3 triangle in figure 5.11). The central peak at $v \approx 2$ arises due to Delaunay triangles with two vertices belonging to a single cell, while the third one is located in a neighbouring cell (see T2 triangle in figure 5.11). The first peak at very low values of pore volumes v does not appear for the smaller landing cells, $\alpha = \alpha_1$, α_2, α_3. Indeed, if $\alpha \leq \alpha_3$, the Delaunay triangles that lie within a single landing cell are very rare ($\alpha = \alpha_3$) or they can not exist ($\alpha \leq \alpha_2$). In the case of single-particle per-cell adsorption ($\alpha = \alpha_1$) vertices of each Delaunay triangle are located in three different cells, so that distribution $P(v)$ has only one broad maximum. As can be seen from figure 5.12, the difference between distribution $P(v)$ for regular substrate pattern of squares and for random pattern case decreases with the increase of the cell density $\theta_0^{(cell)}$.
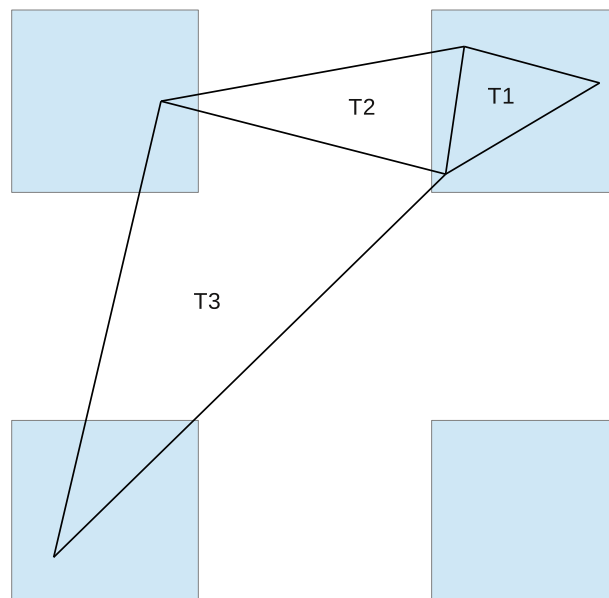
Figure 5.11: Various types of Delaunay triangles (T1, T2, T3) depending on the position of vertices.

(a)

(b)

(c)

(d)

(e)
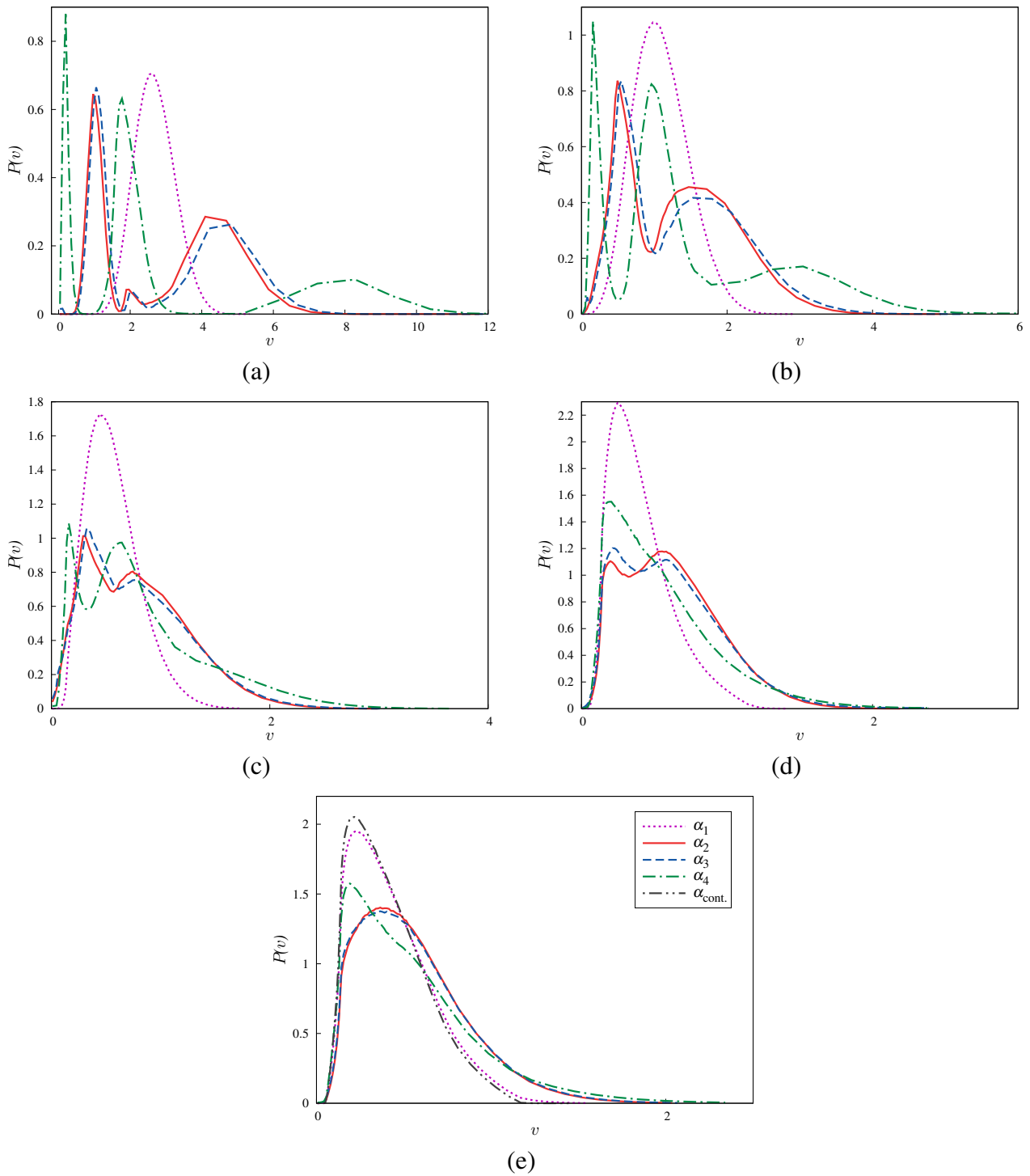
Figure 5.12: Volume distribution of the pores $P(v)$ in the case of heterogeneous surface covered by square cells centred at the vertices of a square lattice for jamming coverings at different values of density of the landing cells corresponding to $\theta_0^{(\text{cell})} = 0.1$ (a), 0.2 (b), 0.3 (c), 0.4 (d), 0.5 (e). The curves in each graph correspond to various values of the cell size, α_k ($k = 1, 2, 3, 4$), as indicated in the legend.

5.2   Rectangular cells

We have also performed numerical simulations of random deposition of identical disks on heterogeneous surfaces covered by rectangles of arbitrary orientation. In these simulations, each landing cell is a rectangle with sides $\alpha = 8$ and $\alpha/\lambda = 1$ (in units of the disk diameter d_0). The choice of the value of aspect ratio λ plays important role in our model. Increasing the aspect ratio of the landing cells (rectangles) leads to the formation of domains of increased regularity. The chosen value of $\lambda = 8$ is large enough to provide a significantly different patterned substrate compared with the case of the square cells. We have verified that usage of different, but large, aspect ratio values λ gives quantitatively very similar results leading to qualitatively the same phenomenology.

5.2.1   Radial distribution function

To characterize the jammed state we studied radial distribution function $g(r)$ and probability distribution $P(v)$ of pore volume v for different values of density of landing cells: $\theta_0^{(cell)} = 0.1, 0.2, 0.3, 0.4,$ 0.45. Figure 5.13 shows the corresponding results for radial distribution function $g(r)$. Comparing the results from figure 5.13 and figures 5.8(b) – 5.8(d), one can see that the first peak near $r/d_0 = 1$ and local maximum at $r/d_0 \gtrsim 2$ of $g(r)$ are more pronounced in the case of elongated rectangular cells than in the case of multi-particle adsorption (MPCA) at squares. This emergence of a better
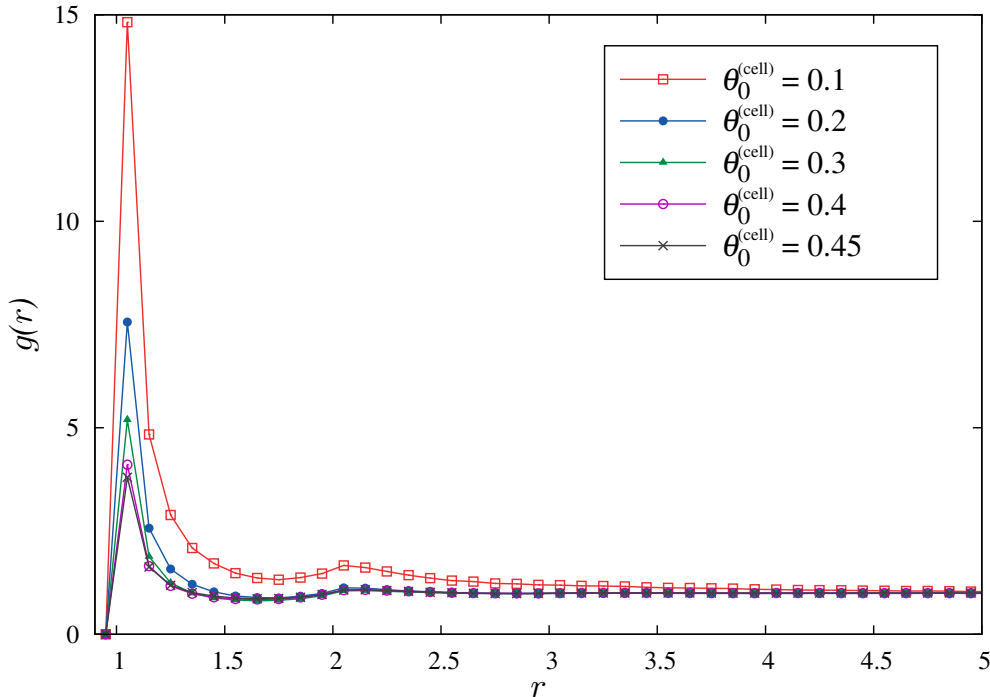
Figure 5.13: Radial distribution function $g(r)$ for jamming coverings as a function of separation r (in units of the disk diameter d_0) obtained from simulations carried out using the heterogeneous surface covered by rectangles of arbitrary orientation. The curves correspond to various values of density $\theta_0^{(cell)} = 0.1, 0.2, 0.3, 0.4, 0.45$, as indicated in the legend.

local order is a correlation effect that develops during the deposition stage due to the formation of arrays of disks within a single elongated rectangular cell.

5.2.2 Volume distribution of pores

Figure 5.14 compares volume distribution of the pores $P(v)$ for jamming coverings corresponding to different densities $\theta_0^{(cell)}$. Similar to the case of MPCA on square cells, here we observe the peak of $P(v)$ at small values of $v \approx 0.2$. As previously mentioned, such small pores are a feature of coverings which occurs when three or more particles can be adsorbed on a single cell. The observed peak of the distribution $P(v)$ broadens when density $\theta_0^{(cell)}$ increases. Deposition of elongated objects at high densities is characterized by compact domains of parallel objects and large islands of unoccupied substrate area. Figure 5.15(a) shows a typical snapshot of the jammed-state covering obtained for rectangular cells of arbitrary orientation and density $\theta_0^{(cell)} = 0.45$. Relatively high local packing of nearly parallel adsorbed rectangles reduces the number of disks effectively adsorbed at a cell. This process is associated with the appearance of larger interstitial voids, which causes peak broadening.
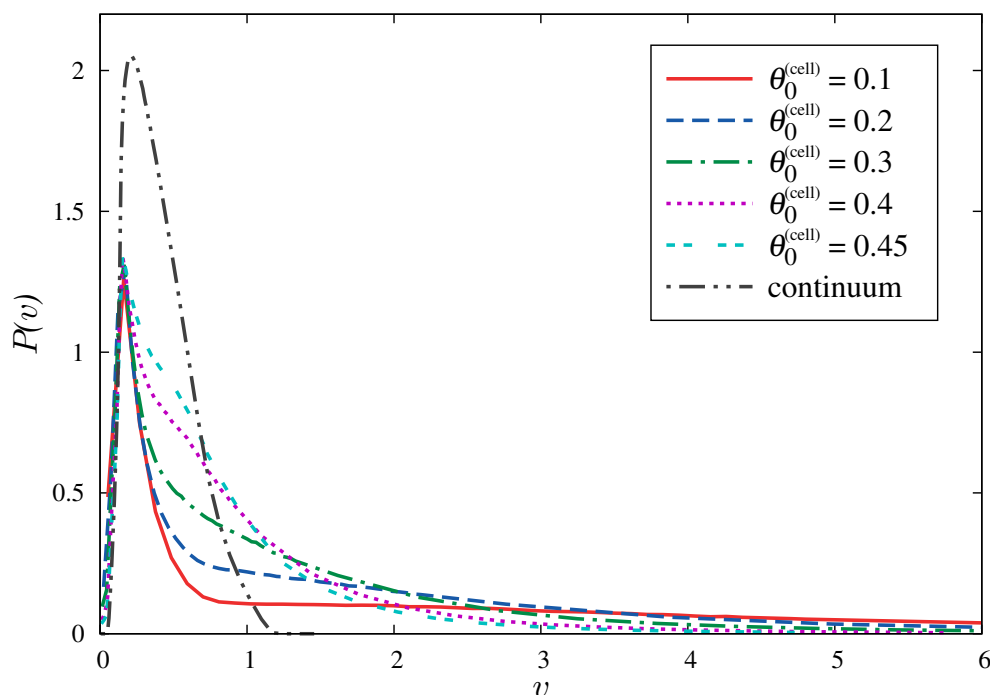
Figure 5.14: obtained from simulations carried out using the heterogeneous surface covered by rectangles of arbitrary orientation. The curves correspond to various values of density $\theta_0^{(cell)} = 0.1$, 0.2, 0.3, 0.4, 0.45, as indicated in the legend. Distribution $P(v)$ for jamming covering in the case of the irreversible disk deposition on a continuous substrate is shown for comparison.

5.2.3 Impact of pattern anisotropy

It is now useful to explore the interplay between the anisotropy in the deposition procedure for landing cells and the structural characteristics of jamming coverings. In this case, the orientation of rectangular cells is fixed to the one preferential direction. The configuration formed in the long time regime is made up of a large number of domains; see figure 5.15(b) for a typical configuration. As expected, any such domain contains parallel cells close to each other. This produces better packing of landing cells and a higher impact of the cell-cell excluded volume interaction on the average cell population. Hence, anisotropic deposition of landing cells lowers the average cell population, which enhances the appearance of larger pores, resulting in a peak broadening. Volume distributions of pores $P(v)$ for jamming coverings of disks corresponding to anisotropic deposition of cells are shown in figure 5.16 with thick lines, while the case of arbitrarily oriented cells from figure 5.14 is drawn with thin lines for comparison. figure 5.16 clearly shows enhanced peak broadening of $P(v)$ in the case of anisotropic deposition of landing cells, which is consistent with the previous discussion.
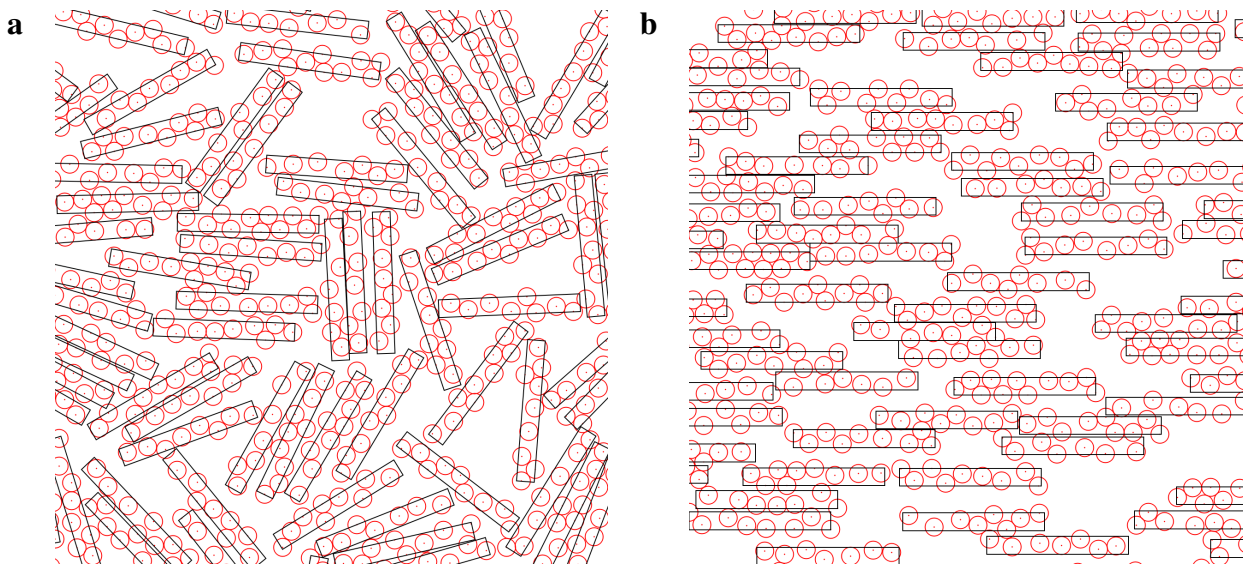
Figure 5.15: Typical jammed-state configuration of a region of size 30×30 (in units of the disk diameter d_0), for $\theta_0^{(\text{cell})} = 0.45$. Orientation of rectangular cells with sides $\alpha = 8$ and $\kappa\alpha = 1$ is (a) arbitrary or (b) fixed to the horizontal direction.
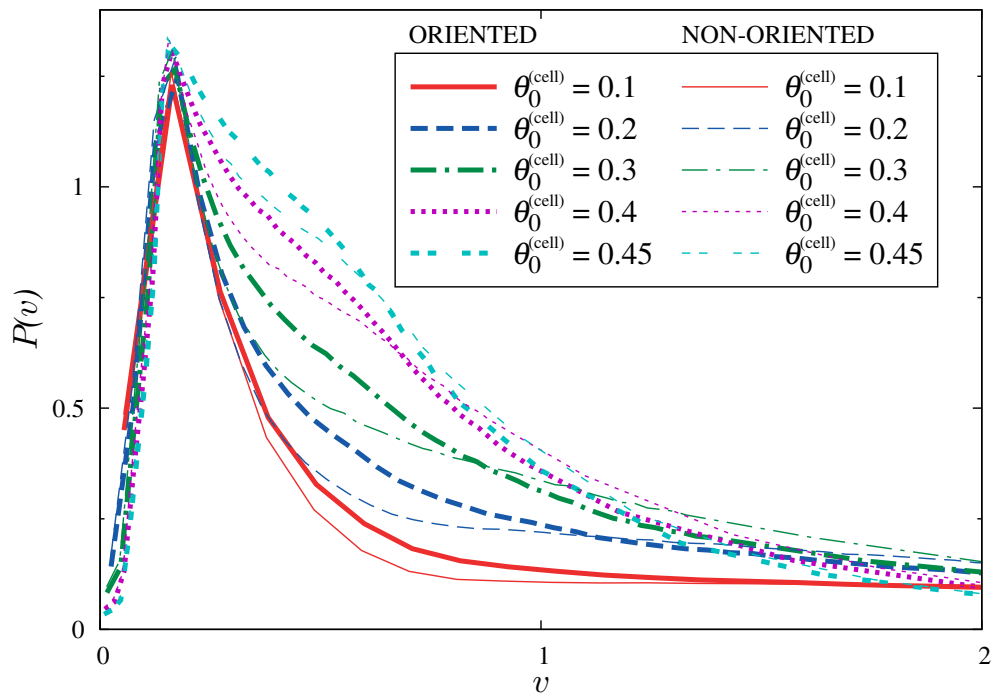
Figure 5.16: Volume distribution of the pores $P(v)$ obtained from simulations carried out using the heterogeneous surface covered by rectangles of fixed orientation (thick lines) and arbitrary orientations (thin lines). The curves correspond to various values of density $\theta_0^{(cell)} = 0.1, 0.2, 0.3, 0.4, 0.45$, as indicated in the legend.

Chapter 6

Adsorption on imprecise lattice

The difference between deposition on finite-size landing cells and lattice RSA is in the particle positions, which can be uncertain within the order of the size of the cell in the former case. Recently, Privman and Yan [1] have analyzed both numerically and analytically extended model of one-dimensional deposition of segments of length a, on a lattice of spacing ℓ between its sites, which instead of just being lattice points are symmetrically broadened (about the lattice points) into segments of width w in which the centres of the depositing objects can land. They reported that even an arbitrarily small imprecision in the lattice-site localization ($w \gtrsim 0$) changes the convergence to jamming from fast, exponential

$$\theta_J - \theta(t) \sim \exp(-t/\sigma), \tag{6.1}$$

to slow, power-law

$$\theta_J - \theta(t) \sim t^{-1/d}. \tag{6.2}$$

In a similar spirit, the study presented in this chapter investigates the rapidity of the approach to the jamming state in the case of *two-dimensional* (2D) pre-patterned substrate. Unlike the models studied in chapter 5, here we analyze deposition on the substrates patterned with a square grid of square-shaped cells onto which the particle can adhere. We consider the process of the irreversible random sequential adsorption (RSA) of fixed size disks. The present chapter focuses on the effect of the presence of a regular substrate pattern on the temporal evolution of the coverage fraction $\theta(t)$. We aim to quantify changes in time coverage behaviour $\theta(t)$ at densities near jamming limit θ_J, associated with different cell sizes and densities.

A regular substrate pattern that consists of identical square cells centred at nodes of a regular square lattice is completely defined by two dimensionless parameters: the length of a cell size α and the length of the smallest gap between two neighbouring cells β (figure. 3.2). These two lengths are measured in the units of the adsorbing particle radius. As described in section 3.3, parameter β determines whether the adsorption is in interacting ($\beta < 1$) or non-interacting mode ($\beta > 1$). Parameter α distinguishes between single vs. multiple particles per cell mode. The phase diagram as defined by Araújo et al. [45] was discussed earlier in section 3.3 and illustrated in figure. 3.3. In this work, we focus on the interacting cell-cell adsorption (ICCA) regime in the case of single-particle per-cell adsorption (SPCA). The non-interacting regime (NICCA) is equivalent to the low cell density limit case discussed in section 5.1.1. We want to investigate the role of the cell-cell interaction and thus we limit this study to the SPCA case where $\alpha < \sqrt{2}/2$, which excludes the interaction of the particles at

the same cell.

6.1 Kinetics

6.1.1 Effect of varying β on the long-time adsorption kinetics

We simulate the adsorption on a substrate with a regular pattern consisting of square cells that are comparable in size to the adsorbing particles and that satisfy the SPCA condition $\alpha < \sqrt{2}/2$. We chose the three values of cell size: $\alpha = 0.3$, 0.5, and 0.7. Figures 6.1(a) – 6.1(c) illustrate the kinetics of the irreversible deposition of disks. The plots of the time coverage behaviour $\theta(t)$ are given for the three chosen values of α and various values of the gap β between the cells, in the range from $\beta = 0$ (continuous substrate and ICCA regime) to $\beta = 1$ (upper limit of the parameter β, above which the NICCA occurs). These 2D plots enable us to analyze how the time evolution of the coverage $\theta(t)$ in

(a)

(b)

(c)
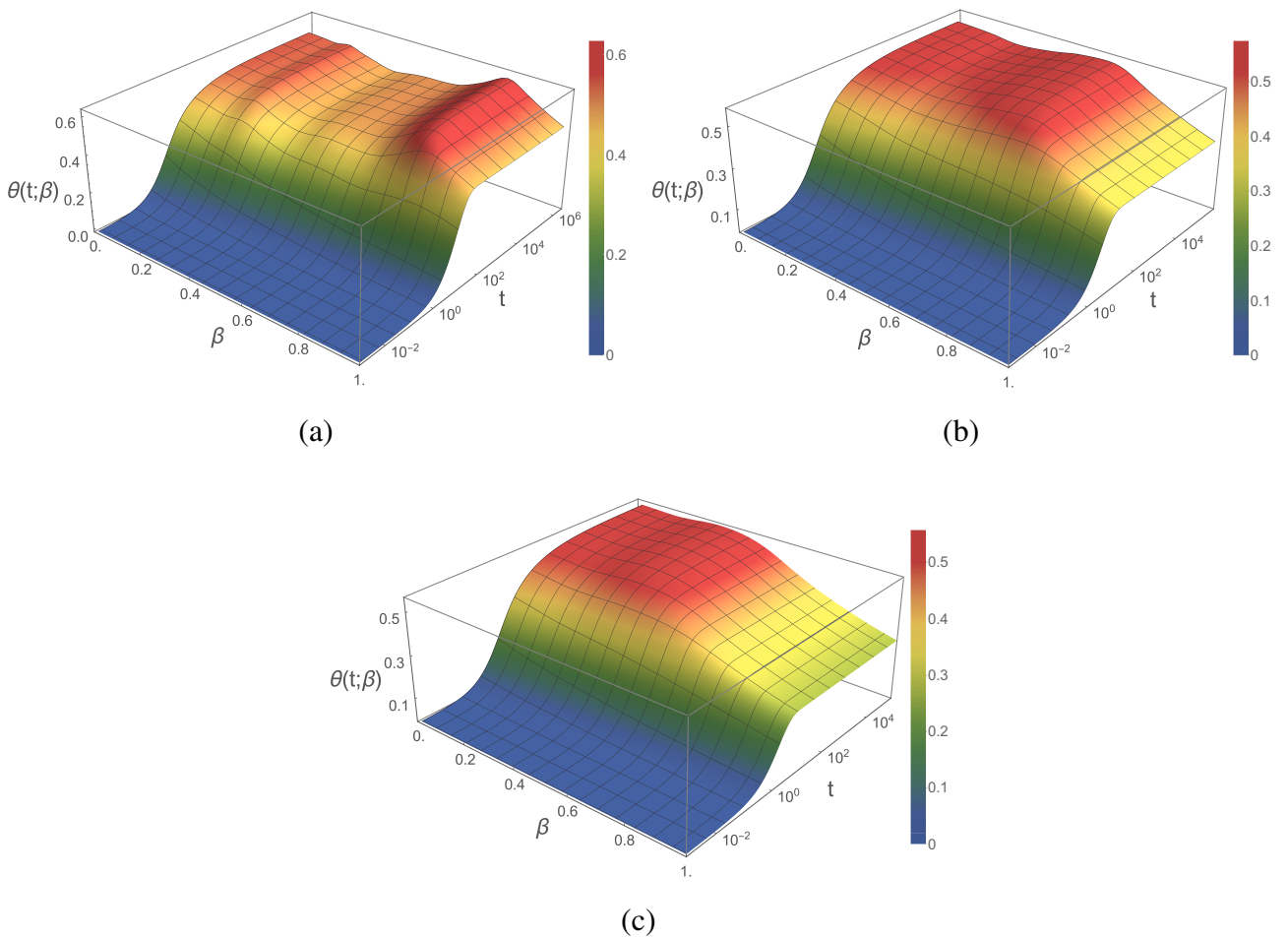
Figure 6.1: Time evolution of the coverage fraction $\theta(t)$ depending on the gap size β between two neighbouring landing cells (in units of the disk diameter d_0), for the three values of cell size, $\alpha = 0.3$ (a), 0.5 (b), and 0.7 (c). For each α, the gap β between cells is varied in the range [0, 1], with the step of 0.02.

the case of SPCA depends on the gap size β between the landing cells.

It can be seen that for a fixed size of landing cells α, coverage $\theta(t)$ in the early stage of the deposition process increases faster when the gaps between the cells are smaller. Indeed, at very early times of the process, when the coverage fraction $\theta(t)$ is small, the deposited objects do not "feel" the presence of the other ones, and the coverage grows rapidly in time. Then, the adsorption process has an overall rate proportional to the surface density of landing cells onto which the particles can adhere. Since the flux of incoming particles is fixed, the overall rate at which the coverage $\theta(t)$ increases is progressively reduced with the increase of the gap between the landing cells.

At a late enough time, when the coverage fraction is sufficiently high and "excluded volumes" of deposited objects begin to overlap, there is a strong dependence of the adsorption rate on the parameter β. The rate of successful adsorption events reduces when the gap size β decreases. This is explained by the larger impact of the cell-cell excluded volume interaction when the cells are closer to each other.

It is interesting to emphasize that the dependence of the jamming coverage θ_J is a non-monotonic function of the gap size β (see figure 6.1). It goes from the jamming coverage value for continuum $\theta_J^{cont} = 0.5472 \pm 0.0002$ [86] ($\beta = 0$), reaches some local minimum ($0 < \beta < 1$), and tends to a definite value which corresponds to the coverings when each cell is occupied by a single particle. Corresponding explanations of such variations of the jamming coverage θ with parameter β are provided later in section 6.3.

6.2   Asymptotic behaviour

To gain a better insight into the complex kinetics of SPCA in the ICCA regime, it is useful to analyze in particular the temporal evolution of the first derivative of coverage $\theta(t)$ with respect to time t. The time derivatives of $\theta(t)$ are calculated numerically from the simulation data. Representative examples of double logarithmic plots of the time derivative $d\theta/dt$ are shown in figures 6.2(a) – 6.2(c), for the three values of cell size, $\alpha =$0.3 (a), 0.5 (b), 0.7 (c). For each α, results are presented for various values of the gap β between the cells in the range $0.60 \leqslant \beta \leqslant 0.98$. In the case of the algebraic behavior of the coverage fraction $\theta(t)$ (see equation (6.2)), a double logarithmic plot of the first time derivative $d\theta/dt \propto t^{-(1+d)/d}$ is a straight line. As seen from figure 6.2, if the values of parameter β for cells of size $\alpha = 0.3, 0.5, 0.7$ do not exceed, respectively, $\approx 0.84, 0.74$ and 0.64, the late time kinetics of the deposition process is similar to the one observed for disks with equal size, adsorbing on a clean substrate. Additionally, thin straight lines with the slope $-3/2$ are shown in figure 6.2, indicating the late time RSA behaviour for clean continuous substrates [5, 36, 49, 50, 71]. However, the same is not valid for large values of the parameter β, regardless of the cell size α (obviously, $\alpha < 1/\sqrt{2} \approx 0.707$ in the case of SPCA). As it can be seen, at the late times of the deposition process the plots of $d\theta/dt$ *vs. t* are not linear on a double logarithmic scale for sufficiently large values of the gap β. The deviation from the power-law (6.2) is particularly pronounced for low densities of landing cells, i.e. when $\beta \lesssim 1$.

Theoretical arguments supporting Feder's law (6.2) have been presented by Swendsen [49] and Pomeau [50]. Their analysis is based on the exclusion of the area of radius d_0 around each disc of

radius $d_0/2$ for selecting the centre of the newly arriving disc. After a certain time, characterizing the beginning of the asymptotic regime, the area that is available to the centre of a new disc consists of small disconnected areas that can be occupied by only one additional disc. When power-law (6.2) holds, a vanishing-small area that is available for the insertion of a new particle can be created with non-zero probability during the deposition process. Arbitrarily small areas are reached with a very small probability for a uniform flux of the arriving disks that attempt deposition. In the case of ICCA-SPCA, since only one particle can fit per cell, the existence of a minimum finite area is related to particles previously adsorbed on neighbouring cells. As seen from figure 6.3(a), particles adsorbed on neighbouring cells can completely overlap the cell when the gap β and cell size α satisfies the relation [81]:

$$\beta + \alpha/2 < 1. \tag{6.3}$$

(a)

(b)

(c)
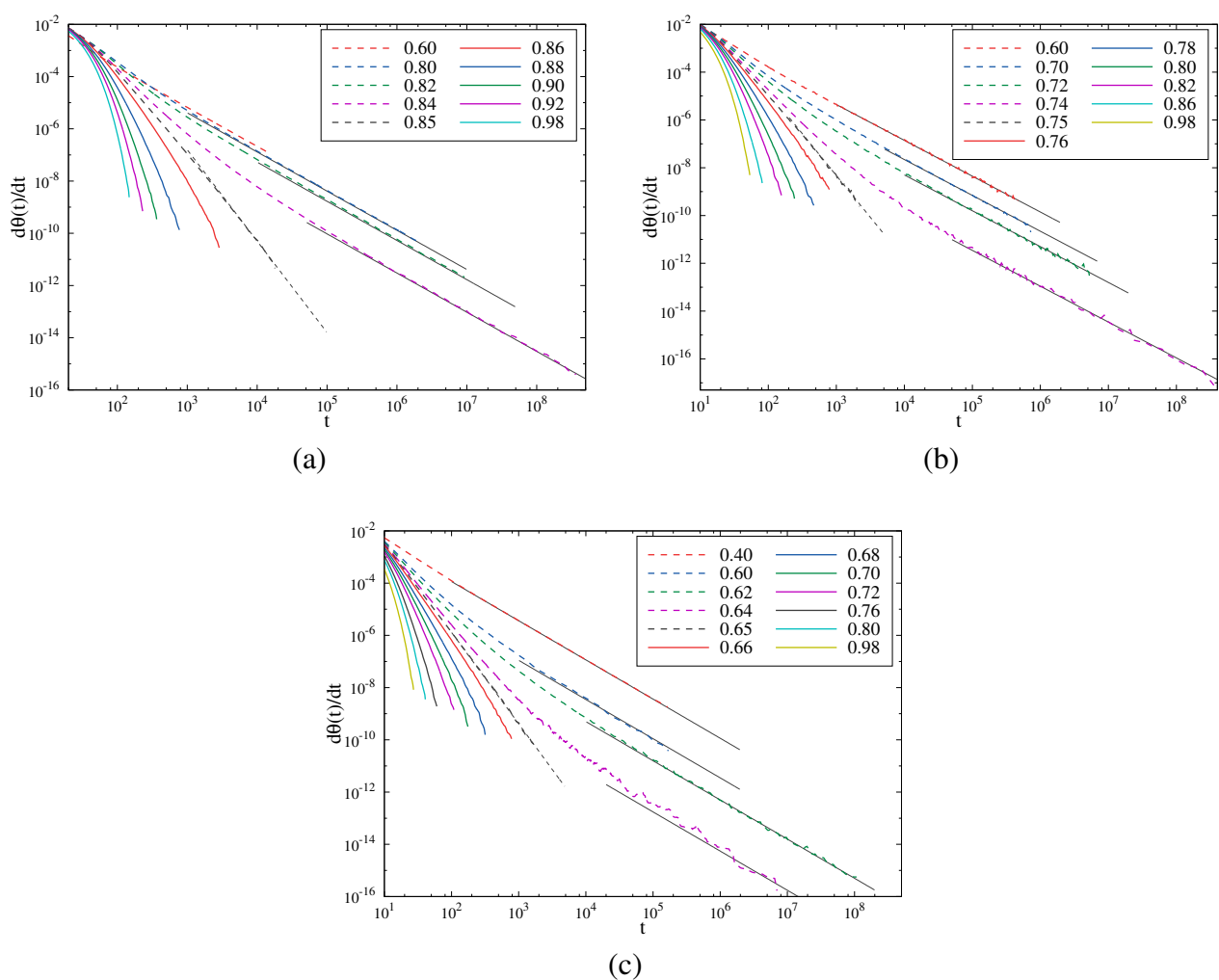
Figure 6.2: Test for the presence of the algebraic law (6.2) in the approach of the coverage $\theta(t)$ to the jamming limit θ_J for different values of cell size, $\alpha = 0.3$ (a), 0.5 (b), and 0.7 (c). The curves in each graph correspond to various values of the gap β between the cells, as indicated in the legend. Straight-line sections of the curves show where the law holds. The solid straight lines have the slope $-3/2$ and are guides for the eye. The dashed straight line has slope -5/2 indicating the late time RSA behaviour of the system for the critical values of the parameter β: (a) $\beta_c = 0.85$, (b) 0.75, (c) 0.65 (see equation (6.4)).

Hence, below the critical value of the parameter β,

$$\beta_c = 1 - \alpha/2, \tag{6.4}$$

there is no minimum *finite* area available to accommodate one particle. However, above the critical value β_c, particles adsorbed on neighbouring cells cannot prevent adsorption inside the cell. Then, there exist finite regions where the centre of a disk can land without overlapping a previously adsorbed particle (see figure 6.3(b)). For the critical value of the gap β_c, the approach to the jamming coverage θ_J with time is still algebraic (6.2), with the exponent that is approximately equal to -3/2 which does not depend on the cell size α. A similar anomalous power-law approach was reported in the literature for the case of adsorption on a one-dimensional imprecise substrate [2, 42]. As explained in more detail in section 3.3, in one dimension the reason for this behaviour lies in a different kind of small hole size distribution in the late phase of the process. The distribution of holes available for particle adsorptions in the late phase of the process for adsorption on a two-dimensional imprecise lattice is out of the scope of this thesis.

Our numerical results suggest that for $\beta_c < \beta < 1$, the asymptotic approach of the coverage fraction $\theta(t)$ to its jamming limit θ_J is neither algebraic nor exponential. Semi-logarithmic plots of the time derivative $d\theta/dt$ are shown in figures 6.4(a) – 6.4(c), for three values of the cell size, $\alpha = 0.3$ (a), 0.5 (b), 0.7 (c). For each α, results are displayed for various values of the parameter β above the corresponding critical values (see equation (6.4)), $\beta_c = 0.85$ (a), 0.75 (b), 0.65 (c). One observes that for the fixed value of cell size α, the time derivatives of $\theta(t)$ decay at the very late times of the deposition process more quickly for the larger values of the gap β between the cells. Interestingly, in the limit of $\beta \to 1$ approach of coverage $\theta(t)$ to the jamming limit θ_J is exponential of the form (6.1). The characteristic timescale σ is found to decrease with the cell size α according to power-law,

(a)   (b)
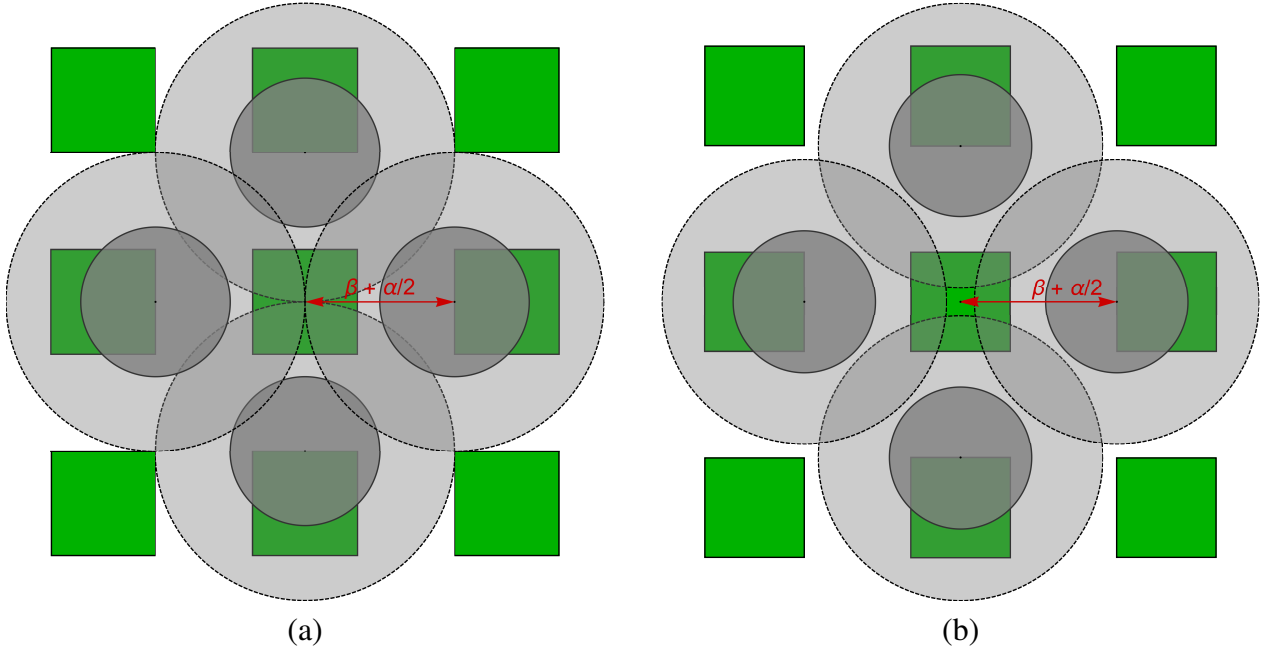
Figure 6.3: Illustration of particles adsorbed in neighbouring cells can prevent adsorption on the central cell: (a) the overlap of the shadowed regions of the four neighbouring particles completely overlap the central cell; (b) particles adsorbed on neighbouring cells cannot prevent adsorption inside the cell.

(a)

(b)

(c)
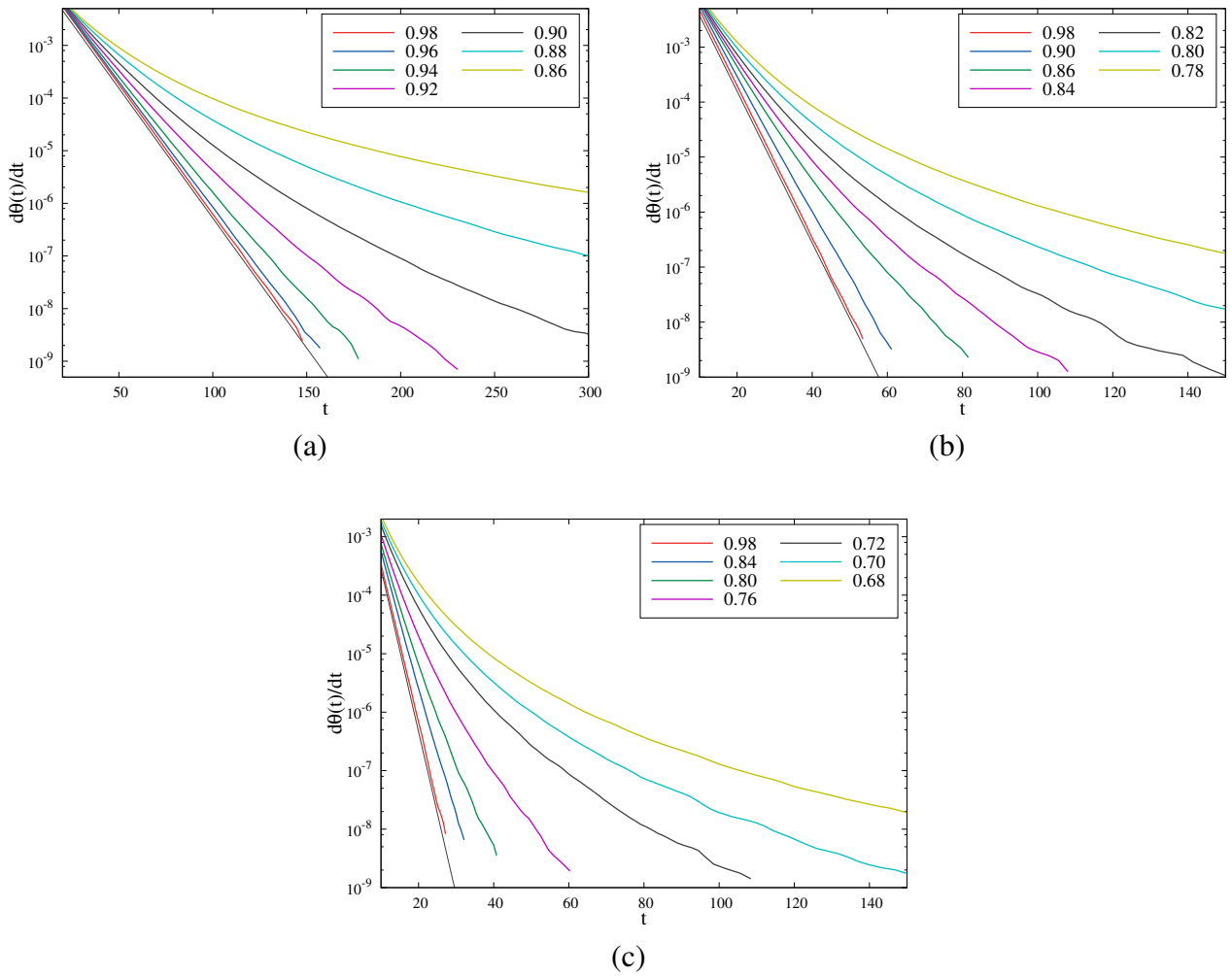
Figure 6.4: Plots of the time derivative of coverage $d\theta/dt$ for the three values of cell size, $\alpha = 0.3$ (a), 0.5 (b), 0.7 (c). As indicated in the legend, the results are reported for values of the gap β above the corresponding critical values (equation (6.4)), $\beta_c = 0.85$ (a), 0.75 (b), 0.65 (c). Additionally, the slanted straight line is shown, indicating the exponential approach to the jamming limit (equation (6.1)), where $\sigma = 8.80$ (a), 3.15 (b), and 1.56 (c).

$\sigma \propto \alpha^{-2.04 \pm 0.02}$. In other words, the relaxation time σ in equation (6.1) is inversely proportional to the cell area. It must be stressed that the appearance of even a slight cell-cell excluded volume interaction violates the exponential asymptotic approach (6.1).

6.3 Jamming coverage

6.3.1 Influence of the pattern on the jamming density θ_J

Let us go back to the analysis of the non-monotonic behaviour of the jamming density θ_J as a function of the gap size β between the landing cells observed in figure 6.1. Dependencies of the jamming

coverage θ_J on the separation distance $\alpha + \beta$ between cell centers are presented in figure 6.5 for the three values of cell size, $\alpha = 0.3$, 0.5 and 0.7. For the case of SPCA, jamming coverage θ_J can be exactly calculated for β larger than the critical value β_c (equation (6.4)) [45]. Indeed, since each cell at late enough time contains the centre of a single deposited particle, the jamming coverage is simply

$$\theta_J^c = \frac{r_0^2 \pi}{(\alpha + \beta)^2} . \tag{6.5}$$

The solid black line in figure 6.5 indicates values of the jamming coverages calculated from equation (6.5). The jammed-state value $\theta_J^{cont} = 0.5472 \pm 0.0002$ [86] of the coverage in the case of the irreversible disks deposition on continuum substrate is marked on the same figure by the horizontal dashed line. When the gap between the cells β starts to increase, cell-cell excluded volume interaction is still strong, but the substrate area that is available for the insertion of a new particle is reduced, which leads to a decrease in the jamming coverage below the value for continuum θ_J^{cont}. As a gap size β increases further, the cell-cell excluded volume interaction weakens, but one expects a higher impact of patterning of the surface on the local particle arrangements. An increase in the pattern-induced tendency for semi-ordering of the coverings leads to the formation of jammed-state deposits of higher density. Then, for sufficiently large values of parameter β, jamming coverage exceeds the jamming limit θ_J^{cont} for continuum substrate and continues to grow with β. In this case, the theoretical value of the highest possible coverage fraction is equal to $\pi/4 \approx 0.7854$. This value corresponds to the local configurations of quadratic symmetry when the disc centres are located at the vertices of a square with a side of $\alpha + \beta = 1$ [87]. However, in the present model this maximum of the jamming coverage θ_J is not reached at $\alpha + \beta = 1$. In figure 6.5 we observe the appearance of three pronounced
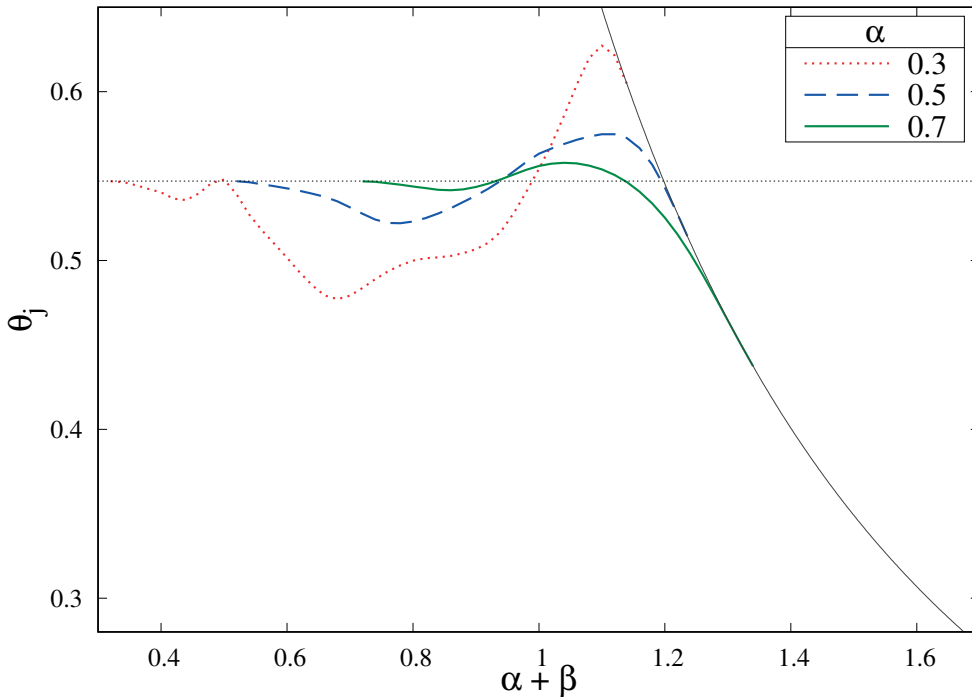
Figure 6.5: Jamming coverage θ_J as a function of separation distance $\alpha + \beta$ (in units of the disk diameter d_0) for various values of the cell size α, as indicated in the legend. The solid black line indicates values of the jamming coverage θ_J^c calculated from equation (6.5).

maxima of θ_J on shifted positions, approximately at $\alpha + \beta = 1.04$, 1.12 and 1.10, for $\alpha = 0.7$, 0.5 and 0.3, respectively. These maxima are not positioned at $\alpha + \beta = 1$ due to the uncertainty in the position of the particle within the cell. Actually, for $\beta \gtrsim 1 - \alpha$ excluded volume interaction with disks belonging to neighbouring cells still substantially lowers the average number of adsorbed disks per cell. As the parameter $\beta > 1 - \alpha$ is increased further to the critical value β_c (equation (6.4)), the average cell population rises, and the jamming coverage θ_J increases until the appearance of large void space between the cells when it falls to the value given by equation (6.5).

We also study the influence of varying α on the jamming coverage θ_J and on the late time kinetics of deposition process. We carried out a series of simulations at fixed $\alpha + \beta = 1.0$, 1.1, and varied cell size α. Numerical results regarding the jamming coverages θ_J for various α are shown in figure 6.6. For $\alpha + \beta = 1.1$, the criteria (6.3) cannot be satisfied if $\alpha < 0.2$. Therefore, for $\alpha < 0.2$ each cell host exactly one particle in the jamming state so that jamming coverage has the constant value $\theta_J = 0.6491$ given by equation (6.5). As $\alpha > 0.2$ increases, the cell-cell exclusion leads to a further reduction of the average cell population, thereby making the jamming coverage lower. However, in the case of $\alpha + \beta = 1$ the jamming coverage $\theta_J(\alpha)$ increases first and reaches the wide maximum at $\alpha \approx 0.5$, after that the curve $\theta_J(\alpha)$ is lowered to the jamming value for continuum substrate θ_J^{cont}. For $\alpha < 1 - \sqrt{2}/2 \approx 0.3$, a cell can only be blocked by disks deposited at the nearest lateral neighbour cells. In that case, for more cell-cell exclusion effects, it is needed a smaller cell size. But, when cells are larger than $1 - \sqrt{2}/2$, a cell can also be blocked by disks deposited at the nearest diagonal neighbour cells, which enhances the cell-cell excluded volume interaction. These two opposite effects that exist when cells increase lead to the formation of the maximum of $\theta_J(\alpha)$ around $\alpha \approx 0.5$. Furthermore, when $\alpha + \beta = 1$ there is discontinuity of the function $\theta_J(\alpha)$ at $\alpha = 0$, since $\theta_J(0) = \pi/4 \approx 0.7854$,
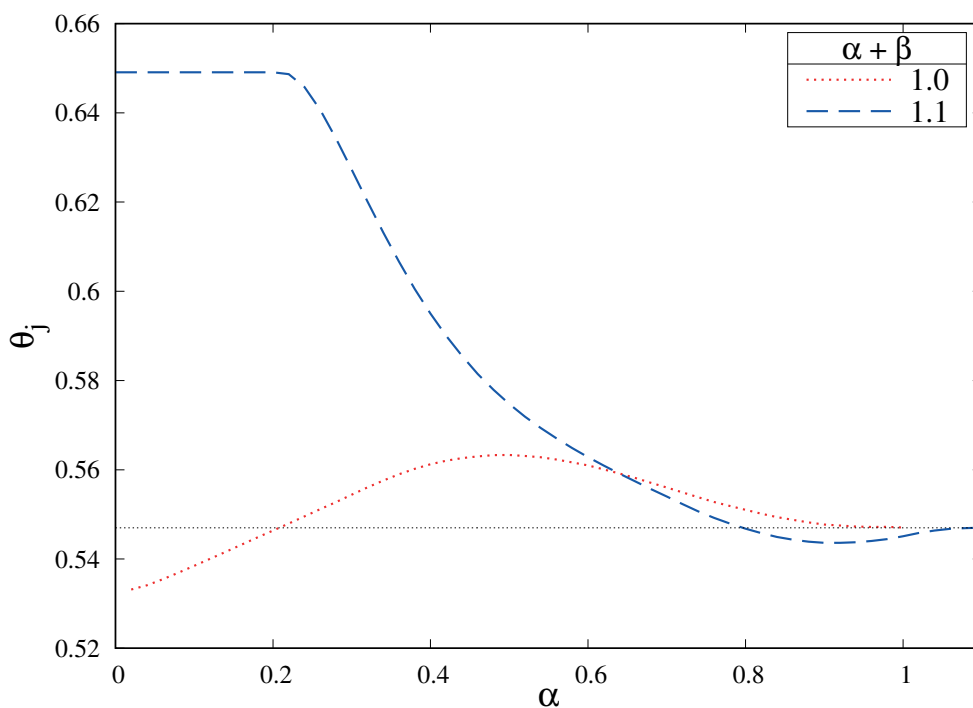
Figure 6.6: Jamming coverage θ_J as a function of cell size α (in units of the disk diameter d_0) for two values of separation distance $\alpha + \beta$, as indicated in the legend.

but $\lim_{\alpha \to 0^+} \theta_J(\alpha) < \theta_J^{\text{cont}} \approx 0.5472$.

6.3.2 Effects of varying α on the long-time adsorption kinetics

It is interesting that in the case when $\alpha + \beta = 1$, the approach to the jamming coverage θ_J is always algebraic, regardless of the size α of the landing cells. As can be seen from figure. 6.7, we find that for $\alpha \geqslant 0.02$ the coverage θ reaches a power-law time-behaviour (6.2) within the length of the simulation. If a cell size α decreases, the value $\beta + \alpha/2$ increases and gets closer to unity when the condition (6.3) ceases to be valid. For very small cells ($\alpha \gtrsim 0$), the coverage growth is slowed down by the creation of a smaller fraction of the layer that is available for the insertion of a new particle. Consequently, when cell size α decreases the onset of long-time power-law behaviour (6.2) shifts to later times (figure 6.7). Generally, this effect occurs when the geometry of the pattern is close to the condition (6.4). In this case, it was necessary to increase the size of the substrate (typically 1024×1024 cells) to gain a convincing confirmation of the power-law approach of the coverage fraction $\theta(t)$ to the jamming limit θ_J at the very late times of the deposition process.

When $\alpha + \beta = 1.1$, although there is no change of jamming coverage θ_J for $\alpha < 0.2$ (figure 6.6), changes in the dynamics of deposition are obvious (see figure 6.8). The criteria (6.3) is satisfied for $\alpha > 0.2$ and then the approach to the jamming limit is consistent with the power law behavior given by equation (6.2). As seen from figure (6.8)(a), at the late times of the deposition process the plots of $d\theta/dt$ vs. t are linear on a double logarithmic scale with the slope of -3/2 for all $\alpha > 0.2$. However, the
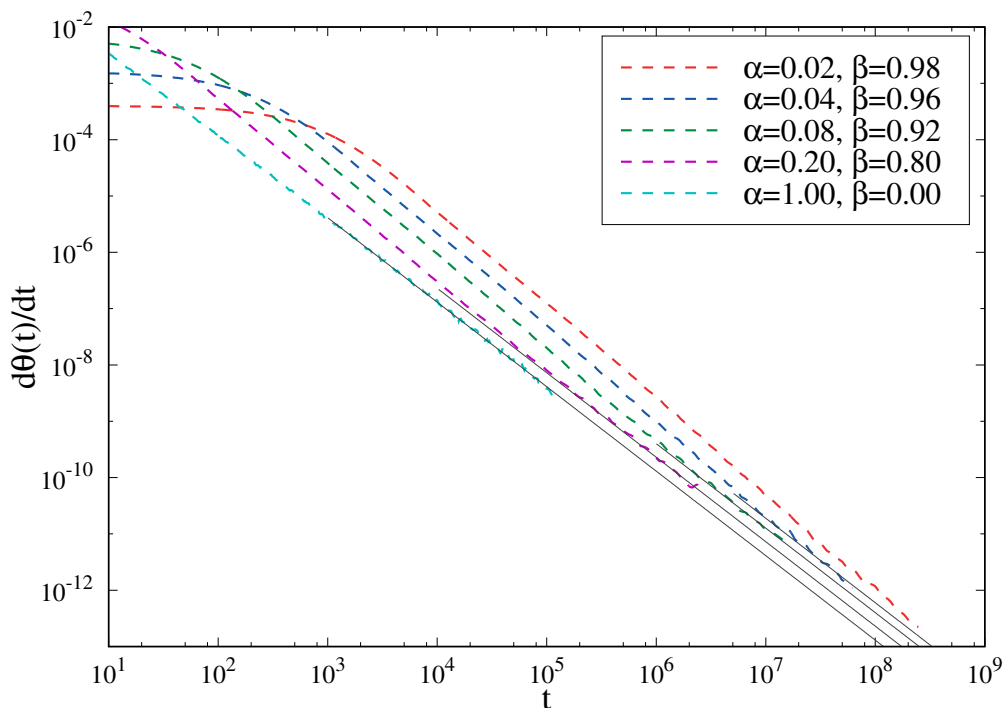
Figure 6.7: Test for the presence of the algebraic law (6.2) in the approach of the coverage $\theta(t)$ to the jamming limit θ_J for different values of parameters α and β that satisfy the condition $\alpha + \beta = 1$ (see legend). Straight-line sections of the curves show where the law holds. The solid straight lines have the slope $-3/2$ and are guides for the eye.

(a)   (b)
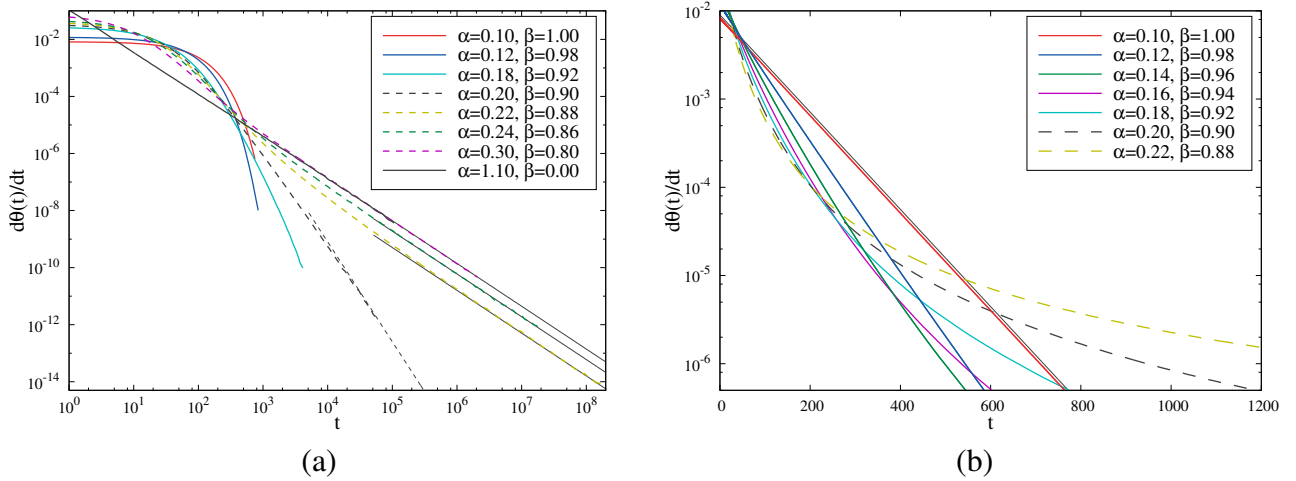
Figure 6.8: Plots of the time derivative of coverage $d\theta/dt$ for different values of parameters α and β that satisfy the condition $\alpha + \beta = 1.1$ (see legends): (a) results are shown on a double logarithmic scale. Solid straight lines have the slope $-3/2$ and are guides for the eye. Dashed straight line has slope -5/2 indicating the late time RSA behavior of the system for the critical value of parameter β, $\beta_c = 0.20$ (see equation (6.4)); (b) results for $\alpha \leqslant 0.22$ are shown on a semi-logarithmic scale. Slanted straight line is shown, indicating the exponential approach to the jamming limit (equation (6.1)), where $\sigma = 78.8$.

slope of $d\theta/dt$ abruptly changes to $\approx -5/2$ when the cell size α reaches the critical value of $\alpha = 0.2$ (see equation (6.4)). By reducing the size of cells below the critical value $\alpha = 0.2$, algebraic approach disappears. Under conditions when the cell size α decreases towards non-interacting condition ($\alpha \to 0.10^+$, $\beta \to 1.0^-$), asymptotic approach of the coverage fraction $\theta(t)$ to its jamming limit θ_J becomes closer to the exponential law (6.1) (see figure 6.8(b)).

6.4 Structural properties of the jammed state

To gain additional insight into the late time kinetics of the deposition process onto a nonuniform substrate, it is useful to analyze in particular the spatial distribution of particles inside the cells. In figures. 6.9, 6.10, and 6.11 we show the spatial distribution of particles inside the cell at the jammed state, for $\alpha = 0.3$, 0.5 and 0.7, respectively, and the twelve different values of parameter $\beta \in [0.02$ 0.98]. To calculate these probability distributions, we divided cell space in mesh with 40×40 bins and counted the number of particles falling into bins. The data are averaged over 100 independent runs for each of the investigated substrate patterns with 256×256 landing cells. Spatial distribution of particles shown in figures 6.9 – 6.11 are accompanied by corresponding radial distribution functions $g(r)$ (or pair-correlation functions) defined as

$$g(r) = \frac{S}{N^2} \left\langle \sum_{i=1}^{N} \sum_{j=1}^{N} \delta \left[\vec{r} - (\vec{r}_j - \vec{r}_i) \right] \right\rangle, \tag{6.6}$$

where $\vec{r}$ is the position vector of a point over the adsorption plane (measured from the centre of an adsorbed particle), δ is the Dirac delta function, $\vec{r}_i$ and $\vec{r}_j$ are the position vectors of the particles i

and j, respectively, and angle brackets mean the ensemble average. Here, S is the surface area, and N is the total number of particles adsorbed over this area. Radial distribution $g(r)$ gives information about the long-range inter-particle correlations and their organization [15, 47]. This function can be interpreted as an averaged probability of finding a particle at the distance r from another particle, with the centre located at $r = 0$. For sake of convenience, the distance r is usually normalized by using the particle radius $d_0/2$ as a scaling variable. In the absence of external forces, when the system can be considered isotropic, the vector $\vec{r}$ can be replaced with the radial coordinate r and the pair correlation function may be calculated more directly by converting equation (6.6) to the form

$$g(r) = \frac{S}{N} \frac{\overline{N}_a(r)}{2\pi r \Delta r}, \tag{6.7}$$

where $\overline{N}_a$ is the averaged number of particles within the annulus of the radius r and the thickness Δr.

To discuss the effect of the parameter β on the spatial distribution of particles inside the cell at the jammed state, let us first consider the fixed value $\alpha = 0.3$, with varying $\beta = 0.02 - 0.98$, as shown in figure 6.9. In the case of the ICCA regime, the temporal evolution of the coverage $\theta(t)$ towards its jamming state value θ_J is a two-stage process. At very early times of the process, when the coverage fraction is small, the coverage grows rapidly in time. Particles adsorbed during this stage are homogeneously distributed in the cells. At a late enough time, when the coverage fraction is sufficient to make the geometry of the unoccupied substrate complex, the growth of the coverage fraction $\theta(t)$ requires the filling of holes that are large enough for the insertion of an additional particle. Consequently, the structure of the spatial distribution of particles inside the cell is determined by the late stage of the deposition process. For $\beta \leqslant 0.02$, particles are distributed uniformly throughout the whole substrate and the shape of radial distribution $g(r)$ is the same as in the case of RSA of disks on a continuous substrate. Since the cell-cell excluded volume interaction is changing with β, the spatial distribution of particles inside the cell reveals various preferential regions. From the probability distribution plots in figure 6.9, we can identify various regions such as corners (f), sides (g), interior ring (h), central square (i), central peak (j), etc., that are predominantly populated with particles. For β below the critical value β_c (equation (6.4)) particles adsorb preferentially at the cell edges. Approaching the critical value of $\beta_c = 0.85$ ($\alpha = 0.30$), the probability of deposition in the centre of a cell increases. Close to the critical value, we observe the appearance of a pronounced peak of probability distribution in the centre of the cell. In addition, as parameter β is increased, one observes that the radial distribution functions $g(r)$ become more detailed with peaks becoming sharper. There is also peak splitting, related to a weaker excluded volume interaction between particles deposited into different cells. For the large $\beta = 0.98$, since adsorption on an empty cell is weakly constrained by particles previously adsorbed on a neighbouring one, adsorption can occur, with almost equal probability all over the cell (figure 6.9(l)). The radial distribution function now shows a series of well-developed peaks which correspond to the various cell-defined distances in the square lattice matrix. Finally, in the NICCA regime ($\beta > 1$), the adsorption inside cells is entirely uniform and the shape of the radial distribution function $g(r)$ is no longer changing (not shown here).

Numerical simulations for the other cell sizes, $\alpha = 0.5$, 0.7, produce qualitatively similar results for the spatial distribution of particles inside the cell leading to qualitatively the same phenomenology (see figures 6.10 and 6.11). However, increasing the value of α in the NICCA-SPCA regime increases the uncertainty in the position of the particle within the cell, i.e., it leads to peak broadening of the radial distribution function $g(r)$.
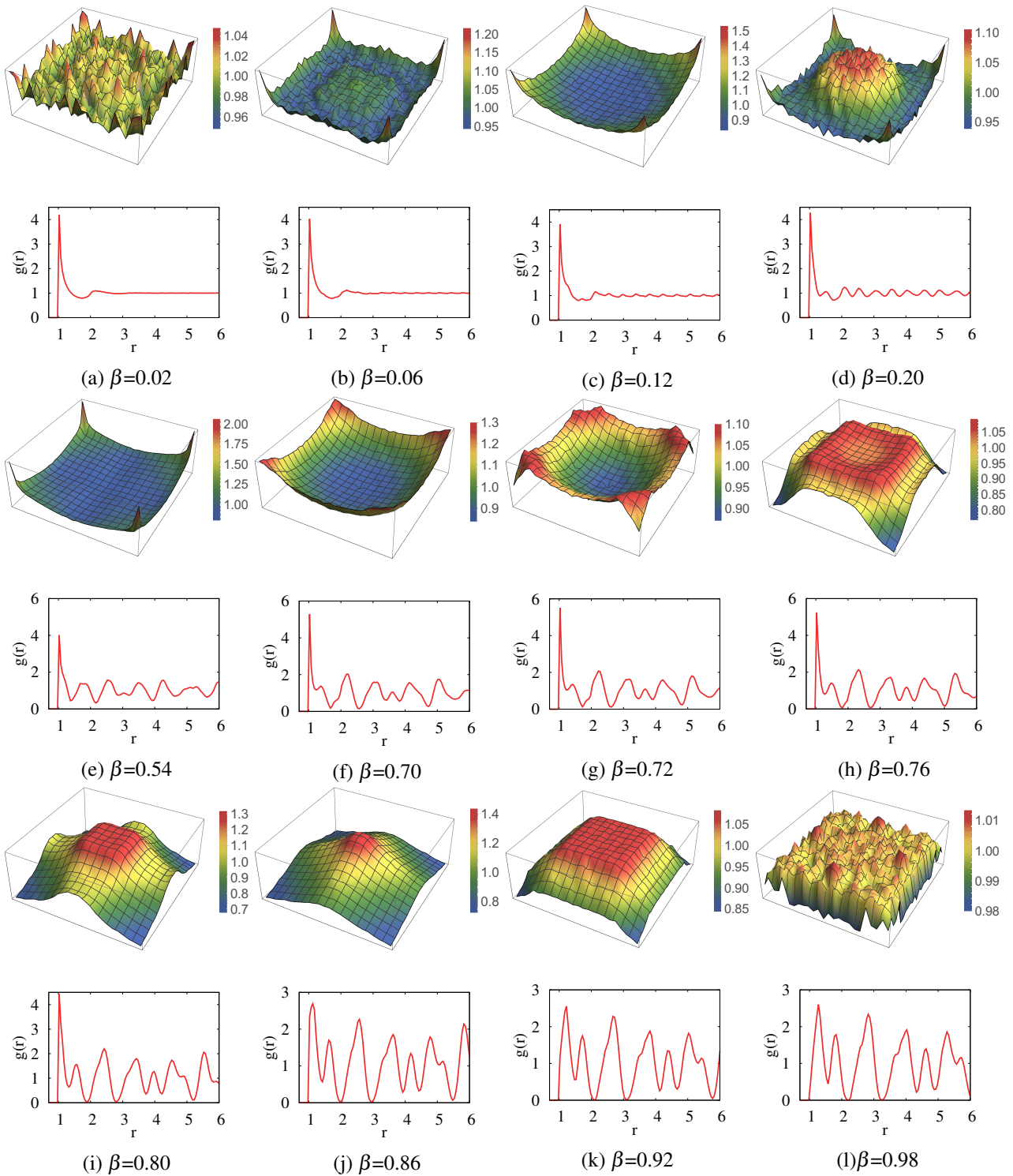
Figure 6.9: Spatial distribution of particles inside the cell and radial distribution function $g(r)$ at the jammed state, for the fixed value of cell size $\alpha = 0.3$ and different values of parameter β.
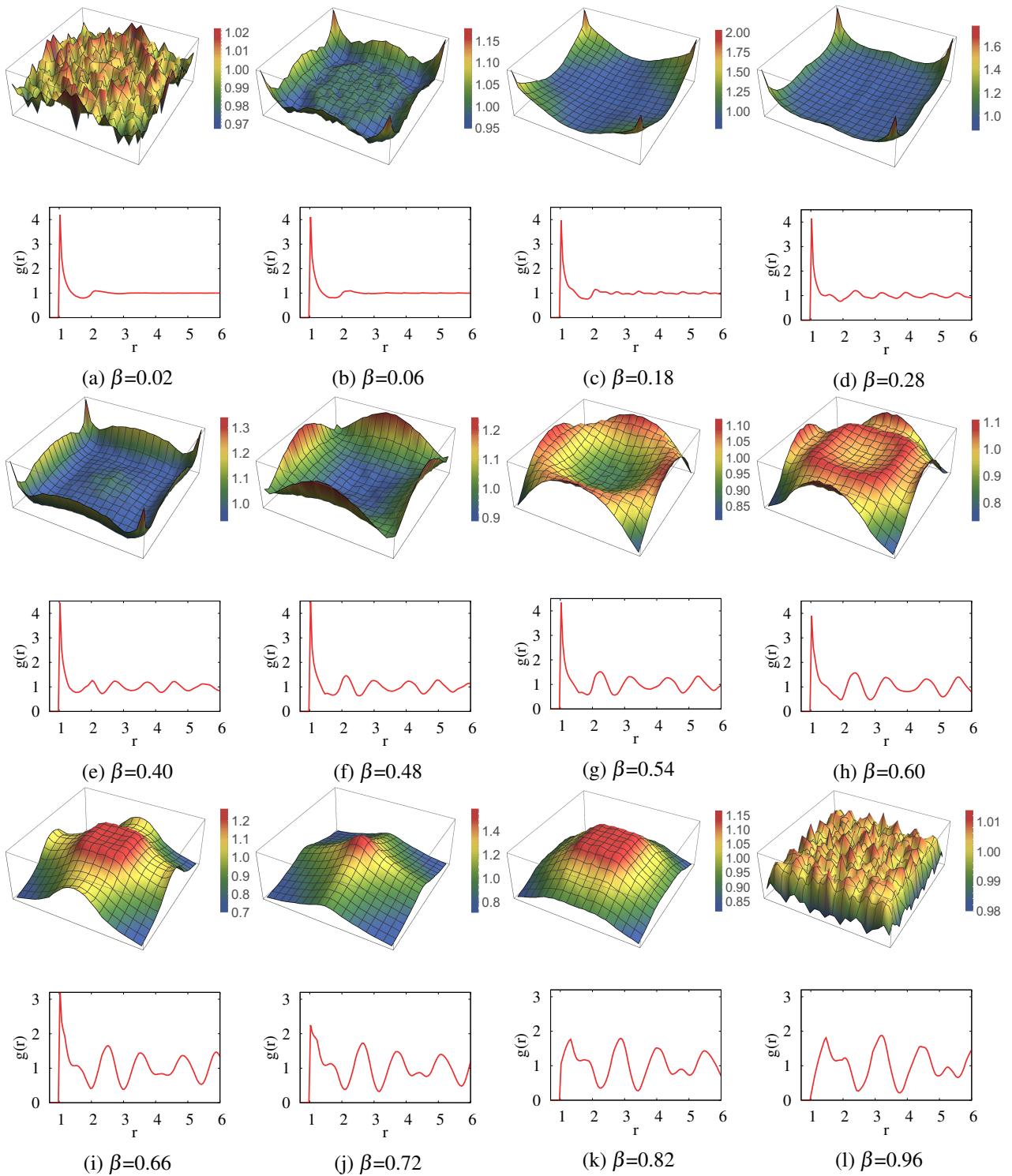
Figure 6.10: Spatial distribution of particles inside the cell and radial distribution function $g(r)$ at the jammed state, for the fixed value of cell size $\alpha = 0.5$ and different values of parameter β.
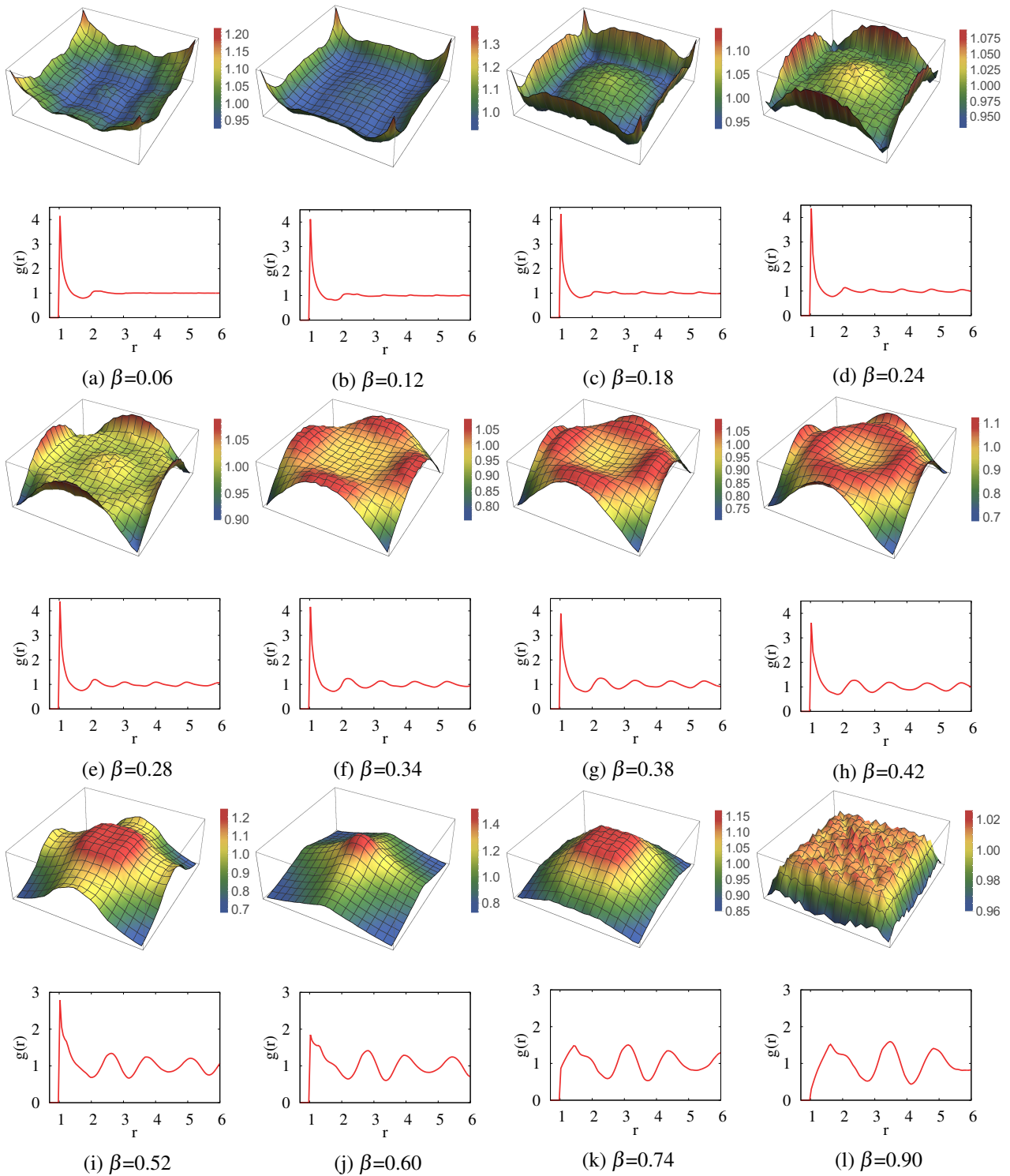
Figure 6.11: Spatial distribution of particles inside the cell and radial distribution function $g(r)$ at the jammed state, for the fixed value of cell size $\alpha = 0.7$ and different values of parameter β.

Chapter 7

Conclusions

In this thesis, we have used the Random Sequential Adsorption model to numerically investigate the deposition of identical spherical particles of fixed radius onto a flat heterogeneous substrate. A surface heterogeneities consisted of square or elongated rectangle adsorption cells with the typical geometrical cell length comparable with the size of the particles. A particle is irreversibly adsorbed at a random position on the substrate if it does not overlap any of previously adsorbed particles and if it touches one of the cells on the substrate. The equivalent model is the adsorption of two-dimensional disks (sphere projections), without overlapping already adsorbed disks and with a condition that the disk centres lie in the adsorption cells. We studied the influence of the cell size, density and arrangement of the landing cells and emphasized the influence of substrate inhomogeneities on the coverage growth rate and the geometry of the final (jammed) state. It was shown that manipulation of the substrate pattern can yield monolayer deposits with desired properties.

In the first part of this thesis research, we presented the results of numerical simulations of RSA deposition on randomly patterned substrates, with a focus on the jammed-state properties. We found that for a given density of landing cells, the highest jamming coverage and the fastest kinetics of the deposition process can be achieved in the single-particle per-cell adsorption (SPCA) case. Because the densification kinetics is dictated by geometric exclusion effects, the coverage kinetics is severely slowed down in the multiple-particles per-cell adsorption (MPCA) case.

To examine the short scale structure in the jammed-state coverings, we evaluated the radial correlation function $g(r)$ which measures the particle density-density correlation at distance r for various shapes and sizes of the landing cells. The oscillation of $g(r)$ quickly decays for all densities of landing cells $\theta_0^{(cell)}$, which means that long-range order does not exist in the system. In the MPCA case, the peak of $g(r)$ which appears at a unit distance is the most pronounced for low densities of landing cells $\theta_0^{(cell)}$. This is opposite to what is observed under SPCA conditions when the shape of radial distribution $g(r)$ is more structured at higher adsorption cell densities $\theta_0^{(cell)}$.

The morphology of deposited disks has been analyzed through the distribution of pore volumes. The pore is defined as the free area of a Delaunay triangle. Its volume distribution is sensitive to small structural changes in the covering and it, therefore, describes the degree to which the cell size and cell density affect the deposit morphology. We have found that pore volumes have a distribution

with a long tail, particularly at low densities of adsorption cells $\theta_0^{(cell)}$. The distribution $P(v)$ becomes narrower and more localized around the low values of volumes v with the increase of cell density $\theta_0^{(cell)}$. In the case of the largest cells that we examined ($\alpha_4 = \sqrt{2}$), we observed the pronounced peak of distribution $P(v)$ at low values of volume $v = 0.15 - 0.20$, which appears due to the presence of configurations with three or more disks on a single landing cell. We have also studied the influence of a regular substrate pattern on the volume distribution of the pores $P(v)$. At low cell densities, $\theta_0^{(cell)}$, distribution function $P(v)$ shows well-developed peaks which correspond to the various types of Delaunay triangles. A triangle can have three or two vertices in the same cell or all three vertices in three different cells. Cell-cell excluded volume interaction increases with the cell density $\theta_0^{(cell)}$ so that distribution $P(v)$ for regular substrate pattern of squares becomes similar to distribution $P(v)$ for random pattern case at densities near the jamming limit of adsorption cells.

Numerical simulations of Random Sequential Adsorption on heterogeneous substrates composed of elongated rectangular adsorption cells have shown that the shape of the pore distribution function $P(v)$ is affected by the anisotropy in the deposition procedure for landing cells. It is shown that anisotropic deposition of landing cells lowers the average cell population and reduces the number of small pores. Our results suggest that the porosity of deposit (pore volumes) can be controlled by the size and shape of landing cells, and by the anisotropy of the cell deposition procedure. The radial correlation function $g(r)$ for jamming coverings of disks corresponding to anisotropic deposition of rectangles is quite similar to $g(r)$ for the case of the isotropic landing-cell pattern.

The second part of this thesis research considered a pattern with the equal square cells, positioned in a square-lattice matrix. Analysis of numerical simulation of RSA of disk-shaped particles is focused on the kinetics of the deposition process in the interacting cell-cell adsorption (ICCA) regime. An efficient numerical algorithm was implemented to simulate the disk deposition in the case of single-particle per-cell adsorption (SPCA).

It was demonstrated that the two geometrical parameters, the cell size α and the cell-cell separation β, have a striking influence on the kinetic properties of a deposition process, as well as on the in-cell particle population. By studying the temporal evolution of the first derivative of coverage $\theta(t)$ we have found that the asymptotic approach of the coverage fraction $\theta(t)$ to its jamming limit θ_J is algebraic if the parameters α and β satisfy the simple condition $\beta + \alpha/2 < 1$. If this relation is valid, particles adsorbed on neighbouring cells can block adsorption inside the central cell, so that there is no minimum finite area available for adsorption. A vanishing-small area can be created with non-zero probability and an asymptotic approach to the jamming limit in the late stage of the deposition process obeys the power law.

If the geometry of the pattern does not satisfy the criteria $\beta + \alpha/2 < 1$, the approach of the coverage fraction $\theta(t)$ to the jamming limit is not consistent with the power-law behaviour. The existence of the minimum finite area where the centre of a disk can land without overlapping a previously adsorbed particle is a sufficient condition for deviation from the algebraic asymptotic approach. When the geometry of the pattern approaches towards non-interacting condition ($\beta \to 1.0^-$), the asymptotic approach of the coverage fraction $\theta(t)$ to its jamming limit θ_J becomes closer to the exponential law. It must be stressed that the appearance of even a slight cell-cell excluded volume interaction violates the exponential asymptotic approach. Consequently, changing the pattern in our numerical model allows interpolating the deposition kinetics between the continuum limit and the lattice-like behaviour.

We found that the asymptotic approach obeys a power-law t^{-p} with a different exponent $p = 3/2$ on the critical line in the parameter phase space (α, β), determined by equation $\beta + \alpha/2 = 1$. This line is the boundary of the standard power-law asymptotic behaviour phase with $p = 1/2$. A similar anomalous power-law approach was reported in the literature for the case of adsorption on a one-dimensional imprecise substrate [2, 42]. We are the first to observe and document this kind of behaviour in two-dimensional RSA systems. In one dimension, this behaviour is explained by a different kind of small hole size distribution in the late phase of the process. For the normal power-law approach, this distribution is constant in the limit of the hole size zero, while for the anomalous power-law approach the small hole distribution vanishes linearly in the same limit. The distribution of holes available for particle adsorptions in the late phase of the process for adsorption on a two-dimensional imprecise lattice is out of the scope of this thesis and this topic could be addressed in further research.

To examine the short scale structure in the jammed-state coverings, we evaluated the spatial distribution of particles inside the cell and the radial distribution function $g(r)$. Interesting, non-trivial spatial distributions are observed, with local order resulting not only from the constraint of the pattern but also due to steric effects that make certain insertions of particles impossible owing to an effective high local density. Close to the critical values of parameter β determined with $\beta_c = 1 - \alpha/2$, we observe the appearance of the pronounced peak of probability distribution in the centre of the cell. Hence, by tuning the pattern parameters on the critical values, it is possible to obtain jammed-state covering with a highly ordered structure.

In the available literature, various models of thin-film formation were used to investigate the impact of particle properties on the kinetics of adsorption and the structure of the jammed state. With technological advances and the development of methods to modify substrate surfaces, more studies are devoted to the influence of the substrate on the deposition process. This direction of research is largely unexplored and leaves a lot of space for further research. For example, our research can be extended to different particle and cell shapes, as well as to different substrate patterns. The relaxation processes in the deposit formation with weaker particle-cell interaction play a more important role and can not be neglected. Inter-particle interactions, hydrodynamic interactions, and external forces like gravitation and electromagnetic forces can also be incorporated into an extended model. The experimental measurements of monolayer deposit formations are extremely difficult to realize, especially when it comes to kinetics. This makes numerical simulations an indispensable tool for advancing our understanding of the adsorption process.

Appendix A

Dense packing of equal disks in a square

In this work, we investigated the adsorption of equal hard disks on square cells of different sizes and arrangements. But what is the maximal number of disks that can fit into a square cell of a given size? Or stated differently, what is the minimal square cell that can contain centres of n non-overlapping disks? Finding and prooving the most optimal configuration might be easy for up to 5 disks, but the cases of 6 and more disks require more creativity and more profound mathematical knowledge.

This appendix lists the sizes of minimal squares that contain the centres of up to ten disks, along with the coordinates of disk centres in the optimal configuration (see figures A.1 - A.9). Next to each figure, we give the exact values [88–91], except for the case of 10 disks where we cite approximate numerical values proposed and proved by Groot et al. [92]. It is interesting that the optimal solution for $n = 10$ is not symmetric and the side of the minimal square is calculated as the smallest real root of the polynomial of degree 18.

Rigorous mathematical proofs exist for $n = 2$ to 30, and for $n = 36$. Best known solutions for up to $\approx 10^4$ disks are summarized in a web page maintained by Eckard Specht [93], most of which found numerically.
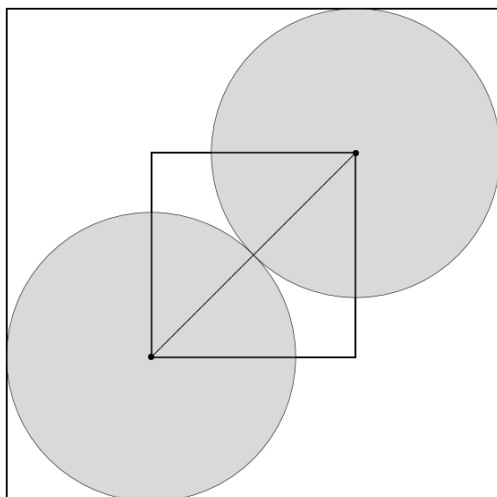
Figure A.1: Dense packing of $n = 2$ disks in a square

$a_2 = \sqrt{2}/2$
$P_1 = (0,\ 0)$
$P_2 = (\sqrt{2}/2,\ \sqrt{2}/2)$
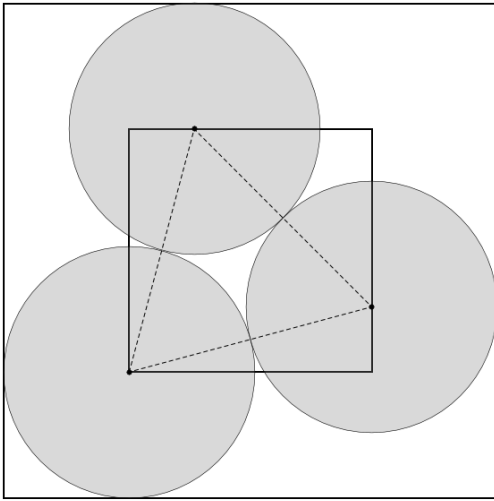
Figure A.2: Dense packing of $n = 3$ disks in a square

$a_3 = (\sqrt{6} + \sqrt{2})/4$
$P_1 = (0,\ 0)$
$P_2 = ((\sqrt{6} - \sqrt{2})/4,\ (\sqrt{6} + \sqrt{2})/4)$
$P_3 = ((\sqrt{6} + \sqrt{2})/4,\ (\sqrt{6} - \sqrt{2})/4)$
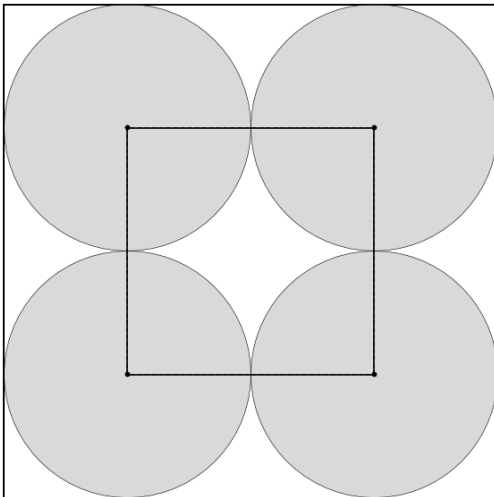
Figure A.3: Dense packing of $n = 4$ disks in a square

$a_4 = 1$
$P_1 = (0,\ 0)$
$P_2 = (0,\ 1)$
$P_3 = (1,\ 0)$
$P_4 = (1,\ 1)$
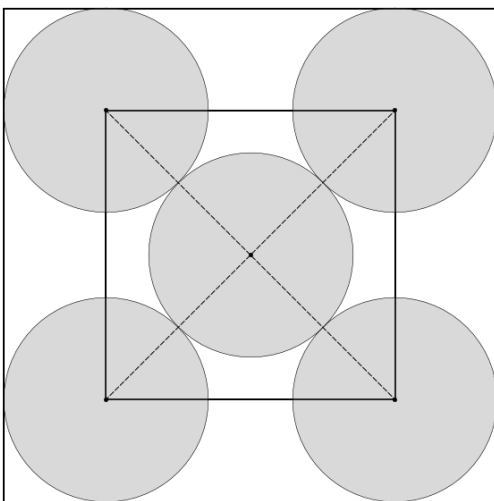
Figure A.4: Dense packing of $n = 5$ disks in a square

$a_5 = \sqrt{2}$
$P_1 = (0,\ 0)$
$P_2 = (\sqrt{2},\ \sqrt{2})$
$P_3 = (0,\ \sqrt{2})$
$P_4 = (\sqrt{2},\ 0)$
$P_5 = (\sqrt{2}/2,\ \sqrt{2}/2)$
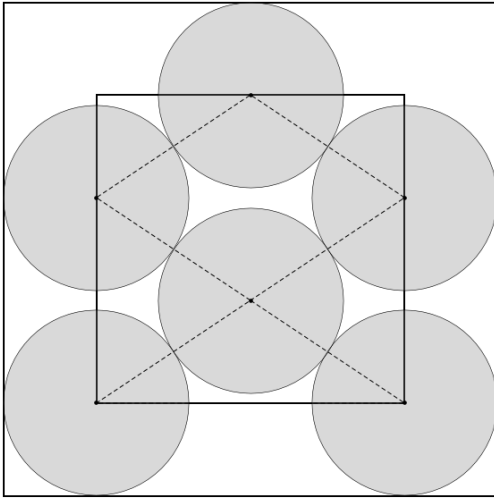
Figure A.5: Dense packing of $n = 6$ disks in a square

$a_6 = \frac{6}{\sqrt{13}}$
$P_1 = (0, 0)$
$P_2 = \left(\frac{6}{\sqrt{13}}, 0\right)$
$P_3 = \left(\frac{3}{\sqrt{13}}, \frac{2}{\sqrt{13}}\right)$
$P_4 = \left(0, \frac{4}{\sqrt{13}}\right)$
$P_5 = \left(\frac{6}{\sqrt{13}}, \frac{4}{\sqrt{13}}\right)$
$P_6 = \left(\frac{3}{\sqrt{13}}, \frac{6}{\sqrt{13}}\right)$
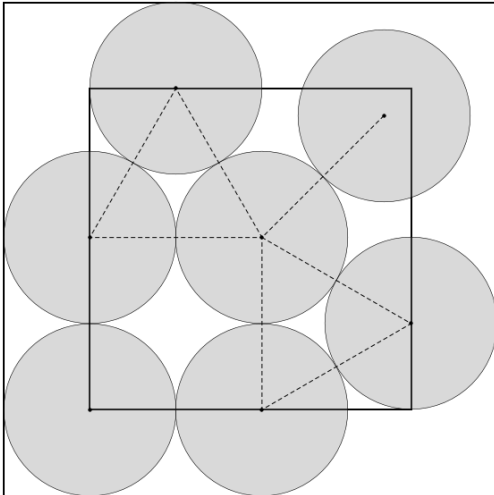
Figure A.6: Dense packing of $n = 7$ disks in a square

$a_7 = 1 + \sqrt{3}/2$
$P_1 = (0, 0)$
$P_2 = (1, 0)$
$P_3 = (1, 1)$
$P_4 = (0, 1)$
$P_5 = (1 + \sqrt{3}/2, 1/2)$
$P_6 = (1/2, 1 + \sqrt{3}/2)$
$P_7 = (1 + \sqrt{2}/2, 1 + \sqrt{2}/2)$
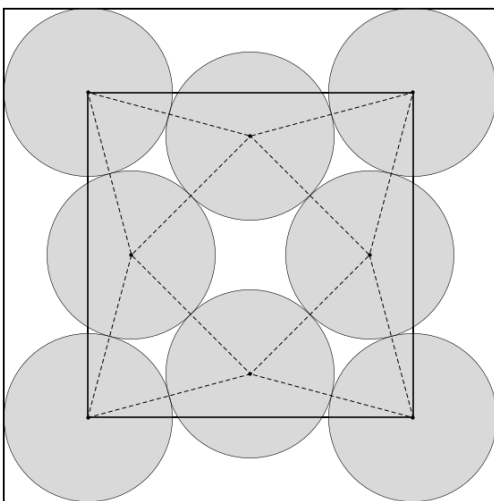
Figure A.7: Dense packing of $n = 8$ disks in a square

$a_8 = (\sqrt{6} + \sqrt{2})/2$
$P_1 = (0, 0)$
$P_2 = ((\sqrt{6} + \sqrt{2})/2, 0)$
$P_3 = ((\sqrt{6} + \sqrt{2})/2, (\sqrt{6} + \sqrt{2})/2)$
$P_4 = (0, (\sqrt{6} + \sqrt{2})/2)$
$P_5 = ((\sqrt{6} + \sqrt{2})/4, (\sqrt{6} - \sqrt{2})/4)$
$P_6 = ((\sqrt{6} + \sqrt{2})/4, (\sqrt{6} + 3\sqrt{2})/4)$
$P_7 = ((\sqrt{6} - \sqrt{2})/4, (\sqrt{2} + \sqrt{6})/4)$
$P_8 = ((\sqrt{6} + 3\sqrt{2})/4, (\sqrt{6} + \sqrt{2})/4)$
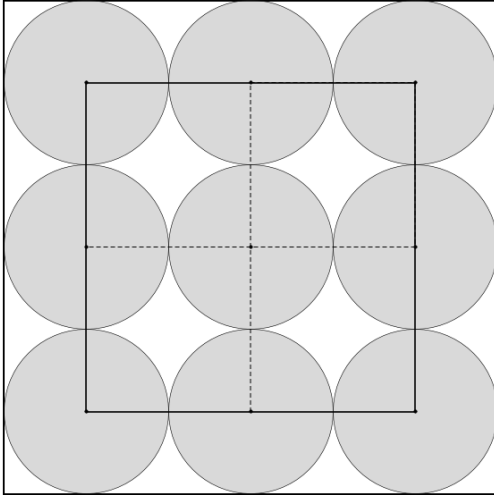
Figure A.8: Dense packing of $n = 9$ disks in a square

$a_9 = 2$
$P_1 = (0, 0)$
$P_2 = (0, 1)$
$P_3 = (0, 2)$
$P_4 = (1, 0)$
$P_5 = (1, 1)$
$P_6 = (1, 2)$
$P_7 = (2, 0)$
$P_8 = (2, 1)$
$P_9 = (2, 2)$
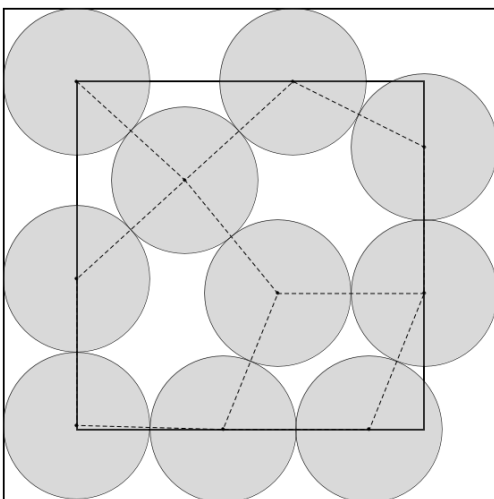
Figure A.9: Dense packing of $n = 10$ disks in a square

$a_{10} = 2.87372076161906$
$P_1 = (0, 0.027244965467)$
$P_2 = (0.999628787029, 0)$
$P_3 = (1.999628787029, 0)$
$P_4 = (1.373720761619, 0.927391607978)$
$P_5 = (2.373720761619, 0.927391607978)$
$P_6 = (0, 1.027244965467)$
$P_7 = (0.739425948012, 1.700482863543)$
$P_8 = (2.373720761619, 1.927391607977)$
$P_9 = (0, 2.373720761619)$
$P_{10} = (1.478851896025, 2.373720761619)$

References

[1] V. Privman and H. Yan, *Random sequential adsorption on imprecise lattice*, The Journal of Chemical Physics **144**, 244704, (2016).

[2] A. Verma and V. Privman, *Nonstandard convergence to jamming in random sequential adsorption: The case of patterned one-dimensional substrates*, Physica A: Statistical Mechanics and its Applications **491**, 560–573, (2018).

[3] I. R. Epstein, *Kinetics of large-ligand binding to one-dimensional lattices: theory of irreversible binding*, Biopolymers **18**, 765–788, (1979).

[4] P. R. Van Tassel, P. Viot, and G. Tarjus, *A kinetic model of partially reversible protein adsorption*, The Journal of Chemical Physics **106**, 761–770, (1997).

[5] J. Feder, *Random sequential adsorption*, J. Theoret. Biol. **87**, 237–254, (1980).

[6] S. Ravichandran and J. Talbot, *Mobility of Adsorbed Proteins: A Brownian Dynamics Study*, Biophysical Journal **78**, 110–120, (2000).

[7] V. Privman, *Recent Theoretical Results for Nonequilibrium Deposition of Submicron Particles*, The Journal of Adhesion **74**, 421–440, (2000).

[8] J. A. Liddle, Y. Cui, and P. Alivisatos, *Lithographically directed self-assembly of nanostructures*, Journal of Vacuum Science & Technology B: Microelectronics and Nanometer Structures Processing, Measurement, and Phenomena **22**, 3409–3414, (2004).

[9] A. V. Subashiev and S. Luryi, *Random sequential adsorption of shrinking or expanding particles*, Phys. Rev. E **75**, 011123, (2007).

[10] O. Gromenko and V. Privman, *Random sequential adsorption of objects of decreasing size*, Phys. Rev. E **79**, 011104, (2009).

[11] R. D. Deshmukh, G. A. Buxton, N. Clarke, and R. J. Composto, *Nanoscale Block Copolymer Templates Decorated by Nanoparticle Arrays*, Macromolecules **40**, 6316–6324, (2007).

[12] J. W. Evans and D. R. Burgess, *Irreversible reaction on a polymer chain with range two cooperative effects*, The Journal of Chemical Physics **79**, 5023–5028, (1983).

[13] J. F. Marques, A. B. Lima, N. A. M. Araújo, and A. Cadilhe, *Effect of particle polydispersity on the irreversible adsorption of fine particles on patterned substrates*, Phys. Rev. E **85**, 061122, (2012).

[14] O. Gromenko, V. Privman, and M. L. Glasser, *Random Sequential Adsorption Model of Damage and Crack Accumulation: Exact One-Dimensional Results*, Journal of Computational and Theoretical Nanoscience **5**, 2119–2123, (2008).

[15] J. W. Evans, *Random and cooperative sequential adsorption*, Rev. Mod. Phys. **65**, 1281 – 1329, (1993).

[16] V. Privman (Ed.), *Nonequilibrium Statistical Mechanics in One Dimension*, Cambridge University Press, Cambridge, UK, 1997.

[17] P. J. Flory, *Intramolecular Reaction between Neighboring Substituents of Vinyl Polymers*, J. Am. Chem. Soc. **61**, 1518, (1939).

[18] A. Rènyi, *On a One-Dimensional Problem Concerning Random Space-Filling*, Publ. Math. Inst. Hung. Acad. Sci. **3**, 109–127, (1958).

[19] B. Widom, *Random Sequential Addition of Hard Spheres to a Volume*, The Journal of Chemical Physics **44**, 3888–3894, (1966).

[20] R. D. Vigil and R. M. Ziff, *Random sequential adsorption of unoriented rectangles onto a plane*, The Journal of Chemical Physics **91**, 2599–2602, (1989).

[21] J. Talbot, G. Tarjus, and P. Schaaf, *Unexpected asymptotic behavior in random sequential adsorption of nonspherical particles*, Phys. Rev. A **40**, 4808–4811, (1989).

[22] P. Viot and G. Tarjus, *Random Sequential Addition of Unoriented Squares: Breakdown of Swendsen's Conjecture*, Europhysics Letters (EPL) **13**, 295–300, (1990).

[23] J. D. Sherwood, *Random sequential adsorption of lines and ellipses*, Journal of Physics A: Mathematical and General **23**, 2827–2833, (1990).

[24] R. M. Ziff and R. D. Vigil, *Kinetics and fractal properties of the random sequential adsorption of line segments*, J. Phys. A: Math. Gen. **23**, 5103 – 5108, (1990).

[25] R. D. Vigil and R. M. Ziff, *Kinetics of random sequential adsorption of rectangles and line segments*, The Journal of Chemical Physics **93**, 8270–8272, (1990).

[26] B. J. Brosilow, R. M. Ziff, and R. D. Vigil, *Random sequential adsorption of parallel squares*, Phys. Rev. A **43**, 631–638, (1991).

[27] S. S. Manna and N. M. Švrakić, *Random sequential adsorption: line segments on the square lattice*, J. Phys. A: Math. Gen. **24**, L671 – L676, (1991).

[28] N. M. Švrakić and M. Henkel, *Kinetics of irreversible deposition of mixtures*, J. Phys. I France **1**, 791–795, (1991).

[29] P. Viot, G. Tarjus, S. M. Ricci, and J. Talbot, *Random sequential adsorption of anisotropic particles. I. Jamming limit and asymptotic behavior*, J. Chem. Phys. **97**, 5212, (1992).

[30] P. Meakin and R. Jullien, *Random-sequential adsorption of disks of different sizes*, Phys. Rev. A **46**, 2029–2038, (1992).

[31] B. Bonnier, Y. Leroyer, and E. Pommiers, *Random sequential adsorption of line segments: universal properties of mixtures in 1, 2 and 3D lattices*, J. Phys. I France **2**, 379–384, (1992).

[32] Z. Adamczyk, B. Siwek, M. Zembala, and P. Weroński, *Influence of Polydispersity on Random Sequential Adsorption of Spherical Particles*, Journal of Colloid and Interface Science **185**, 236–244, (1997).

[33] Z. Adamczyk, B. Siwek, and P. Weroński, *NOTE:Adsorption of colloid particles at partially covered surface*, Journal of Colloid and Interface Science **195**, 261–263, (1997).

[34] Z. Adamczyk and P. Weroński, *Random sequential adsorption on partially covered surfaces*, The Journal of Chemical Physics **108**, 9851–9858, (1998).

[35] J. W. Lee, *Irreversible random sequential adsorption of mixtures*, Colloids Surf. A **165**, 363 – 372, (2000).

[36] B. Bonnier, *Random sequential adsorption of binary mixtures on a line*, Phys. Rev. E **64**, 066111, (2001).

[37] G. Kondrat, *The effect of impurities on jamming in random sequential adsorption of elongated objects*, The Journal of Chemical Physics **124**, 054713, (2006).

[38] P. B. Shelke, M. D. Khandkar, A. G. Banpurkar, S. B. Ogale, and A. V. Limaye, *Universality of the power-law approach to the jamming limit in random sequential adsorption dynamics*, Phys. Rev. E **75**, 060601, (2007).

[39] M. Cieśla, G. Pająk, and R. M. Ziff, *Shapes for maximal coverage for two dimensional random sequential adsorption*, Phys. Chem. Chem. Phys. **17**, 24376–24381, (2015).

[40] L. Reeve and J. Wattis, *Random sequential adsorption with two components: Asymptotic analysis and finite size effects*, Journal of Physics A: Mathematical and Theoretical **48**, (2015).

[41] X. Jin, N. H. L. Wang, G. Tarjus, and J. Talbot, *Irreversible adsorption on non-uniform surfaces: the random site model*, J. Chem. Phys. **97**, 4256, (1993).

[42] B. Bonnier, Y. Leroyer, and E. Pommiers, *Random sequential adsorption on a dashed line*, Journal of Physics A: Mathematical and General **28**, 1847–1860, (1995).

[43] Z. Adamczyk, P. Weroński, and E. Musiał, *Irreversible adsorption of hard spheres at random site (heterogeneous) surfaces*, J. Chem. Phys. **116**, 4665, (2002).

[44] Z. Adamczyk, P. Weroński, and E. Musiał, *Colloid Particle Adsorption at Random Site (Heterogeneous) Surfaces*, Journal of Colloid and Interface Science **248**, 67–75, (2002).

[45] N. A. M. Araújo, A. Cadilhe, and V. Privman, *Morphology of fine-particle monolayers deposited on nanopatterned substrates*, Phys. Rev. E **77**, 031603, (2008).

[46] Z. Adamczyk, *Particles at Interfaces: Interactions, Deposition, Structure*, Interface Science and Technology 9. Elsevier, Academic Press, 2006, ISBN 9780123705419.

[47] T. M. Truskett, S. Torquato, S. Sastry, P. G. Debenedetti, and F. H. Stillinger, *Structural precursor to freezing in the hard-disk and hard-sphere systems*, Phys. Rev. E **58**, 3083–3088, (1998).

[48] E. L. Hinrichsen, J. Feder, and T. Jøssang, *Geometry of random sequential adsorption*, J. Stat. Phys. **44**, 793–827, (1986).

[49] R. H. Swendsen, *Erratum: Dynamics of random sequential adsorption*, Phys. Rev. A **24**, 3285–3285, (1981).

[50] Y. Pomeau, *Some asymptotic estimates in the random parking problem*, J. Phys. A: Math. Gen. **13**, L193–L196, (1980).

[51] F. Downton, *A Note on Vacancies on a Line*, Journal of the Royal Statistical Society. Series B (Methodological) **23**, 207–214, (1961).

[52] E. S. Page, *The Distribution of Vacancies on a Line*, Journal of the Royal Statistical Society. Series B (Methodological) **21**, 364–374, (1959).

[53] N. A. M. Araújo and A. Cadilhe, *Gap-size distribution functions of a random sequential adsorption model of segments on a line*, Phys. Rev. E **73**, 051602, (2006).

[54] N. A. M. Araújo and A. Cadilhe, *Jammed state characterization of the random sequential adsorption of segments of two lengths on a line*, Journal of Statistical Mechanics: Theory and Experiment **2010**, P02019, (2010).

[55] P. Philippe and D. Bideau, *Numerical model for granular compaction under vertical tapping*, Phys. Rev. E **63**, 051304, (2001).

[56] P. Richard, P. Philippe, F. Barbe, S. Bourles, X. Thibault, and D. Bideau, *Analysis by x-ray microtomography of a granular packing undergoing compaction*, Phys. Rev. E **68**, 020301(R), (2003).

[57] T. Aste, *Variations around disordered close packing*, J. Phys.: Condens. Matter **17**, S2361 – S2390, (2005).

[58] T. Aste, *Volume fluctuations and geometrical constraints in granular packs*, Phys. Rev. Lett. **96**, 018002, (2006).

[59] D. Arsenović, S. B. Vrhovac, Z. M. Jakšić, L. Budinski-Petković, and A. Belić, *Simulation Study of Granular Compaction Dynamics under vertical tapping*, Phys. Rev. E **74**, 061302, (2006).

[60] P. Su and R. L. Scot Drysdale, *A comparison of sequential Delaunay triangulation algorithms*, Computational Geometry **7**, 361–385, (1997).

[61] C. B. Barber, D. P. Dobkin, and H. Huhdanpaa, *The quickhull algorithm for convex hulls*, ACM Trans. Math. Softw. **22**, 469, (1996).

[62] Wikipedia contributors, *Delaunay triangulation*, Wikipedia, The Free Encyclopedia , (2021).

[63] F. Aurenhammer, *Voronoi diagrams – A survey of a fundamental geometric data structure*, ACM Comput. Surv. **23**, 345, (1991).

[64] R. S. Nord and J. W. Evans, *Irreversible immobile random adsorption of dimers, trimers, ... on 2D lattices*, The Journal of Chemical Physics **82**, 2795–2810, (1985).

[65] R. Nord, *Irreversible random sequential filling of lattices by monte carlo simulation*, Journal of Statistical Computation and Simulation **39**, 231–240, (1991).

[66] K. J. Vette, T. W. Orent, D. K. Hoffman, and R. S. Hansen, *Kinetic model for dissociative adsorption of a diatomic gas*, The Journal of Chemical Physics **60**, 4854–4861, (1974).

[67] M. C. Bartelt and V. Privman, *Kinetics of irreversible multilayer adsorption: One-dimensional models*, J. Chem. Phys. **93**, 6820, (1990).

[68] Lj. Budinski-Petković and U. Kozmidis-Luburić, *Random sequential adsorption on a triangular lattice*, Phys. Rev. E **56**, 6904, (1997).

[69] Lj. Budinski-Petković, S. B. Vrhovac, and I. Lončarević, *Random sequential adsorption of polydisperse mixtures on discrete substrates*, Phys. Rev. E **78**, 061603, (2008).

[70] B. Bonnier, D. Boyer, and P. Viot, *Pair correlation function in random sequential adsorption processes*, Journal of Physics A: Mathematical and General **27**, 3671–3682, (1994).

[71] D. J. Burridge and Y. Mao, *Recursive approach to random sequential adsorption*, Phys. Rev. E **69**, 037102, (2004).

[72] P. Parisse, D. Luciani, A. D'Angelo, S. Santucci, P. Zuppella, P. Tucceri, A. Reale, and L. Otta-viano, *Patterning at the nanoscale: Atomic force microscopy and extreme ultraviolet interference lithography*, Mater. Sci. Eng. B **165**, 227–230, (2009).

[73] T. Kraus, L. Malaquin, H. Schmid, W. Riess, N. D. Spencer, and H. Wolf, *Nanoparticle printing with single-particle resolution*, Nat. Nanotechnol. **2**, 570–576, (2007).

[74] R. J. Kershner, L. D. Bozano, C. M. Micheel, A. M. Hung, A. R. Fornof, J. N. Cha, C. T. Rettner, M. Bersani, J. Frommer, P. W. K. Rothemund, and G. M. Wallraff, *Placement and orientation of individual DNA shapes on lithographically patterned surfaces*, Nat. Nanotechnol. **4**, 557–561, (2009).

[75] A. del Campo, C. Greiner, I. Alvarez, and E. Arzt, *Patterned Surfaces with Pillars with Controlled 3D Tip Geometry Mimicking Bioattachment Devices*, Adv. Mater. **19**, 1973–1977, (2007).

[76] X. Jin, J. Talbot, and N. H. L. Wang, *Analysis of steric hindrance effects on adsorption kinetics and equilibria*, AIChE J. **40**, 1685, (1994).

[77] C. Oleyar and J. Talbot, *Reversible adsorption on random site surface*, Physica A **376**, 27 – 37, (2007).

[78] Z. Adamczyk, B. Siwek, P. Weronski, and E. Musial, *Irreversible adsorption of colloid particles at heterogeneous surfaces*, Appl. Surf. Sci. **196**, 250, (2002).

[79] Z. Adamczyk, K. Jaszczółt, A. Michna, B. Siwek, L. Szyk-Warszyńska, and M. Zembala, *Irreversible adsorption of particles on heterogeneous surfaces*, Adv. Colloid Interface Sci. **118**, 25–42, (2005).

[80] A. Cadilhe, N. A. M. Araújo, and V. Privman, *Random sequential adsorption: from continuum to lattice and pre-patterned substrates*, J. Phys.: Condens. Matter **19**, 065124, (2007).

[81] N. Araújo, *Nonequilibrium thin-film growth: kinetics of deposition and post evolution relaxation*, LAP LAMBERT Academic Publishing, 2010, ISBN 9783838369419.

[82] M. Mascagni and A. Srinivasan, *Algorithm 806: SPRNG: a scalable library for pseudorandom number generation*, ACM Transactions on Mathematical Software **26**, 436–461, (2000).

[83] D. Stojiljković, J. R. Šćepanović, S. B. Vrhovac, and N. M. Švrakić, *Structural properties of particle deposits at heterogeneous surfaces*, Journal of Statistical Mechanics: Theory and Experiment **2015**, P06032, (2015).

[84] P. Nielaba, V. Privman, and J. S. Wang, *Journal of Physics A: Mathematical and General Kinetics of multilayer adsorption: Monte Carlo studies of models without screening*, J. Phys. A: Math. Gen. **23**, L1187, (1990).

[85] Lj. Budinski-Petković and U. Kozmidis-Luburić, *Jamming configurations for irreversible deposition on a square lattice*, Physica A **236**, 211 – 219, (1997).

[86] E. L. Hinrichsen, J. Feder, and T. Jøssang, *Random packing of disks in two dimensions*, Physical Review A **41**, 4199–4209, (1990).

[87] P. G. Szabó, M. C. Markót, T. Csendes, E. Specht, L. G. Casado, and I. García, *New approaches to circle packing in a square: with program codes*, volume 6, Springer Science & Business Media, 2007.

[88] B. Schwartz, *Separating points in a square*, J. of Recreational Mathematics **3**, 195–204, (1970).

[89] K. J. Nurmela and P. R. J. Östergård, *More Optimal Packings of Equal Circles in a Square*, Discrete & Computational Geometry **22**, 439–457, (1999).

[90] J. Schaer and A. Meir, *On a Geometric Extremum Problem*, Canadian Mathematical Bulletin **8**, 21–27, (1965).

[91] J. Schaer, *The Densest Packing of 9 Circles in a Square*, Canadian Mathematical Bulletin **8**, 273–277, (1965).

[92] C. Groot, R. Peikert, and D. Würtz, *The Optimal Packing of Ten Equal Circles in a Square*, IPS Research Report **90-12**, (1990).

[93] Eckard Specht, *The best known packings of equal circles in a square (up to N = 10000)*, 2018, http://hydra.nat.uni-magdeburg.de/packing/csq/.

Biography of the author

Danica Stojiljković was born on August 19th, 1981 in Kruševac, Serbia. She went to Mathematical high school in Belgrade, and subsequently, in 2000, started studies of Theoretical and experimental physics at the Faculty of Physics, University of Belgrade. She wrote her diploma thesis entitled "The method of efficent calculation of energy spectra in functional formalism", conducted under the mentorship of Dr. Aleksandar Bogojević and graduated in 2005 (GPA 9.93/10). In 2005 Danica Stojiljković started undergraduate studies in the department of "Theoretical physics of the condensed state of matter" at the Faculty of Physics, UoB. Under guidance of Dr. Aleksandar Bogojević she worked on the subjects of the functional formalism applications and development of Monte Carlo simulations. She started PhD studies in 2016 in the department of "Physics of condensed matter and statistical physics" at the Faculty of Physics, UoB, under the supervision of Dr. Slobodan Vrhovac. So far, Danica Stojiljković have published 5 research papers in peer-review international journals:

1. D. Stojiljkovic and S. B. Vrhovac, *Kinetics of Particle Deposition at Heterogeneous Surfaces*, Physica A 488, 16-29 (2017)
2. J. R. Scepanovic, D. Stojiljkovic, Z. M. Jaksic, Lj. Budinski-Petkovic, and S. B. Vrhovac, *Response Properties in the Adsorption-desorption Model on a Triangular Lattice*, Physica A 451, 213 (2016)
3. D. Stojiljkovic, J. R. Scepanovic, S. B. Vrhovac, and N. M. Svrakic, *Structural Properties of Particle Deposits at Heterogeneous Surfaces*, J. Stat. Mech.-Theory Exp. 2015, P06032 (2015)
4. A. Balaz, I. Vidanovic, D. Stojiljkovic, D. Vudragovic, A. Belic, and A. Bogojevic, *SPEEDUP Code for Calculation of Transition Amplitudes Via the Effective Action Approach*, Commun. Comput. Phys. 11, 739 (2012)
5. D. Stojiljkovic, A. Bogojevic, and A. Balaz, *Efficient Calculation of Energy Spectra Using Path Integrals*, Phys. Lett. A 360, 205 (2006).

Two of these papers (1. and 3.) are directly related to the research presented in this thesis. She presented her research at 3 international and one national conference, and edited one book of proceedings of an international conference.

Danica Stojiljković is employed at the Institute of Physics in Belgrade since 2007. Her scientific work was supported by the national research project ON171017 "Modeling and Numerical Simulations of Complex Many-Particle Systems" and integrated project III43007, funded by the Ministry of Education, Science, and Technological Development of the Republic of Serbia. From 2008 till 2010 she was engaged as liason officer for FP7 projects SEE-GRID-SCI and EGEE-III, the position that was based at CERN, Geneva, Switzerland. From 2012-2017 she was a member of the European Particle Physics Communication Network. She was engaged on several other FP7 projects such as HP-SEE, PRACE-1IP, PRACE-2IP and PRACE-3IP.

Изјава о ауторству

Име и презиме аутора – **Даница Стојиљковић**

Број индекса – **2016/8021**

Изјављујем

да је докторска дисертација под насловом

Kinetics and Morphology of Particle Deposition at Heterogeneous Surfaces

(Кинетика и морфологија депозиције честица на хетерогеним површинама)

- резултат сопственог истраживачког рада;

- да дисертација у целини ни у деловима није била предложена за стицање друге дипломе према студијским програмима других високошколских установа;

- да су резултати коректно наведени и

- да нисам кршила ауторска права и користила интелектуалну својину других лица.

У Београду,   2022   **Потпис аутора**

_____

Изјава о истоветности штампане и електронске верзије докторског рада

Име и презиме аутора – **Даница Стојиљковић**

Број индекса – **2016/8021**

Студијски програм – Физика кондензоване материје и статистичка физика

Наслов рада – **Kinetics and Morphology of Particle Deposition at Heterogeneous Surfaces**

(Кинетика и морфологија депозиције честица на хетерогеним површинама)

Ментор – **др Слободан Врховац**

Изјављујем да је штампана верзија мог докторског рада истоветна електронској верзији коју сам предала ради похрањивања у **Дигиталном репозиторијуму Универзитета у Београду**.

Дозвољавам да се објаве моји лични подаци везани за добијање академског назива доктора наука, као што су име и презиме, година и место рођења и датум одбране рада.

Ови лични подаци могу се објавити на мрежним страницама дигиталне библиотеке, у електронском каталогу и у публикацијама Универзитета у Београду.

У Београду,   2022   **Потпис аутора**

_____

Изјава о коришћењу

Овлашћујем Универзитетску библиотеку „Светозар Марковић" да у Дигитални репозиторијум Универзитета у Београду унесе моју докторску дисертацију под насловом:

Kinetics and Morphology of Particle Deposition at Heterogeneous Surfaces

(Кинетика и морфологија депозиције честица на хетерогеним површинама)

која је моје ауторско дело.

Дисертацију са свим прилозима предала сам у електронском формату погодном за трајно архивирање.

Моју докторску дисертацију похрањену у Дигиталном репозиторијуму Универзитета у Београду и доступну у отвореном приступу могу да користе сви који поштују одредбе садржане у одабраном типу лиценце Креативне заједнице (Creative Commons) за коју сам се одлучила.

1. Ауторство (CC BY)

2. Ауторство – некомерцијално (CC BY-NC)

3. Ауторство – некомерцијално – без прерада (CC BY-NC-ND)

4. **Ауторство – некомерцијално – делити под истим условима (CC BY-NC-SA)**

5. Ауторство – без прерада (CC BY-ND)

6. Ауторство – делити под истим условима (CC BY-SA)

(Молимо да заокружите само једну од шест понуђених лиценци.
Кратак опис лиценци је саставни део ове изјаве).

У Београду,   2022   **Потпис аутора**

_____

1. **Ауторство.** Дозвољавате умножавање, дистрибуцију и јавно саопштавање дела, и прераде, ако се наведе име аутора на начин одређен од стране аутора или даваоца лиценце, чак и у комерцијалне сврхе. Ово је најслободнија од свих лиценци.

2. **Ауторство – некомерцијално.** Дозвољавате умножавање, дистрибуцију и јавно саопштавање дела, и прераде, ако се наведе име аутора на начин одређен од стране аутора или даваоца лиценце. Ова лиценца не дозвољава комерцијалну употребу дела.

3. **Ауторство – некомерцијално – без прерада.** Дозвољавате умножавање, дистрибуцију и јавно саопштавање дела, без промена, преобликовања или употребе дела у свом делу, ако се наведе име аутора на начин одређен од стране аутора или даваоца лиценце. Ова лиценца не дозвољава комерцијалну употребу дела. У односу на све остале лиценце, овом лиценцом се ограничава највећи обим права коришћења дела.

4. **Ауторство – некомерцијално – делити под истим условима.** Дозвољавате умножавање, дистрибуцију и јавно саопштавање дела, и прераде, ако се наведе име аутора на начин одређен од стране аутора или даваоца лиценце и ако се прерада дистрибуира под истом или сличном лиценцом. Ова лиценца не дозвољава комерцијалну употребу дела и прерада.

5. **Ауторство – без прерада.** Дозвољавате умножавање, дистрибуцију и јавно саопштавање дела, без промена, преобликовања или употребе дела у свом делу, ако се наведе име аутора на начин одређен од стране аутора или даваоца лиценце. Ова лиценца дозвољава комерцијалну употребу дела.

6. **Ауторство – делити под истим условима.** Дозвољавате умножавање, дистрибуцију и јавно саопштавање дела, и прераде, ако се наведе име аутора на начин одређен од стране аутора или даваоца лиценце и ако се прерада дистрибуира под истом или сличном лиценцом. Ова лиценца дозвољава комерцијалну употребу дела и прерада. Слична је софтверским лиценцама, односно лиценцама отвореног кода.